Genetic and Functional Evaluation of Aminoacyl-tRNA Synthetase Mutations in Patients with Peripheral Neuropathy

by

Heather M. McLaughlin

A dissertation submitted in partial fulfillment
of the requirements for the degree of
Doctor of Philosophy
(Human Genetics)
in The University of Michigan
2012

Doctoral Committee:

Assistant Professor Anthony Antonellis, Chair
Professor Miriam H. Meisler
Professor John V. Moran
Associate Professor Thomas M. Glaser
Assistant Professor Asim Beg

"The significance and joy in my science comes in those occasional moments of discovering something new and saying to myself, 'So that's how God did it.'"

Henry Schaefer

To my husband Chris,
For his love, patience, and encouragement

ACKNOWLEDGEMENTS

The completion of a doctoral thesis is a great undertaking, and a project of this magnitude would not be possible without the support, guidance, and sacrifice of many mentors, colleagues, friends, and family.

I would like to extend my deepest gratitude to my advisor, Tony Antonellis, for his patience, support, and encouragement. I joined Tony's lab at a time when I was frustrated with science and unsure if I had chosen the right career path. Looking back, joining Tony's lab was one of the best decisions I made during my graduate career. Tony has not only provided me with the opportunity to explore various model systems and design my own experiments, he has also given me the freedom to develop new ideas and work independently on my own projects. Tony has been instrumental in improving my writing and presentation abilities, which has allowed me to publish several papers in distinguished journals and attend excellent scientific meetings. Tony has created an enjoyable environment in the lab and I will never forget our lab lunches, happy hours, and champagne toasts. I thank Tony for his guidance during my graduate career, and I hope to use the skills I have learned from him to effectively mentor my own students and staff in the future.

I would also like to thank my committee members Miriam Meisler, John Moran, Thomas Glaser, and Asim Beg for their guidance, recommendations, and encouragement throughout the duration of my thesis. I have had the opportunity to work with many wonderful collaborators and clinicians and would like to thank them for their contributions to this thesis, especially Ya-Ming Hou and Reiko Sakaguchi for their work on ARS enzyme kinetics. Thank you to members of the Antonellis lab, both past and present, for their friendship and encouragement, especially Kira Charney for her "British" accent, Chani Hodonsky for her never-ending supply of baked goods, Megan for teaching me about drop bears, Bill for his enthusiastic love for Jimmy John's, and Chetna for her cheery attitude. I would also like to thank members of the Meisler lab for their discussion and recommendations during lab meetings. Thanks to Tom Wilson for teaching me the art of tetrad dissection. Finally, a big thanks to Asim Beg for teaching me everything I know about *C. elegans*, and to Georgie Nicholl and Gisselle Velez for warmly inviting me into the Beg lab.

I would like to end with thanking all of the people who made my life enjoyable outside of the lab. A special thanks to Cheryl Jacobs Smith, Kaanan Shah, Valerie Schaibley, Stephanie Coomes, Kadee Luderman, and Ilea Swinehart for many glasses of wine and episodes of Grey's Anatomy. Thanks to my dear friends Sarah Gray, Christina Pries, Amanda Schneider, Jen Yager, and Beth DuRoss for always lending an ear. Thank you to my family for always believing in me. Finally, thank you to my husband Chris for being such a loving and devoted husband, for being so supportive of my career and aspirations, and for agreeing to move to Boston so that I can follow my dreams.

TABLE OF CONTENTS

LIST OF FIGURES

Figure

LIST OF TABLES

Table

LIST OF APPENDICES

Appendix

ABSTRACT

Charcot-Marie-Tooth (CMT) disease comprises a group of clinically and genetically heterogeneous peripheral neuropathies mainly characterized by distal muscle weakness and wasting, and impaired sensation in the extremities. CMT disease is the most common inherited peripheral neuropathy, with a prevalence of ~1 in 2,500 individuals. While CMT disease is relatively common, our understanding of the genes mutated in patients with CMT disease and the mechanism by which these mutations lead to peripheral neuropathy remains incomplete. Genes encoding aminoacyl-tRNA synthetases (ARSs) have been implicated in CMT disease with an axonal pathogenesis. ARSs are ubiquitously expressed, essential enzymes, responsible for covalently attaching amino acids to their cognate tRNA molecules, thus completing an essential step of protein translation. To improve our understanding of the genetic and functional mechanisms by which ARS mutations lead to disease, we sought to: (1) identify and characterize ARS gene mutations in a cohort of patients with CMT disease and no known disease-causing mutation; (2) evaluate the functional consequences of disease-associated ARS mutations; and (3) develop a multi-cellular model system for assessing the toxicity of ARS alleles in neurons. Our genetic analyses led to the discovery of missense and frameshift lysyl-tRNA synthetase (*KARS*) gene mutations in a compound heterozygous patient with CMT disease and additional non-neurological sequelae, and the discovery of missense alanyl-tRNA synthetase (*AARS*) gene mutations in two families with CMT2N. Using a combination of biochemical analyses and yeast viability assays, we determined that

disease-associated *AARS* and *KARS* mutations lead to impaired enzyme activity. Finally, we developed a *C. elegans* model system for evaluating the effect of ARS mutations on peripheral nerve axons *in vivo,* and discovered that overexpression of a mutant AARS enzyme leads to morphological defects. Together, these studies underscore the critical role of ARS enzymes in peripheral nerve function and suggest that impaired aminoacylation may be a central component to disease pathology. In summary, my dissertation research has advanced our understanding of the genetic and functional role of ARS enzymes in peripheral neuropathies and will provide a platform for further investigating the molecular pathology of ARS-related CMT disease.

CHAPTER 1

Introduction to Inherited Peripheral Neuropathies

Overview of the Peripheral Nervous System

The peripheral nervous system (PNS) is composed of all neurons and glial cells outside of the brain and spinal cord. Three structures predominate the PNS: sensory neurons, motor neuron axons, and Schwann cells (Purves *et al.*, 2001). Sensory neurons are afferent neurons with cell bodies originating in the dorsal root ganglia. Sensory neurons process stimuli from the external environment (light, touch, sound) and convey these sensory signals to the central nervous system (CNS) (Levitan and Kaczmarek, 2002). Motor neurons are efferent neurons with cell bodies originating from the ventral region of the spinal cord. Motor neurons relay messages from the CNS to the skeletal muscles, glands, and other effector tissues (Levitan and Kaczmarek, 2002). Sensory and motor neurons possess two types of continuous projections that facilitate information transfer to and from the cell body, or soma (Waxman *et al.*, 1995). Dendrites are short, branched projections along which signals from upstream neurons can be transmitted to the soma. In contrast, axons are long, narrow projections that serve to deliver electrical impulses away from the cell body (in the case of motor neurons) or towards the cell body (in the case of sensory neurons). Schwann cells are the principal glia of the PNS and exist in non-myelinating and myelinating forms. Myelinating Schwann cells provide trophic support

and electrical insulation to nearby axons, and can produce an elaborate myelin sheath that envelops a subset axons in the PNS (Gilbert, 2010).

Nerve cell axons serve as the primary conduit for transferring electrical impulses, proteins, organelles, receptors, and various trophic factors from the soma to the axon terminus (Dyck and Thomas, 2005b; Waxman *et al.*, 1995). Axon length varies, with the largest axons spanning up to a meter in length. For example, the largest nerve in the human body, the sciatic nerve, spans from the base of the spine down to the lower limbs and into the foot (Dyck and Thomas, 2005b). The extensive length of large axons presents a unique problem to peripheral nerves; nerve signaling and axonal transport must be supported over great distances throughout the life of the neuron. Defects in these processes, or in the axonal structure itself, are highly detrimental to the nerve cell and the PNS as a whole.

Peripheral Neuropathies

Peripheral neuropathies are a clinically heterogeneous group of diseases that affect the peripheral nerves. Peripheral neuropathies are relatively common, and are estimated to affect 2-8% of the population worldwide (Martyn and Hughes, 1997). Broadly, peripheral neuropathies can be subdivided into three distinct subtypes: (1) acquired peripheral neuropathies; (2) peripheral neuropathies associated with systemic disorders; and (3) inherited peripheral neuropathies (Dyck and Thomas, 2005b). Acquired peripheral neuropathies often result from nerve trauma, tumors, inflammation, nutritional deficiencies, and alcoholism. For example, Guillain-Barré Syndrome commonly presents

following a respiratory or gastrointestinal infection and leads to an autoimmune-mediated attack of the nervous system (Pritchard, 2010). Peripheral neuropathies can also be associated with systemic disorders. For example, complications from diabetes, such as chronically high blood glucose levels, can lead to oxidative and inflammatory damage to peripheral nerves (Vincent *et al.*, 2011). Inherited peripheral neuropathies are the result of heritable genetic lesions, often occurring in genes important for peripheral nerve function. Examples of inherited peripheral neuropathy include Dejerine-Sottas syndrome (DSS), hereditary neuropathy with liability to pressure palsies (HNPP), and Charcot-Marie-Tooth (CMT) disease (Martyn and Hughes, 1997). The various forms of inherited peripheral neuropathy are often distinguished by disease onset and symptomatic features. For example, DSS is characterized by infantile onset of moderate to severe lower and upper extremity weakness and loss of sensation, whereas HNPP is distinguished by the presence of repeated focal pressure neuropathy (Dyck and Thomas, 2005a). CMT disease is the focus of this dissertation and will be discussed at length in the next section.

Inherited Peripheral Neuropathies: Charcot-Marie-Tooth Disease

The most common inherited peripheral neuropathies are a group of disorders collectively referred to as CMT disease. CMT disease was first described in 1886 by Drs. Jean-Martin Charcot and Pierre Marie from France, and Dr. Howard Henry Tooth from England, as a hereditary disorder giving rise to distal limb weakness and wasting, being maximal in the lower extremities (Charcot and Marie, 1886; Tooth, 1886). CMT disease is estimated to affect ~1 in 2,500 individuals worldwide, making it the most common inherited peripheral neuropathy (Skre, 1974). CMT disease has emerged as a clinically and

genetically heterogeneous disorder. While the overall clinical presentation may vary, patients with CMT disease commonly display a phenotype consisting of: impaired motor function, muscle wasting, reduced or absent deep-tendon reflexes, impaired sensation in the extremities, pes cavus, steppage gait, and variable reduction in motor nerve conduction velocities (MNCVs) or amplitudes (hereafter referred to as the "classical" CMT disease phenotype) (Dyck and Lambert, 1968; Murakami *et al.*, 1996). CMT disease does not typically affect patient lifespan; however, disease symptoms can lead to ambulatory loss, limb amputation, and other morbidity (*e.g.,* use of orthotics).

Broadly, CMT disease can be divided into two distinct categories based mainly upon electrophysiological criteria gained from MNCV studies. MNCV analyses are performed by providing electrical stimulation at one point along the nerve and measuring the latency of the response (*i.e.,* the amount of time it takes for the electrical impulse to reach the muscle supplied by the nerve) (Dyck and Thomas, 2005b). MNCV values are calculated by dividing the distance between the point of stimulation and the muscle measured in millimeters by the latency in milliseconds. Patients with median MNCVs < 38 ms^{-1} and the discovery of classical "onion bulb" formations of concentric Schwann cell lamellae upon cross-sectional analysis of nerve biopsies are considered to have "demyelinating" CMT (Dyck and Thomas, 2005a). Conversely, patients with normal (>45 ms^{-1}) MNCVs, along with reduced amplitudes of evoked motor nerve response, are considered to have "axonal" CMT (Dyck and Lambert, 1968; Harding and Thomas, 1980). While CMT disease is mainly divided into demyelinating and axonal forms, the idea of an intermediate form of CMT has been gaining popularity amongst clinicians because it can

be helpful in guiding genetic diagnoses. Intermediate CMT is distinguished by the presence of patients with demyelinating or axonal features in a single family, or the presence of MNCVs in the intermediate range (25-45 ms^{-1}) in an individual patient (Nicholson and Myers, 2006).

Demyelinating and axonal forms of CMT disease can be further divided into six subtypes based upon inheritance pattern: CMT disease type I (CMT1), CMT disease type II (CMT2), CMT disease type IV (CMT4), X-linked CMT (CMTX), dominant intermediate CMT (CMTDI), and recessive intermediate CMT (CMTRI) (Table 1.1). CMT1, an autosomal dominant, demyelinating form of CMT disease, is the most common form of CMT disease and is estimated to affect ~60-70% of patients with CMT disease (Dyck and Thomas, 2005b). To date, six subtypes of CMT1 have been described, with the majority of the genes implicated being important for Schwann cell function and myelination. (Table 1.1) (Hayasaka *et al.*, 1993; Kovach *et al.*, 1999; Lupski *et al.*, 1991; Mersiyanova *et al.*, 2000; Saporta *et al.*, 2011; Street *et al.*, 2003; Warner *et al.*, 1998).

CMT2, an autosomal dominant, axonal form of CMT disease, is estimated to affect ~30-40% of patients with CMT disease (Dyck and Thomas, 2005b). Currently, a total of 16 subtypes of CMT2 have been described (Table 1.1) (Antonellis *et al.*, 2003; Auer-Grumbach *et al.*, 2010; Crimella *et al.*, 2010; De Jonghe *et al.*, 1999; De Sandre-Giovannoli *et al.*, 2002; Evgrafov *et al.*, 2004; Gallardo *et al.*, 2008; Georgiou *et al.*, 2002; Latour *et al.*, 2010; Leal *et al.*, 2009; Marrosu *et al.*, 1998; Tang *et al.*, 2005; Verhoeven *et al.*, 2003; Weedon *et al.*, 2011; Zhao *et al.*, 2001; Zuchner *et al.*, 2004). In

Table 1.1 Genes Implicated in Charcot-Marie-Tooth Disease

CMT Subtype	OMIM[1]	Class	Inheritance[2]	Gene	Reference
CMT1A	118220	Demy	AD	*PMP22*	Lupski *et al.*, 1991
CMT1B	118200	Demy	AD	*MPZ*	Hayasaka *et al.*, 1993b
CMT1C	601098	Demy	AD	*LITAF*	Street *et al.*, 2003
CMT1D	607678	Demy	AD	*EGR2*	Warner *et al.*, 1998
CMT1E	118300	Demy	AD	*PMP22*	Kovach *et al.*, 1999
CMT1F	607734	Demy	AD	*NEFL*	Mersiyanova *et al.*, 2000
CMT2A1	118210	Axonal	AD	*KIF1B*	Zhao *et al.*, 2001
CMT2A2	609260	Axonal	AD	*MFN2*	Zuchner *et al.*, 2004
CMT2B	600882	Axonal	AD	*RAB7*	Verhoeven *et al.*, 2003
CMT2B1	605588	Axonal	AR	*LMNA*	De Sandre-Giovannoli *et al.*, 2002
CMT2B2	605589	Axonal	AR	*MED25*	Leal *et al.*, 2009
CMT2C	606071	Axonal	AD	*TRPV4*	Auer-Grumbach *et al.*, 2010
CMT2D	601472	Axonal	AD	*GARS*	Antonellis *et al.*, 2003
CMT2E	607684	Axonal	AD	*NEFL*	Mersiyanova *et al.*, 2000
CMT2F	606595	Axonal	AD	*HSPB1*	Evgrafov, *et al.*, 2004
CMT2I	607677	Axonal	AD	*MPZ*	Marrosu *et al.*, 1998
CMT2J	607736	Axonal	AD	*MPZ*	De Jonghe *et al.*, 1999
CMT2K	607831	Axonal	AD	*GDAP1*	Cuesta *et al.*, 2002
CMT2L	608673	Axonal	AD	*HSPB8*	Tang, *et al.*, 2005
CMT2M	606482	Axonal	AD	*DNM2*	Fabrizi *et al.*, 2007a
CMT2N	613287	Axonal	AD	*AARS*	Latour *et al.*, 2010
CMT2O	614228	Axonal	AD	*DYNC1H1*	Weedon, *et al.*, 2011
CMT4A	214400	Demy	AR	*GDAP1*	Baxter *et al.*, 2002
CMT4B1	601382	Demy	AR	*MTMR2*	Bolino *et al.*, 2000
CMT4B2	604563	Demy	AR	*SBF2*	Senderek *et al.*, 2003a
CMT4C	601596	Demy	AR	*SH3TC2*	Senderek, *et al.*, 2003c
CMT4D	601455	Demy	AR	*NDRG1*	Kalaydjieva *et al.*, 2000
CMT4E	605253	Hypomy	AR	*EGR2*	Warner *et al.*, 1998
CMT4H	609311	Demy	AR	*FDG4*	Delague *et al.*, 2007
CMT4J	611228	Demy	AR	*FIG4*	Chow *et al.*, 2007
CMTX1	302800	Mixed	XD	*GJB1*	Bergoffen *et al.*, 1993
CMTX5	311070	Mixed	XR	*PRPS1*	Kim *et al.*, 2007
CMTDIB	606482	Mixed	AD	*DNM2*	Zuchner *et al.*, 2005
CMTDIC	608323	Mixed	AD	*YARS*	Jordanova *et al.*, 2006
CMTDIE	614455	Mixed	AD	*INF2*	Boyer *et al.*, 2011
CMTRIA	608340	Mixed	AR	*GDAP1*	Senderek *et al.*, 2003b
CMTRIB	613641	Mixed	AR	*KARS*	McLaughlin, *et al.*, 2010

[1]OMIM (Online Mendelian Inheritance in Man) phenotype accession number
[2] AD (autosomal dominant); AR (autosomal recessive); XD (X-linked dominant); XR (X-linked recessive)

contrast to genes implicated in CMT1, the majority of the genes mutated in patients with CMT2 are critical for axonal maintenance and health.

CMT4 comprises a group of autosomal recessive demyelinating forms of CMT disease. A total of eight forms of CMT4 have been described (Table 1.1) (Baxter *et al.*, 2002; Bolino *et al.*, 2000; Chow *et al.*, 2007; Delague *et al.*, 2007; Kalaydjieva *et al.*, 2000; Senderek *et al.*, 2003c; Senderek *et al.*, 2003a; Warner *et al.*, 1998). Patients with CMT4 present with the classical CMT phenotype; however, it is usually more severe and often includes other systemic symptoms such as deafness, glaucoma, scoliosis, and loss of ambulation. CMT4 accounts for less than 10% of patients with CMT disease, but can be more prevalent in consanguineous populations (Bernard *et al.*, 2006).

CMTX affects ~10-20% of patients with CMT disease (Ionasescu *et al.*, 1993). There are five subtypes of CMTX, including both dominant and recessive forms, however only two loci have been implicated in disease onset (Table 1.1) (Bergoffen *et al.*, 1993; Kim *et al.*, 2007). CMTX demonstrates both axonal and demyelinating features and is often suspected in pedigrees with an absence of male-to-male transmission (Bergoffen *et al.*, 1993; Hahn *et al.*, 1990).

Intermediate CMT is the least common form of CMT disease and can be inherited in either a dominant or recessive manner. To date, five forms of intermediate CMT have been described (Table 1.1) (Boyer *et al.*, 2011; Jordanova *et al.*, 2006; McLaughlin *et al.*, 2010; Senderek *et al.*, 2003b; Zuchner *et al.*, 2005).

Mechanisms of Demyelinating Charcot-Marie-Tooth Disease

A total of 19 forms of CMT disease include demyelinating pathology (Table 1.1). Mutations in several genes important for Schwann cell function and peripheral nerve axon myelination have been implicated in demyelinating CMT disease including *PMP22, MPZ*, *GJB1* and *LITAF*. CMT1A, the most common subtype of CMT1, is caused by mutations in the peripheral myelin protein 22 (*PMP22*) gene (Lupski *et al.*, 1991). *PMP22* encodes a 22 kDa membrane protein expressed in all myelinated fibers in the PNS (Snipes *et al.*, 1992). The gene dosage of the *PMP22* gene, and the amount of PMP22 present in compact myelin, appears to be critical for Schwann cell function. For example, loss-of-function mutations in *PMP22,* or deletion of a 1.7 Mb region at the *PMP22* locus leads to hereditary neuropathy with liability to pressure palsies (HNPP), while gain-of-function mutations in *PMP22,* or duplication of the same 1.7 Mb region gives rise to CMT1A (Chance *et al.*, 1993; Valentijn *et al.*, 1992).

The myelin protein zero (*MPZ*) gene encodes a 30 kDa integral membrane glycoprotein (Ishaque *et al.*, 1980). Missense and frameshift mutations in the *MPZ* gene have been implicated in CMT1B and Dejerine-Sottas syndrome (DSS) (Hayasaka *et al.*, 1993). MPZ accounts for ≥ 50% of the protein in peripheral myelin and is essential for myelin assembly and stabilization (Greenfield *et al.*, 1973). MPZ is a member of the immunoglobulin superfamily and engages in cell-adhesion activity, forming *cis*-homotetramers that interact in *trans* with homotetramers on adjacent membranes (Inouye *et al.*, 1999; Thompson *et al.*, 2002). It is predicted that these tetrameric interactions

serve to keep the concentric layers of Schwann cell myelin intact. Loss-of-function mutations affecting myelin compaction are predicted to be responsible for CMT1B, whereas gain-of-function mutations effecting tetramerization are predicted to be responsible for DSS (Warner *et al.*, 1996).

Insertions, deletions, frameshift, and missense mutations in another gene important for peripheral nerve myelin, the connexin 32 gene (*GJB1*), cause CMTX1, a demyelinating peripheral neuropathy (Bergoffen *et al.*, 1993). The connexin 32 protein is widely expressed in many tissues, including uncompacted myelin, where it likely functions as a gap junction protein, allowing the radial diffusion of small molecules and ions between layers of the myelin sheath (Kumar and Gilula, 1996; Scherer *et al.*, 1995). Mutations in the *GJB1* gene are predicted to result in impediment of gap junction formation or alteration of the conduction properties of assembled gap junctions, and often result in retention of connexin 32 proteins at the cell surface, in the cytoplasm, or in the Golgi apparatus (Deschenes *et al.*, 1997; Yum *et al.*, 2002).

While *PMP22, MPZ,* and *GJB1* mutations underscore the critical role of peripheral nerve myelin proteins and components in demyelinating peripheral neuropathy, the roles of other proteins implicated in demyelinating CMT disease remain speculative. For example, missense mutations in the lipopolysaccharide-induced tumor necrosis factor-alpha factor (*LITAF*) gene have been implicated in CMT1C (Street *et al.*, 2003). The LITAF protein localizes to aggresomes and is thought to be involved in ubiquitin-mediated lysosomal protein degradation and membrane turnover (Eaton *et al.*, 2012; Saifi

et al., 2005). Mutations in *LITAF* may lead to impaired protein degradation and subsequent toxicity to Schwann cells. Interestingly, the PMP22 protein undergoes rapid turnover, and overexpression of *PMP22*, or inhibition of the ubiquitin proteasome pathway, results in perinuclear protein aggregates (Pareek *et al.*, 1997; Ryan *et al.*, 2002). It is possible that LITAF plays a role in the degradation of PMP22 and other peripheral nerve myelin membrane proteins.

Mechanisms of Axonal Charcot-Marie-Tooth Disease

There are a total of 23 forms of CMT that comprise axonal pathology (Table 1.1). Elucidation of the genetic causes of axonal CMT, along with the pathogenic mechanisms by which mutations in these genes lead to axonal CMT, has provided substantial knowledge towards the understanding of proteins and pathways responsible for the health and maintenance of PNS axons. Together, these studies have revealed a diverse array of cellular processes important for proper axon function including axonal transport, cytoskeletal integrity, and mitochondrial dynamics (Figure 1.1).

Neurons, and their associated axons, constitute the longest, most polarized cells in the human body. Axons must be supported over long distances, often spanning up to a meter in length (Dyck and Thomas, 2005b). Axonal function is achieved, in part, by coordinated transport of proteins, lipids, organelles, synaptic vesicles, and other macromolecules to and from the axon terminal via axonal transport along microtubules (Levitan and Kaczmarek, 2002). Anterograde axonal transport serves to convey cargo

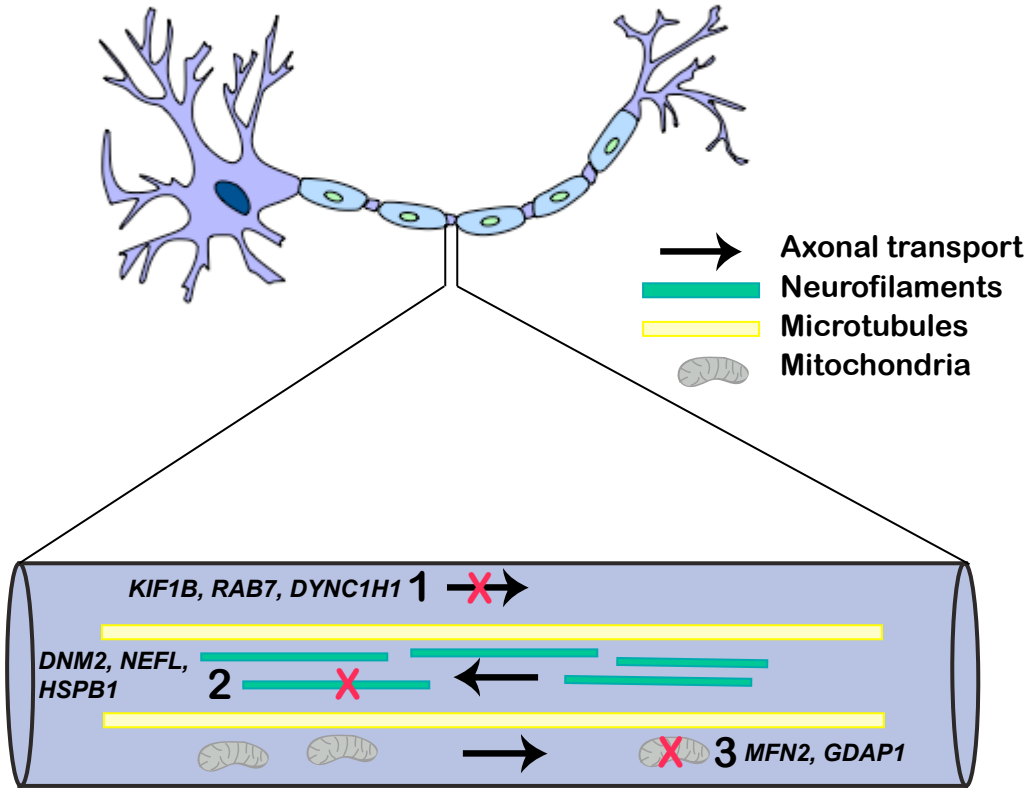

Figure 1.1 Mechanisms of Axonal Charcot-Marie-Tooth Disease. A neuron is schematically depicted with a cell body on the left and an axon protruding toward the right. Schwann cells are depicted as ovals wrapping around the axon. Below, an enlarged segment of the axon is shown. Three mechanisms leading to axonal CMT disease are represented: (1) defective axonal transport; (2) diminished cytoskeletal integrity; and (3) abnormal mitochondrial dynamics.

towards the axon terminal, while retrograde axonal transport is responsible for transporting cargo towards the soma. Anterograde and retrograde transport are facilitated via adenosine triphosphate (ATP)-dependent kinesins and dyneins, respectively (Alberts, 2008). Kinesins consist of a dimer of globular head domains and two light chains, attached by a α-helix (Lodish, 2008). The kinesin head domain binds ATP and microtubules, while the tail domain binds membrane vesicles. Dynein also contains a dimer of head domains, but requires interactions with other microtubule-associated proteins to facilitate axonal transport (Lodish, 2008). Microtubules consist of α- and β-tubilin dimers that polymerize end to end, with the α-tubulin subunit of one dimer associating with the β-tubulin subunit of the next dimer (Lodish, 2008). This arrangement imparts polarity to polymerized microtubules; the end with the α-subunit exposed is designated the (+) end, while the end with the β-subunit exposed is designated the (-) end. Kinesins are (+) end-directed motor proteins, while dyneins are (-) end-directed motor proteins (Lodish, 2008).

Mutations in several genes involved in axonal transport have been implicated in axonal CMT disease including *KIF1Bβ, RAB7,* and *DYNC1H1* (Figure 1.1). A missense mutation in isoform β of the kinesin family member 1B (*KIF1B)* gene, was identified in a single family with CMT2A1 (Zhao *et al.*, 2001). Patients with CMT2A1 display the classical CMT phenotype, although some patients also report mild inward curvature of the lumbar spine (*i.e.,* lordosis) (Saito *et al.*, 1997). KIF1Bβ, a member of the kinesin family of microtubule motors, is widely distributed in neuronal cell bodies and axons and is responsible for transport of synaptic vesicle precursors (Zhao *et al.*, 2001).

Examination of axonal transport in *Kif1b*$^{+/-}$ mice revealed a decrease of synaptic precursors specifically at the nerve terminals, and not in the cell body, supporting the hypothesis that haploinsufficiency of KIF1Bβ leads to impaired axonal transport (Zhao *et al.*, 2001).

A second protein important for axonal transport, the ras-related protein 7 (RAB7), is a guanosine triphosphate (GTP)ase responsible for controlling late endocytic trafficking (Cantalupo *et al.*, 2001). RAB7 has been implicated in retrograde axonal transport of neurotrophins and their receptors, a family of proteins important for the growth and survival of neurons (Deinhardt *et al.*, 2006; Saxena *et al.*, 2005). Missense *RAB7* mutations have been identified in patients with CMT2B (Verhoeven *et al.*, 2003). CMT2B is distinguished by the presence of sensory loss, foot ulcers, and infections that often lead to amputation of the phalanges (Verhoeven *et al.*, 2003). All disease-associated mutations identified to date map to the nucleotide-binding site of RAB7, and while RAB7 mutant enzymes are able to effectively bind GTP, they all display impaired GTPase activity along with a reduced affinity for guanine nucleotides (Spinosa *et al.*, 2008). These data support the hypothesis that *RAB7* mutations lead to diminished GTPase activity, which may result in impaired retrograde transport of proteins important for axonal function.

Mutations in the cytoplasmic dynein heavy chain 1 (*DYNC1H1*) gene have been reported in patients with CMT2O (Weedon *et al.*, 2011). As reviewed above, dyneins are molecular motors that participate in retrograde axonal transport along microtubules.

DYNC1H1 subunits dimerize to form the core of the dynein complex. Missense mutations in the *DYNC1H1* gene lead to dynein instability and decreased affinity for microtubules (Harms *et al.*, 2012) Moreover, *Dynchc1* mutant mouse models display defects in fast retrograde transport and develop progressive motor neuron degeneration (Hafezparast *et al.*, 2003). Together, functional evaluation of *KIF1Bβ, RAB7,* and*, DYNC1H1* mutations in patients with CMT disease has served to highlight the critical role of axonal transport in neurodegenerative disease.

Proper axonal transport relies on the integrity of the axonal cytoskeletal support system (Figure 1.1). The axonal cytoskeleton consists of an intricate network of neurofilaments, microtubules, actin microfilaments, and other associated proteins (Waxman *et al.*, 1995). Missense and frameshift mutations in one gene important for cytoskeletal stability, dynamin 2 (*DNM2*), have been implicated in CMT2M and in CMTDIB (Fabrizi *et al.*, 2007a; Zuchner *et al.*, 2005). Patients with CMT2M have an axonal form of CMT disease, while most families with CMTDIB display intermediate CMT features, with MNCVs spanning 24-54 m/s (Fabrizi *et al.*, 2007a; Kennerson *et al.*, 2001). DNM2 is a GTPase that modulates a wide array of cellular processes including intracellular membrane trafficking, endocytosis, and cytoskeletal assembly via regulation of actin and microtubule networks (Cao *et al.*, 2005; Kessels *et al.*, 2006). While wild-type DNM2 co-localizes with vesicular (*e.g.* endosomal vesicles) and filamentous (*e.g.* microtubules, actin) structures, mutant DNM2 localizes almost exclusively to the microtubule cytoskeleton and leads to disorganized microtubules (Zuchner *et al.*, 2005). These data

indicate that mutations in *DNM2* may lead to disruption of the microtubule cytoskeleton resulting in impaired axonal transport.

Neurofilaments, members of the intermediate filament family, constitute the majority of the axon cytoskeleton (Waxman *et al.*, 1995). Neurofilaments are composed of light, medium, and heavy chains, termed NEFL, NEFM, and NEFH, respectively. Together, neurofilaments coassemble *in vivo* to form highly organized heteropolymers, for which the presence of NEFL is required (Geisler and Weber, 1981). Neurofilaments maintain axonal caliber and support axonal growth, transport, and signaling. Mutations in two genes important for neurofilament assembly have been identified in patients with CMT: neurofilament light chain (*NEFL*) and heat shock protein beta-1 (*HSPB1*). Insertions, deletions, and missense mutations in the *NEFL* gene were identified in patients with CMT2E, a subtype of CMT distinguished by the development of "claw hand" deformities (when the muscles in the hand tighten and curl inward) (Fabrizi *et al.*, 2004; Georgiou *et al.*, 2002; Mersiyanova *et al.*, 2000). Sural nerve biopsies of CMT2E patients reveal profound cytoskeletal abnormalities including accumulation of focal NEFL aggregates, axonal swelling, and secondary demyelination (Fabrizi *et al.*, 2007b).

CMT2F, a CMT subtype that also features claw hand deformities, is caused by missense mutations in the *HSBP1* gene (Evgrafov *et al.*, 2004). The HSPB1 protein associates with NEFL, and mutant HSPB1 leads to neurofilament network disruption and aggregation of NEFL (Zhai *et al.*, 2007). *DMN2*, *NEFL*, and *HSPB1* mutations highlight the important role of neurofilament organization in the structural integrity of the axon and reveal that

disruption of cytoskeletal networks can lead to axonal transport obstruction resulting in impaired transport of proteins, organelles, and other important factors to the axon terminal.

Mitochondria are dynamic organelles that continually undergo fusion and fission events. Mitochondrial fusion occurs when two mitochondria merge together, while mitochondrial fission occurs when a single mitochondrion splits into two (Alberts, 2008). Fusion and fission are essential for mitochondrial processes including ATP production, electron transport chain support, calcium storage, and apoptosis (Figure 1.1) (Voet *et al.*, 1999). Interestingly, mutations in the mitofusin 2 gene (*MFN2)* and the ganglioside-induced differentiation-associated protein 1 gene (*GDAP1*), both responsible for controlling mitochondrial dynamics, have been implicated in CMT2A2 and CMT2K, respectively (Crimella *et al.*, 2010; Zuchner *et al.*, 2004). CMT2A2 is characterized by the classical CMT phenotype with occasional optic atrophy. CMT2A2 accounts for up to 20% of patients with CMT2, and is caused by missense mutations in the *MFN2* gene (Verhoeven *et al.*, 2006; Zuchner *et al.*, 2004). MFN2 is anchored to the outer mitochondrial membrane and plays a pivotal role in mitochondrial fusion events (Santel and Fuller, 2001). Mitochondria undergo both fast, persistent transport, and also periods of slower activity, or stationary periods. Analysis of mitochondrial transport in cells expressing mutant MFN2 proteins revealed a dramatic decrease of fast, persistent transport accompanied by longer latencies between anterograde and retrograde transport and smaller, fragmented axonal mitochondria (Misko *et al.*, 2010). These data indicate that

MFN2 is required for mitochondrial trafficking and that MFN2 mutant proteins disrupt mitochondrial transportation.

The ganglioside-induced differentiation-associated protein 1 (*GDAP1*) gene encodes another outer mitochondrial membrane protein essential to mitochondrial dynamics. Splice-site, frameshift, insertion, deletion, and missense mutations in the *GDAP1* gene are associated with CMT2K. Patients with CMT2K display the classical CMT phenotype, however, several patients also experience vocal cord paresis (Crimella *et al.*, 2010; Cuesta *et al.*, 2002; Sahin-Calapoglu *et al.*, 2009). The majority of CMT2K-associated *GDAP1* mutations disrupt mitochondrial fusion leading to elevated reactive oxygen species (ROS) levels and an increased susceptibility to apoptosis (Niemann *et al.*, 2009). Combined, *MFN2* and *GDAP1* mutations underscore the essential role of mitochondrial dynamics in peripheral nerve axon health. Impaired mitochondrial transport and disrupted metabolite production may deprive the axon of key metabolites and promote neuronal apoptosis or further interrupt axonal transport, especially in distal portions of the axon.

Aminoacyl-tRNA Synthetases Implicated in Charcot-Marie-Tooth Disease

Aminoacyl-tRNA synthetase (ARS) genes encode a class of enzymes responsible for tRNA charging, the process of covalently linking amino-acids onto their cognate tRNA molecules (Delarue, 1995). Demonstrating their fundamental importance, ARSs are ubiquitously expressed, essential enzymes that are encoded in the genomes of all multi- and unicellular species. ARS enzymes may function as monomers, dimers, or tetramers,

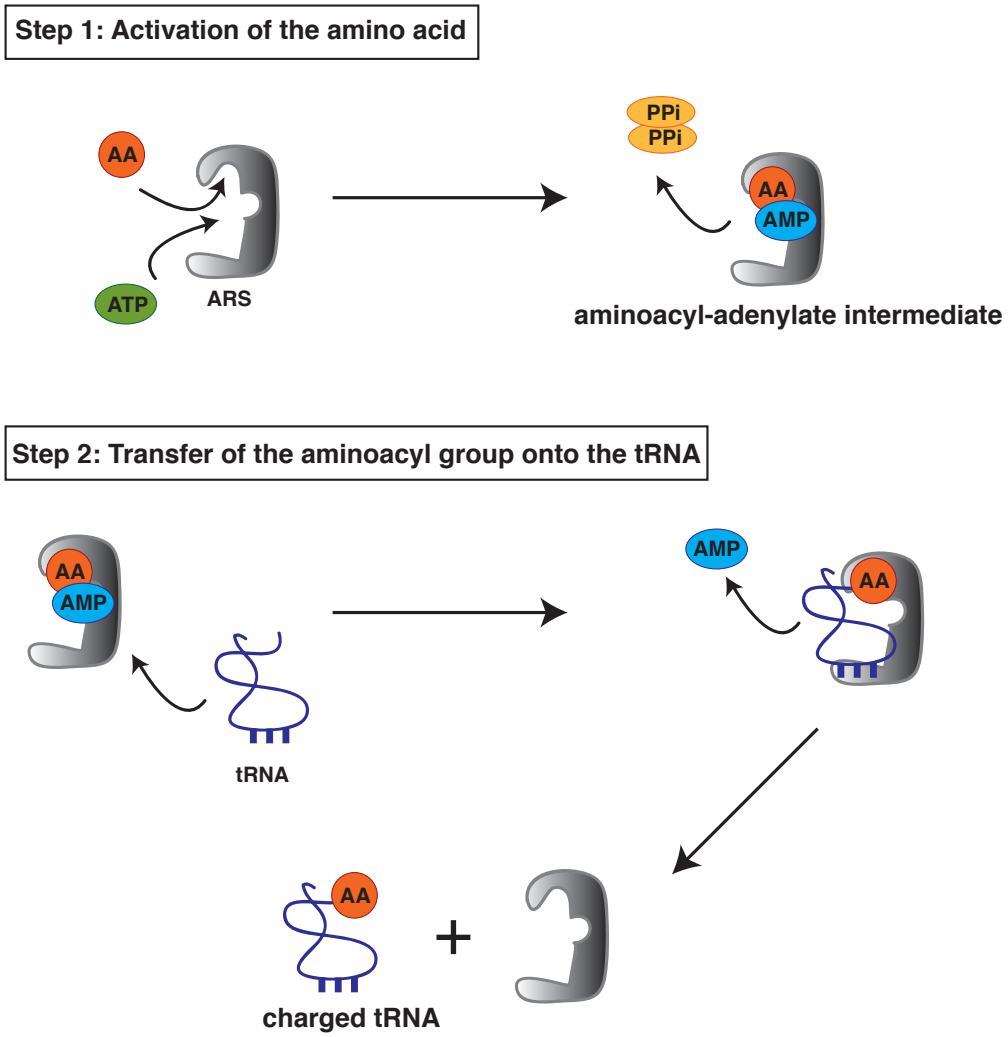

Figure 1.2 The Aminoacylation Reaction. Each aminoacyl-tRNA synthetase (ARS) charges a specific tRNA molecule with its cognate amino acid (AA) via a two-step aminoacylation reaction. In the activation step (Step 1), the ARS binds the AA and an adenosine triphosphate (ATP) molecule to form an aminoacyl-adenylate intermediate, resulting in the release of two pyrophosphate molecules (PPi). In the transfer step (Step 2), the tRNA binds the ARS via its anticodon-binding domain, the AA is ligated onto the tRNA, and an AMP molecule is released. After release of the aminoacylated tRNA, the ARS is free to charge another tRNA molecule.

and each ARS is responsible for charging a specific tRNA via a two-step aminoacylation reaction (Figure 1.2). In the first (activation) step, the ARS binds the amino-acid and an ATP molecule to form the aminoacyl-adenylate intermediate, releasing two pyrophosphate molecules. In the second (transfer) step, the tRNA binds the ARS via an anticodon-binding domain, the amino-acid is ligated onto the tRNA, and an AMP molecule is released. The charged tRNA is then utilized for protein translation and the ARS is free to charge another tRNA molecule.

The human nuclear genome harbors 37 ARS loci: 17 ARS loci encode ARS enzymes that charge tRNAs exclusively in the cytoplasm, 17 ARS loci encode ARS enzymes that charge tRNAs in the mitochondria, and 3 ARS loci encode bifunctional ARS enzymes (Table 1.2). Bifunctional ARS enzymes are able to charge tRNAs in both the cytoplasm and in the mitochondria via use of an alternative splicing mechanism which leads to the inclusion of a mitochondrial targeting sequence (Collins and Lambowitz, 1985; Mudge *et al.*, 1998; Rinehart *et al.*, 2005; Tolkunova *et al.*, 2000).

The fidelity of protein synthesis relies on correct attachment of amino-acids to their cognate tRNA molecules. Errors in aminoacylation result in misincorporation of amino-acids onto the growing polypeptide chain and may lead to subsequent protein misfolding and degradation. The fidelity of the aminoacylation reaction is achieved via a "double-sieve" editing mechanism, reducing the overall error rate to one in 10^4-10^5 aminoacylation events (Zaher and Green, 2009). The double-sieve model consists of pre-transfer editing, occurring prior to aminoacyl-adenylate intermediate formation, and post-

Table 1.2 Human Aminoacyl-tRNA Synthetase Genes

Gene Symbol	Gene Name	Cell Compartment
AARS	alanyl-tRNA synthetase	cytoplasmic
CARS	cysteinyl-tRNA synthetase	cytoplasmic
DARS	aspartyl-tRNA synthetase	cytoplasmic
EPRS	glutamyl-prolyl-tRNA synthetase	cytoplasmic
FARSA	phenylalanyl-tRNA synthetase α subunit	cytoplasmic
FARSB	phenylalanyl-tRNA synthetase β subunit	cytoplasmic
HARS	histidyl-tRNA synthetase	cytoplasmic
IARS	isoleucyl-tRNA synthetase	cytoplasmic
LARS	leucyl-tRNA synthetase	cytoplasmic
MARS	methionyl-tRNA synthetase	cytoplasmic
NARS	asparaginyl-tRNA synthetase	cytoplasmic
RARS	arginyl-tRNA synthetase	cytoplasmic
SARS	seryl-tRNA synthetase	cytoplasmic
TARS	threonyl-tRNA synthetase	cytoplasmic
VARS	valyl-tRNA synthetase	cytoplasmic
WARS	tryptophanyl-tRNA synthetase	cytoplasmic
YARS	tyrosyl-tRNA synthetase	cytoplasmic
AARS2	alanyl-tRNA synthetase 2	mitochondrial
CARS2	cysteinyl-tRNA synthetase 2	mitochondrial
DARS2	aspartyl-tRNA synthetase 2	mitochondrial
EARS2	glutamyl-tRNA synthetase 2	mitochondrial
FARS2	phenylalanyl-tRNA synthetase 2	mitochondrial
HARS2	histidyl-tRNA synthetase 2	mitochondrial
IARS2	isoleucyl-tRNA synthetase 2	mitochondrial
LARS2	leucyl-tRNA synthetase 2	mitochondrial
MARS2	methionyl-tRNA synthetase 2	mitochondrial
NARS2	asparaginyl-tRNA synthetase 2	mitochondrial
PARS2	prolyl-tRNA synthetase 2	mitochondrial
RARS2	arginyl-tRNA synthetase 2	mitochondrial
SARS2	seryl-tRNA synthetase 2	mitochondrial
TARS2	threonyl-tRNA synthetase 2	mitochondrial
VARS2	valyl-tRNA synthetase 2	mitochondrial
WARS2	tryptophanyl-tRNA synthetase 2	mitochondrial
YARS2	tyrosyl-tRNA synthetase 2	mitochondrial
GARS	glycyl-tRNA synthetase	bifunctional
KARS	lysyl-tRNA synthetase	bifunctional
QARS	glutamyl-tRNA synthetase	bifunctional

transfer editing, occurring after the amino-acid is transferred onto the tRNA (Fersht, 1977). The first "course sieve" excludes amino-acids larger than the cognate amino-acid at the amino-acid activation site (Baldwin and Berg, 1966; Fersht, 1977). The second "fine sieve" targets incorrectly charged tRNA molecules for hydrolysis (Eldred and Schimmel, 1972). Several ARS enzymes contain internal editing domains that participate in fine sieve editing and hydrolysis and thereby ensure fidelity of aminoacyl-tRNA formation.

Throughout evolution, several ARS enzymes have acquired secondary, non-canonical functions (Table 1.3) (Andreev *et al.*, 2012; Arif *et al.*, 2009; Ko *et al.*, 2000; Ko *et al.*, 2001; Lee *et al.*, 2004; Otani *et al.*, 2002; Park *et al.*, 2012; Park *et al.*, 2005; Stark and Hay, 1998; Wakasugi and Schimmel, 1999a, b; Wakasugi *et al.*, 2002). Three ARS enzymes have been shown to participate in transcriptional or translational regulation: glutamyl-prolyl-tRNA synthetase (EPRS) is a part of the gamma-interferon-activated inhibitor of translation complex, GARS participates in internal ribosome entry site (IRES) initiation in polio virus, and KARS suppresses microphthalmia transcription factor (MITF) transcriptional activity (Andreev *et al.*, 2012; Arif *et al.*, 2009; Lee *et al.*, 2004). In addition, several ARS enzymes are involved in the immune response. For example, GARS participates in the adaptive immunity against tumor initiation, KARS serves as a pro-inflammatory cytokine, tryptophanyl-tRNA synthetase (WARS) serves as an angiostatic cytokine, and YARS serves as an angiogenic cytokine (Otani *et al.*, 2002; Park *et al.*, 2012; Park *et al.*, 2005; Wakasugi and Schimmel, 1999a, b; Wakasugi *et al.*, 2002).

Table 1.3 Human Non-Canonical ARS Functions

Gene Name	Non-canonical Function	Reference
EPRS	translational silencing	Arif *et al.*, 2009
GARS	immune response	Park *et al.*, 2012
GARS	translational initiation	Andreev *et al.*, 2012
KARS	transcriptional regulation	Lee *et al.*, 2004
KARS	HIV virion packaging	Stark *et al.*, 1998
KARS	inflammatory cytokine	Park *et al.*, 2005
MARS	rRNA biogenesis	Ko *et al.*, 2000
QARS	apoptotic inhibition	Ko *et al.*, 2001
WARS	angiostatic cytokine	Otani *et al.*, 2002; Wakasugi *et al.*, 2002
YARS	angiogenic cyotkine	Wakasugi *et al.*, 1999a; Wakasugi *et al.*, 1999b
YARS	immune response	Wakasugi *et al.*, 1999b

Interestingly, despite the essential nature of ARS enzymes for all cell types, mutations in three genes encoding an ARS enzyme have been implicated in CMT disease with an axonal pathogenesis including: glycyl-tRNA synthetase (*GARS*) in patients with CMT2D, tyrosyl-tRNA synthetase (*YARS*) in patients with CMTDIC, and alanyl-tRNA synthetase (*AARS*) in patients with CMT2N (Antonellis *et al.*, 2003; Jordanova *et al.*, 2006; Latour *et al.*, 2010).

Missense mutations were first reported in the *GARS* gene in four families with dominant axonal CMT2D or distal spinal muscular atrophy type V (dSMA-V) (Antonellis *et al.*, 2003). CMT2D and dSMA-V are characterized by pronounced muscle weakness and wasting in the upper extremities and is distinguished by distal sensory loss in patients with CMT2D that is not observed in patients with dSMA-V.

CMTDIC is an intermediate form of CMT characterized by MNCVs in the intermediate range (25-45 m/s) and the presence of both demyelinating and axonal features upon histological evaluation (Nicholson and Myers, 2006). An insertion and two missense *YARS* mutations have been identified in three families with CMTDIC (Jordanova *et al.*, 2006).

Finally, a single missense *AARS* mutation was identified in two French families with CMT2N (Latour *et al.*, 2010). CMT2N encompasses classical CMT features including distal muscle weakness and wasting that is more pronounced in the lower extremities.

While mutations in genes encoding bifunctional or cytoplasmic-specific ARS enzymes have been implicated in dominant CMT disease, mutations in genes encoding mitochondrial-specific ARS enzymes have been implicated in an array of recessive diseases with diverse clinical manifestations (Table 1.4). Two of these diseases lack neuronal involvement: missense mutations in the mitochondrial seryl-tRNA synthetase (*SARS2*) gene lead to hyperuricemia, pulmonary hypertension, renal failure, and alkalosis (HUPRA) syndrome, while missense mutations in the mitochondrial tyrosyl-tRNA synthetase (*YARS2*) gene lead to myopathy, lactic acidosis, and sideroblastic anemia-2 (Belostotsky *et al.*, 2011; Pierce *et al.*, 2011). The three remaining mitochondrial ARS-related diseases encompass some form of neuronal involvement. Mutations in the mitochondrial histidyl-tRNA synthetase (*HARS2*) gene lead to Perrault syndome (Pierce *et al.*, 2011). Perrault syndrome is characterized by sensorineural deafness in affected males and females and ovarian dysgenesis in affected females. (Pierce *et al.*, 2011) Patients homozygous for mitochondrial arginyl-tRNA synthetase (*RARS2*) gene mutations display severe developmental delay and reduced cerebellar volume, a phenotype classified as pontocerebellar hypoplasia type 6 (PCH6) (Edvardson *et al.*, 2007). Finally, missense and nonsense mutations in the mitochondrial aspartyl-tRNA synthetase (*DARS2*) gene lead to leukoencephalopathy with brain stem and spinal cord involvement and lactate elevation (LBSL) (Scheper *et al.*, 2007). While LBSL does include peripheral nervous system involvement, none of the diseases associated with mitochondrial ARS mutations have fully recapitulated the CMT disease phenotype.

Table 1.4 Mitochondrial tRNA Synthetases Implicated in Human Disease

Gene	Disease	Symptoms[1]	Reference
DARS2	Leukoencephalopathy with brain stem and spinal cord involvement and lactate elevation	LE, MS, PNS, A, E, MR	Scheper, *et al.*, 2007
HARS2	Perrault syndrome	O, D, MR, CNS, PNS	Pierce *et al.*, 2011
RARS2	pontocerebellar hypoplasia type 6	MR, CNS	Edvardson *et al.*, 2007
SARS2	HUPRA syndrome	R, EA, P, H, D	Belostotsky *et al.*, 2011
YARS2	myopathy, lactic acidosis, and sideroblastic anemia-2	SA, L, M, LA	Pierce *et al.*, 2011

[1]LE (leukoencephalopathy); MS (muscle spasticity); A (ataxia); E (epilepsy); O (ovarian dysgenesis); D (sensorineural hearing loss); MR (mental retardation); CNS (central nervous system involvement); PNS (peripheral nervous system involvement); R (renal failure); EA (electrolyte abnormalities); P (pulmonary hypertension); H (hypotonia); D (delayed development); SA (sideroblastic anemia); L (lethargy); M (muscle weakness); LA (lactic acidemia)

Proposed Mechanisms of Aminoacyl-tRNA Synthetase-Related Peripheral Neuropathy

The exact mechanism by which *GARS, YARS*, and *AARS* mutations lead to an axonal peripheral neuropathy remains unclear. Here, I will outline the proposed disease mechanisms and review the culmination of data gleaned from previous functional studies on disease-associated *GARS* and *YARS* mutations. Several mechanisms of ARS-related peripheral neuropathy have been proposed: (1) impaired tRNA charging; (2) impaired ARS localization to PNS axons; (3) a toxic gain-of-function effect; (4) mitochondrial dysfunction; and (5) a loss of an undiscovered neuronal-specific secondary function (Figure 1.3) (Antonellis and Green, 2008; Motley *et al.*, 2010).

ARS enzymes supply the cell with an essential pool of charged tRNAs for use in protein translation. In the context of long, terminally differentiated neurons, impaired aminoacylation activity could lead to insufficient levels of proteins critical for axonal function and maintenance. Certain lines of evidence support an impaired tRNA charging mechanism for ARS-related peripheral neuropathy. First, functional assays evaluating the ability of mutant human GARS and YARS enzymes to catalyze the aminoacylation reaction *in vitro* revealed that five out of eight mutants tested display a reduction in aminoacylation activity (Froelich and First, 2011; Jordanova *et al.*, 2006; Nangle *et al.*, 2007; Storkebaum *et al.*, 2009; Xie *et al.*, 2007) (Table 1.5). Second, *in vivo* yeast genetic complementation assays determining the ability of human *GARS* and *YARS* mutants, modeled in the corresponding yeast orthologs (*GRS1* and *TYS1*, respectively), to rescue deletion of the endogenous yeast gene, revealed that six out of eight enzymes lead to

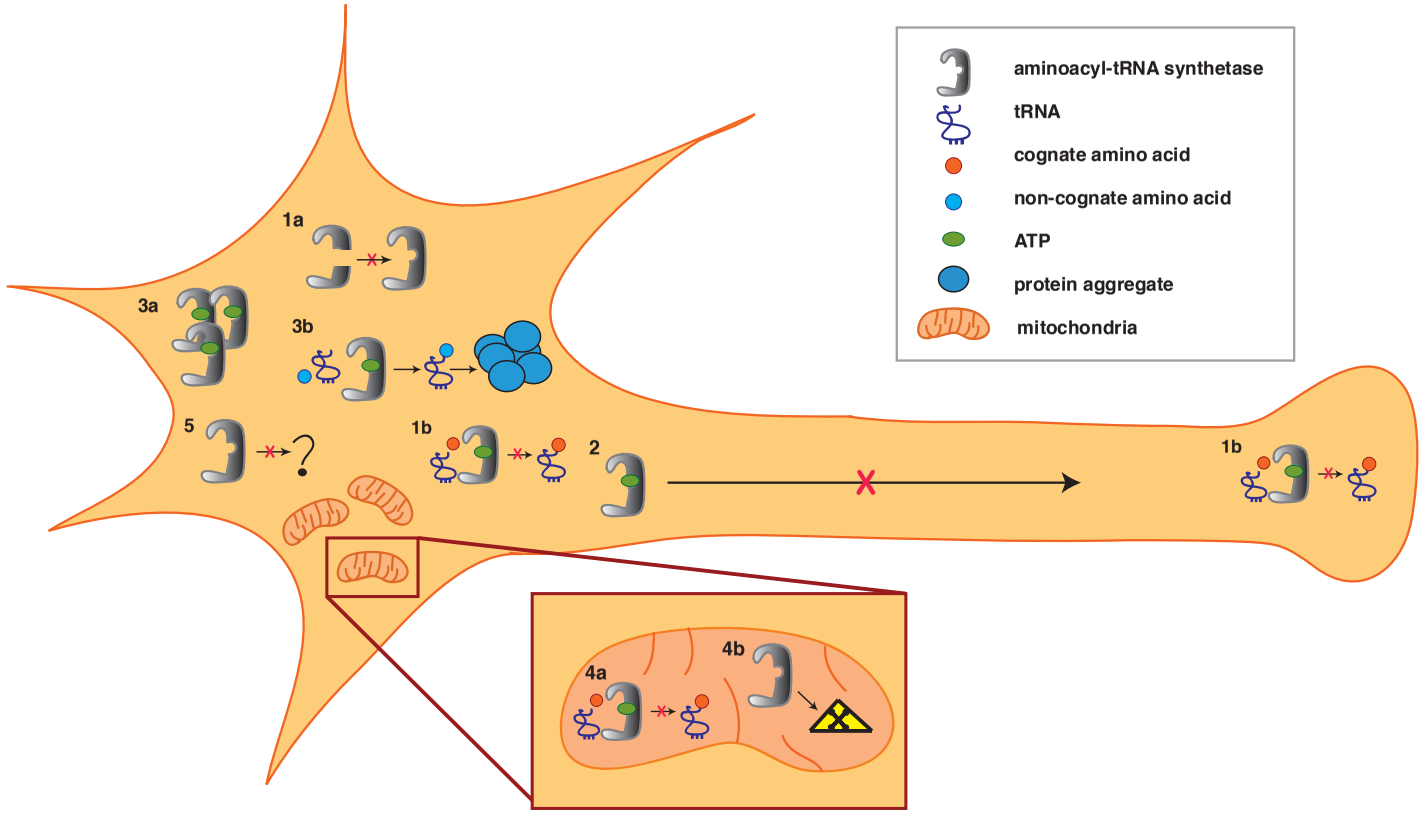

Figure 1.3 Proposed Mechanisms of Aminoacyl-tRNA Synthetase-Related Peripheral Neuropathy. A neuron is schematically depicted with a cell body on the left and an axon protruding to the right. Below, and enlarged segment of a mitochondrion is shown. Mutations in aminoacyl-tRNA synthetase may lead to a number of defects in the neuron including: (1a) defective ARS dimerization; (1b) impaired tRNA charging leading to aminoacyl-tRNA deficiency in the axon; (2) abnormal cellular localization or axonal transport of the mutant ARS; (3a) accumulation of mutant ARS enzymes; (3b) mis-acylation of tRNA resulting in misfolded protein aggregates; (4a) impaired tRNA charging in the mitochondria; (4b) mitochondrial toxicity; and (5) loss of neuronal-specific non-canonical ARS function(s).

Table 1.5 Loss-of-function Characteristics of Disease-Associated ARS Mutations

Gene	Variant	Biochemistry[1]	Yeast[1]	Localization[1]	Fly neurons[1]	References
GARS	E71G	N	N	N	Y	Nangle *et al*., 2007; Antonellis *et al*., 2006; Chihara *et al*. 2007,
GARS	L129P	Y	Y	Y	Y	Nangle *et al*., 2007; Antonellis *et al*., 2006; Chihara *et al*. 2007
GARS	G240R	Y	N	Y	UT	Nangle *et al*., 2007; Antonellis *et al*., 2006
GARS	H418R	UT	Y	Y	UT	Antonellis *et al*., 2006
GARS	D500N	N	UT	UT	UT	Nangle *et al*., 2007
GARS	G526R	Y	Y	Y	UT	Xie *et al*., 2007; Antonellis *et al*., 2006
YARS	G41R	Y	Y	Y	UT	Jordnanova *et al*., 2006, Storkebaum, *et al*., 2009, Froelich, *et al*., 2011
YARS	del153-156	Y	Y	UT	UT	Jordnanova *et al*., 2006, Storkebaum, *et al*., 2009
YARS	E196K	Y	Y	Y	UT	Jordnanova *et al*., 2006, Storkebaum, *et al*., 2009, Froelich, *et al*., 2011

[1] N (no loss-of-function affect detected); Y (loss-of-function effect present); UT (untested)

reduced yeast viability (Antonellis *et al.*, 2006; Jordanova *et al.*, 2006; Storkebaum *et al.*, 2009) (Table 1.5). Importantly, all of the *GARS* and *YARS* mutations identified to date have shown a loss-of-function effect in some capacity, with the exception of D500N *GARS*, which has only been evaluated with regard to aminoacylation capacity (Table 1.5). It is important to note that while many *GARS* and *YARS* mutations result in loss-of-function effects, aminoacylation and yeast genetic complementation assays are essentially testing the ability of mutants to function as a homodimer, without the presence of a wild-type subunit, and therefore cannot not provide a clear picture of what is happening in a patient heterozygous for *GARS* or *YARS* mutations. Data acquired from *Gars* mouse models argue against a model based solely upon loss of aminoacylation activity. $Gars^{XM256/+}$ mice, generated by inserting a gene-trap in the second intron of the *Gars* gene, have reduced GARS levels but remain phenotypically normal (Seburn *et al.*, 2006). Moreover, ubiquitous overexpression of wild-type human *GARS* in a dominant mouse model of CMT2D does not rescue aminoacylation defects or axonal loss in affected mice (Motley *et al.*, 2011). Together, these data argue against a pure haploinsufficiency model and suggest other mechanisms might be contributing to ARS-related CMT disease.

Impaired localization or axonal transport of proteins important for neuronal function have been implicated in CMT disease and other neurodegenerative disorders (Jellinger, 2010; Niemann *et al.*, 2006). Localization patterns of endogenous and overexpressed forms of both wild-type and mutant GARS and YARS enzymes have been studied extensively. The localization of endogenous GARS was evaluated in a human neuroblastoma cell line (SH-SY5Y) and in human thoracic spinal cord and sural nerve tissue sections by staining

with an anti-GARS antibody. In differentiating SH-SY5Y cells, GARS forms granules in the nucleus, cell body, and neurite projections (Antonellis *et al.*, 2006). Interestingly, the same granules are present in the axons of the ventral horn, dorsal horn, ventral root, dorsal root, and in sural nerve tissue sections (Antonellis *et al.*, 2006). The localization of endogenous YARS was evaluated in SH-SY5Y cells, a mouse neuroblastoma cell line (N2a), and in primary embryonic mouse motor neurons. In differentiating SH-SY5Y and N2a cells, YARS shows granular staining in the growth cone, branch points, and distal portions of projecting neurons, a localization pattern referred to as a "teardrop effect" (Jordanova *et al.*, 2006). A similar localization pattern was identified in primary embryonic mouse motor neurons, where YARS was found to localize throughout the motor neuron and in projecting neurites (Jordanova *et al.*, 2006). Overexpression studies, monitoring the overexpression of EGFP-tagged GARS and YARS proteins, revealed that six out of seven mutant proteins are mislocalized when transiently expressed in MN-1 and N2a cells, respectively (Antonellis *et al.*, 2006; Jordanova *et al.*, 2006). Mislocalization of GARS or YARS enzymes may lead to impaired tRNA charging along the axon, or in the axon terminal, depriving the axon of critical neuronal proteins. Interestingly, tRNAs and ARS enzymes have been identified in the axoplasm of squid axons, mRNAs have been discovered in rat peripheral nerve axons, and ribosomes have been identified in goldfish axons (Black and Lasek, 1977; Koenig, 1979; Taylor *et al.*, 2009). Together, these data indicate that aminoacylation and protein translation likely occur in the periphery, and suggest ARS mutations could adversely affect local protein synthesis in peripheral nerve axons.

A gain-of-function mechanism, whereby mutant ARSs aggregate within the neuron or incorrect amino-acids are ligated onto non-cognate tRNAs resulting in protein aggregation, has also been proposed as a possible mode of ARS-related neuropathy (Antonellis and Green, 2008; Motley *et al.*, 2010). While overexpression of mutant ARS enzymes do not appear to lead to overt aggregation after several days in culture, it is difficult to determine if mutant ARS enzymes would accumulate *in vivo* after several decades of life. Protein aggregation as a result of mis-acylation seems unlikely, as ubiquitin-positive inclusions are absent in the spinal cord and cerebellum of $Gars^{P234KY/+}$ mice (Stum *et al.*, 2011). This is in stark contrast to the ubiquitin-positive inclusions identified in the cerebellum of $Aars^{sti/sti}$ mice homozygous for *Aars* editing-domain mutations that result in mis-incorporation of non-cognate amino-acids onto $tRNA^{Ala}$ (Lee *et al.*, 2006; Stum *et al.*, 2011). Moreover, the phenotype of $Aars^{sti/sti}$ mice differs to that of $Gars^{P234KY/+}$ mice; whereas $Aars^{sti/sti}$ mice display cerebellar Purkinje cell loss and ataxia, $Gars^{P234KY/+}$ mice display abnormal neuromuscular junction morphology and loss of large diameter axons, a phenotype consistent with peripheral neuropathy (Lee *et al.*, 2006; Seburn *et al.*, 2006). Together, these data argue against mis-charging as a disease mechanism for ARS-related peripheral neuropathy. Other gain-of-function mechanisms remain to be fully evaluated. For example, mutant ARSs may shunt the aminoacylation reaction to produce diadenosine tetraphosphate (Ap4A), instead of aminoacyl-tRNA, or mutant ARS enzymes could indiscriminately bind to other cellular RNAs, leading to aberrant RNA stabilization, splicing, and/or transport. Other gain-of-function possibilities will be further explored in Chapter 5.

As reviewed above, impaired mitochondrial function has been implicated in CMT disease. It is possible that ARS mutations are toxic to mitochondria or result in impaired mitochondrial tRNA charging. These events could lead to severe mitochondrial dysfunction resulting in decreased ATP synthesis in the neuron. While *YARS* and *AARS* encode enzymes that charge tRNAs in the cytoplasm, *GARS* encodes a bifunctional tRNA synthetase (Table 1.2). Functional studies utilizing the *Drosophila* olfactory system as a model for dendritic and axonal terminal arborization demonstrate that cytoplasmic ARS mutants lead to arborization defects, while a mitochondrial ARS mutants lack an overt arborization phenotype (Chihara *et al.*, 2007). These data suggest that disruption of cytoplasm-specific aminoacyl-tRNA synthesis leads to CMT disease. As reviewed above, mutations in mitochondrial-specific aminoacyl-tRNA synthetases have been implicated in an array of diseases with widespread manifestations, however none have fully recapitulated a phenotype resembling CMT disease (Table 1.4).

Several tRNA synthetases have acquired secondary, non-canonical functions (Table 1.3) (Andreev *et al.*, 2012; Arif *et al.*, 2009; Ko *et al.*, 2000; Ko *et al.*, 2001; Lee *et al.*, 2004; Otani *et al.*, 2002; Park *et al.*, 2012; Park *et al.*, 2005; Stark and Hay, 1998; Wakasugi and Schimmel, 1999a, b; Wakasugi *et al.*, 2002). It is possible that CMT-associated ARS enzymes possess neuron-specific secondary functions and that disruption of these functions leads to CMT disease. For example *AARS*, *GARS*, and *YARS* could be involved in the transcriptional or translational control of genes important for neuronal function, analogous to the non-canonical functions associated with *KARS* and *EPRS* (Arif *et al.*, 2009; Lee *et al.*, 2004). Alternatively, ARS enzymes could regulate neuronal signaling,

similar to the cytokine activity described for *KARS, YARS,* and *WARS* (Otani *et al.*, 2002; Park *et al.*, 2005; Wakasugi and Schimmel, 1999a, b; Wakasugi *et al.*, 2002). Finally, it is possible that ARSs provide support in response to neuronal stressors in the form of inflammatory signaling, immune response, and apoptotic inhibition as described for *KARS, YARS*, and glutamyl-tRNA synthetase (*QARS*), respectively (Ko *et al.*, 2001; Park *et al.*, 2005; Wakasugi and Schimmel, 1999b). The fact that multiple ARSs have been associated with CMT disease suggests that deficient tRNA charging is the central component to CMT disease pathology. However, it is possible that CMT-associated ARS enzymes share similar, neuronal-specific, secondary functions.

While CMT disease is the most common inherited neurodegenerative disorder, our understanding of the genes mutated in patients with CMT disease and the mechanism by which these mutations lead to peripheral neuropathy remains incomplete. My thesis aims to improve our understanding of the genetic and functional mechanisms by which ARS mutations lead to disease by genetically validating and functionally characterizing ARS gene mutations in patients with CMT disease. These aims will be achieved through a combination of genetic and functional studies. First we will genetically validate each mutation using patient re-sequencing, healthy control screening, and conservation analyses. Next, we will evaluate the effect of each ARS mutation on tRNA charging function using aminoacylation analysis and yeast viability assays. Finally, we will create and validate a *C. elegans* model system for assessing the toxic effects of mutant ARS enzymes in neurons. Together, these studies will provide a platform for further investigating the molecular pathology of ARS-related CMT disease.

CHAPTER 2

Identification and Validation of Aminoacyl-tRNA Synthetase Mutations in Patients with Charcot-Marie-Tooth Disease

The data presented in this chapter were previously published in *The American Journal of Human Genetics* (Volume 87, Issue 4) and in *Human Mutation* (Volume 33, Issue 1) (McLaughlin *et al.*, 2012; McLaughlin *et al.*, 2010). All figures and tables are used with permission from Elsevier (License No. 2827080090840) and John Wiley and Sons (License No. 2822181011090). I performed all of the work presented with three exceptions. First, Garth Nicholson and Jim Lupski performed all clinical examinations and patient sample collections for the *AARS* and *KARS* studies, respectively. Second, the National Institutes of Health Intramural Sequencing Center (NISC) performed the resequencing of 37 ARS genes in the 355 patient samples. Finally, the University of Michigan DNA Sequencing Core performed all DNA sequencing reactions.

Introduction

Disease-associated mutations in three ARS genes have been implicated in CMT disease: glycyl-tRNA synthetase (*GARS*), tyrosyl-tRNA synthetase (*YARS*), and alanyl-tRNA synthetase (*AARS*) (Antonellis *et al.*, 2003; Jordanova *et al.*, 2006; Latour *et al.*, 2010). To investigate the full extent of involvement of ARS genes in peripheral neuropathy, we sought to determine if mutations in additional ARS genes could lead to CMT disease.

Therefore, we analyzed data from a previous mutation analysis performed by resequencing all 37 ARS genes on deoxyribonucleic acid (DNA) samples from a total of 355 patients with CMT disease and no known disease-causing mutation. The identification of additional ARS loci and alleles will: (1) broaden our understanding of the types of ARS genes involved in CMT disease and the cell compartments that are affected (*i.e.,* cytoplasm, mitochondria, or both); (2) provide a thorough categorization of the types of ARS mutations involved in CMT disease (missense, nonsense, etc.); and (3) allow for the additional functional characterization of ARS mutations implicated in CMT disease in an effort to better understand CMT disease mechanisms.This chapter focuses on the genetic validation of variants identified in the alanyl-tRNA synthetase (*AARS*) and lysyl-tRNA synthetase (*KARS*) genes through sequence confirmation, segregation analysis, healthy control screening, and conservation analysis. Based upon data obtained from previous studies evaluating disease-associated *GARS*, *YARS*, and *AARS* mutations, we expect disease-associated ARS mutations to segregate with disease in affected pedigrees, be absent from DNA samples obtained from neurologically normal control populations, and affect highly-conserved amino-acid residues (Antonellis *et al.*, 2003; Jordanova *et al.*, 2006; Latour *et al.*, 2010).

Materials and Methods

Patient Sample Collection

All patient samples were obtained by collaborating physicians after patients were classified as being affected with either CMT disease or a motor neuronopathy, based upon neurological exam. Institutional Review Boards of each participating institution approved the genetic studies and informed consent was obtained from all patients.

DNA Sequencing

A genomic DNA aliquot from each patient was diluted to a working concentration of 10 ng/µl using a NanoDrop 1000. Polymerase chain reaction (PCR) primers were designed to amplify each *AARS* and *KARS* coding exon, as well as at least 20 base pairs of the surrounding introns (Appendix A1). PCR reactions containing 1X PCR supermix (Invitrogen, Grand Island, NY), 200 nM of each primer, and 20 ng of patient DNA using the following touchdown PCR cycling conditions: 96°C for 5 min, followed by 10 cycles of 96°C for 15 sec, 55°C (-0.5°C each cycle) for 15 sec, 72°C for 40 sec, followed by 30 cycles of 96°C for 15 sec, 50°C for 15 sec, 72°C for 40 sec, then a final extension of 72°C for 7 min, and finally a hold at 4°C. A 5-µl aliquot of each PCR reaction was separated on a 1% agarose gel stained with ethidium bromide and visualized to ensure correct product length. The PCR products were purified using the QIAquick PCR purification kit (Qiagen, Valencia, CA), diluted to 50 ng/µl, and sent to the University of Michigan DNA Sequencing Core along with 1 pMol/µl forward primer.

Mutation Analysis

Sanger ABI sequence traces were downloaded directly from the University of Michigan DNA Sequencing Core server. All sequences generated from a given pair of PCR primers were aligned using Sequencher software (Gene Codes, Ann Arbor, MI). The resulting contigs were analyzed by visual inspection to confirm or invalidate each mutation for all probands studied.

Comparative Sequence Analysis

To perform comparative protein sequence analysis, we first employed the NCBI BLAST tool (http://blast.ncbi.nlm.nih.gov/Blast.cgi) to collect AARS and KARS protein orthologs from species indicated below. Amino-acid sequences for AARS were derived from the following accession numbers: human (*Homo sapiens,* NP_001596.2), chimpanzee (*Pan troglodytes,* XP_001169474.1), mouse (*Mus musculus,* NP_666329.2), frog (*Xenopus laevis,* NP_001121342.1), zebrafish (*Danio rerio,* NP_001037775.1), fruit fly (*Drosophila melanogaster,* NP_523511.2), baker's yeast (*Saccharomyces cerevisiae*, NP_014980.1), and bacteria (*Escherichia coli IAI39,* YP_002408816.1). Amino-acid sequences for KARS were derived from the following accession numbers: human (*Homo sapiens*, NP_00112356), chimpanzee (*Pan troglodytes*, XP_511115.2), mouse (*Mus musculus*, NP_444322), zebrafish (*Danio rerio*, NP_001002386), fruitfly (*Drosophila melanogaster*, NP_572573), worm (*Caenorhabditis elegans*, NP_495454), baker's yeast (*Saccharomyces cerevisiae*, NP_010322), and bacteria (*Escherichia sp. 1_1_43*, ZP_0487121). Multiple-species amino-acid sequence alignments were then generated using Clustal W2 software (Larkin *et al.*, 2007). The conservation of each affected amino-acid was determined via visual inspection.

NINDS Control Genotyping

A total of 576 DNA samples isolated from neurologically normal controls were obtained from the National Institute of Neurological Disease (NINDS) and Coriell Institute for Medical Research (Camden, NJ; Panel numbers NDPT079, NDPT082, NDPT084, NDPT090, NDPT093, and NDPT094) and genotyped for each *AARS* and *KARS* variant

using MassARRAY® iPLEX® Gold technology (Sequenom, San Diego, CA). DNA samples were diluted to 5 ng/μl and multiplex locus-specific PCR reactions were performed using primers designed by Sequenom's MassARRAY Designer software (Appendix A2). Locus-specific PCR products were treated with shrimp alkaline phosphatase (SAP) to dephosphorylate unincorporated deoxyribonucleotide triphosphates (dNTPs) (Sequenom, San Diego, CA). Subsequently, primer-extension PCR reactions were performed using mass-modified dideoxynucleotide terminators (Appendix A3). Matrix-assisted laser desorption/ionization time-of-flight (MALDI-TOF) mass spectrometery was used to determine the genotype for each control sample using SpectroTYPER software (Sequenom, Camden, NJ). Each NINDS control sample that tested positive for an *AARS* or *KARS* variant was confirmed by re-sequencing, as described above.

AARS Locus Haplotype Analysis

Microsatellite markers D16S3050, D16S397 and D16S3106 were genotyped for CMT243 and three CEPH Controls: 102-1, 1331-1, and 1332-1 (Coriell Institute for Medical Research, Camden, NJ) using primer sequences obtained from the UCSC genome browser (http://genome.ucsc.edu/cgi-bin/hgGateway) (Appendix A4). The forward primers were 5' labeled with the 6-FAM fluorochrome. Microsatellite markers were amplified in 25-μl PCR reactions containing 10ng DNA, 1X Phusion HF Reaction Buffer, 0.5 uM primers, 200 uM dNTPs, and 1U Phusion High-Fidelity DNA Polymerase (New England Biolabs, Ipswich, MA). The following PCR cycling conditions were used: 98°C for 30 sec, followed by 30 cycles of 98°C for 7 sec, 61°C for 30 sec, 72°C for 5 sec,

then 72°C for 7 min and finally, a hold at 4°C. The products were sent to the University of Michigan DNA Sequencing core (Ann Arbor, MI) for size fractionation using the GeneScan LIZ 500 size standard (Applied Biosystems, Carlsbad, CA). Genotypes were analyzed using GeneMarker version 5.1 software (SoftGenetics LLC, State College, PA).

CpG Content Evaluation

The CpG dinucleotide content of the *AARS* locus (GenBank accession number NM_001605.2) was evaluated using EMBOSS CpG Plot (http://www.ebi.ac.uk/Tools/emboss/cpgplot/) (Rice, *et al.*, 2000) using the following criteria: Observed/Expected ratio > 0.60, percent G + percent C > 50.00, and Length >100.

Sodium Bisulfite Sequencing

Two 2μg samples of genomic DNA isolated from lymphoblasts from unaffected individuals were treated with sodium bisulfite using the EpiTect Bisulfite Kit, according to the manufacturer's protocol (Qiagen, Valencia, CA). Bisulfite-conversion was performed using the following thermocycler conditions: 95°C for 5 min, 60°C for 25 min, 95°C for 5 min, 60°C for 85 min, 95°C for 5 min, 60°C for 175 min, and a hold at 4°C. Bisulfite-treated DNA was bound to the membrane of an EpiTect spin column, washed, desulfonated, washed, and eluted. Sodium bisulfite-treated DNA was amplified in 25-μl PCR reactions containing 10 μg DNA, 1X JumpStart PCR buffer, 0.5 uM primers, 200 uM dNTPs, and 0.05 U JumpStart Taq DNA polymerase (Sigma Aldrich, St. Louis, MO) using PCR primers compatible with sodium bisulfite-converted sequences for *AARS*

exons 7, 8, and 9, and *SOX3* Exon1 (Appendix A5). PCR products were electrophoresed through a 1% agarose gel stained with ethidium bromide. Subsequently, PCR products were excised from the gel and DNA was isolated using the QIAquick Gel Extraction Kit (Qiagen, Valencia, CA) according to the manufacturer's protocol. Amplicons were cloned into the pCR4-TOPO TA vector using the TOPO TA Cloning Kit for Sequencing (Invitrogen, Carlsbad, CA). Twenty resulting clones from each control DNA sample were selected for sequencing at each locus. Bisulfite sequencing data was analyzed using Sequencher 4.8 DNA Sequence Assembly software (Gene Codes, Ann Arbor, MI) and BiQ Analyzer software (Bock, *et al.*, 2005).

Allele Analysis for BAB564

A ~3.7 kb fragment spanning the c.398T>A (L133H) and c.524_525insTT (Y173SfsX7) *KARS* variants was amplified using genomic DNA from patient BAB564. The fragment was amplified in a 50-µl reaction containing 20 µg DNA, 1X Expand High FidelityPLUS PCR buffer, 0.5 uM primers, 200 uM dNTPs, and 2.5U Expand High FidelityPLUS polymerase enzyme (Roche, Madison, WI) using the following cycling parameters: 95°C for 2 min, followed by 30 cycles of 95°C for 15 sec, 55°C for 30 sec, 68°C for 4.5 min, then hold at 4°C. The resulting fragment was TA cloned into the pCR®2.1-TOPO vector using the TOPO-TA Cloning kit (Invitrogen, Carlsbad, CA) according to the manufacturer's directions. Ten clones containing the amplified fragment were subjected to DNA sequencing analysis with the resulting data analyzed using Sequencher 4.8 DNA Sequence Assembly software (Gene Codes, Ann Arbor, MI). Four alleles containing the L133H allele were identified, while the other six alleles contained Y173SfsX7. Codon

numbering for KARS was based upon the reported amino-acid sequence (GenBank accession numbers NM_001130089 and NP_00112356).

Results

Identification of Ten AARS and KARS Variants

Resequencing of the coding regions in 37 ARS genes has led to the discovery of a total of 144 variants in 28 ARS genes (data not shown). This thesis will focus on variants identified in the *AARS* and *KARS* genes. A total of 12 *AARS* and *KARS* variants were initially discovered upon resequencing the patient cohort (Table 2.1). We first sought to determine if these variants were indeed present in the patient samples, or if these variants represent erroneous sequencing calls. To validate each variant, we resequenced patient DNA samples in which *AARS* or *KARS* nucleotide variants were identified using primers corresponding to the exon in which each mutation resides. These efforts confirmed 10 of the 12 sequence variants (Table 2.1). These consisted of six *AARS* variants including: c.986G>A which predicts p.Arg329His (R329H), c.1685C>T which predicts p.Thr562Ile (T562I), c.2185C>T which predicts p.Arg729Trp (R729W), c.2333A>C which predicts p.Glu778Ala (E778A), c.2791G>A which predicts p.Gly931Ser (G931S), and c.2900A>T which predicts p.Lys967Met (K967M). Additionally, we were able to confirm all four *KARS* variants including: c.398T>A which predicts p.Leu133His (L133H), c.524_525insTT which predicts p.Tyr173SerfsX7 (Y173SfsX7), c.906C>G which predicts p.Ile302Met (I302M), and c.1868C>T which predicts p.Thr623Ser (T623S).

Table 2.1 *AARS* and *KARS* Variants Identified in Patients with Peripheral Neuropathy

Gene	cDNA Change	Amino-Acid Change	Confirmed	dbSNP Accession No.[1]	ClinSeq™ Freq.[2]	NINDS Freq.[2]	EVS Freq.[2]	1000 Genomes[3]
AARS	c.439G>T	p.Glu147*	No	N/A	NT	NT	ND	ND
AARS	c.986G>A	p.Arg329His	Yes	N/A	0 / 802	0 / 1,086	ND	ND
AARS	c.1685C>T	p.Thr562Ile	Yes	rs148355156	4 / 802	8 / 1,088	62 / 10,696	D
AARS	c.1961A>T	p.Glu654Val	No	N/A	NT	NT	ND	ND
AARS	c.2185C>T	p.Arg729Trp	Yes	rs138081804	NT	2 / 1,090	7 / 10,751	D
AARS	c.2333A>C	p.Glu778Ala	Yes	N/A	0 / 802	0 / 954	ND	ND
AARS	c.2602G>C	p.Ala868Pro	No	N/A	NT	NT	ND	ND
AARS	c.2602G>A	p.Ala868Thr	No	N/A	NT	NT	ND	ND
AARS	c.2791G>A	p.Gly931Ser	Yes	rs149377346	12 / 802	11 / 1106	94 / 10,664	D
AARS	c.2900A>T	p.Lys967Met	Yes	rs35744709	NT	NT	116 / 10,642	D
KARS	c.398T>A	p.Leu133His	Yes	N/A	0 / 190	0 / 1,036	ND	ND
KARS	c.524_525insTT	p.Tyr173SerfsX7	Yes	N/A	0 / 190	0 / 1,098	ND	ND
KARS	c.906C>G	p.Ile302Met	Yes	rs146955132	0 / 190	0 / 1,094	3 / 10,755	D
KARS	c.1868C>T	p.Thr623Ser	Yes	rs6834	11 / 190	31 / 710	1,517 / 9,241	D

[1]N/A (not applicable)
[2]Frequency indicates number of chromosomes identified; NT (not tested); ND (not detected); D (detected)
[3]D (detected); ND (not detected)

Population Screening of AARS and KARS Variants

We next sought to determine if the *AARS* and *KARS* variants are present in general or control populations. We utilized two publically available databases, the Exome Variant Server (EVS) and the 1000 Genomes (1000G) database, along with data from the ClinSeq™ project, to assess for the presence of each variant in general worldwide populations (1000 Genomes Project Consortium; Biesecker *et al.*, 2009; Exome Variant Server). The ClinSeq™ project is a large-scale, whole-genome resequencing project aimed at achieving a better understanding of cardiovascular disease (Biesecker *et al.*, 2009). The National Institute of Neurological Disorders and Stroke (NINDS) neurologically normal control panels were used as a control population. The NINDS cohort contains samples from male and female individuals, 55-84 years of age, who have provided thorough medical and family histories with no reported neurological disease. The NINDS control panel is particularly useful for evaluating variants identified in patients with neurodegenerative disease, and the presence of a variant in a control population such as the NINDS panel would indicate the variant is a polymorphism, as opposed to a disease-associated variant.

Evaluation of the *AARS* variants revealed the R329H *AARS* and E778A *AARS* variants were not identified in 1,086 and 954 NINDS chromosomes tested, respectively. Neither variant was detected in the ClinSeq™ cohort or in the EVS and 1000G databases. Conversely, T562I *AARS* was detected in 8 out of 1,088 NINDS chromosomes (frequency= 0.0073), R729W *AARS* was detected in 2 out of 1,090 NINDS chromosomes (frequency= 0.0018), and G931S *AARS* was detected and 11 out of 1,106 NINDS

chromosomes (frequency= 0.0099) (Table 2.1). The K967M *AARS* variant is present in dbSNP (rs35744709). Each of the *AARS* variants found in the neurologically normal NINDS controls was also identified in the ClinSeq™ cohort and in the EVS and 1000G databases (Table 2.1). Together, these data indicate that R329H *AARS* and E778A *AARS* are not common polymorphisms.

Evaluation of the *KARS* variants revealed the L133H *KARS* variant was absent in 1,036 NINDS chromosomes tested, the Y173SfsX7 *KARS* variant was absent in 1,098 NINDS chromosomes tested, and the I302M *KARS* was absent in 1,094 NINDS chromosomes tested (Table 2.1). Each variant was also absent in the ClinSeq™ cohort, however, we did identify I302M *KARS* in the EVS (frequency= 0.0002) and 1000G databases. We identified the T623S *KARS* variant in both the NINDS and ClinSeq™ cohorts in 31 out of 710 (frequency= 0.0437), and 11 out of 190 (frequency= 0.0579) chromosomes tested, respectively. Together, these data indicate that L133H *KARS,* Y173SfsX7 *KARS*, and I302M *KARS* are not common polymorphisms.

Alanyl-tRNA Synthetase (AARS) Gene Mutations in Patients with CMT2N

The R329H *AARS* variant (c.986G>A) was identified in family CMT243, a large Australian kindred including nine individuals affected with autosomal dominant CMT disease (Fig. 2.1). The R329H *AARS* variant segregates with disease in all affected family members; while all nine affected family members carry the R329H *AARS* variant, the variant is absent in seven unaffected family members (maximum LOD score=2.41 at

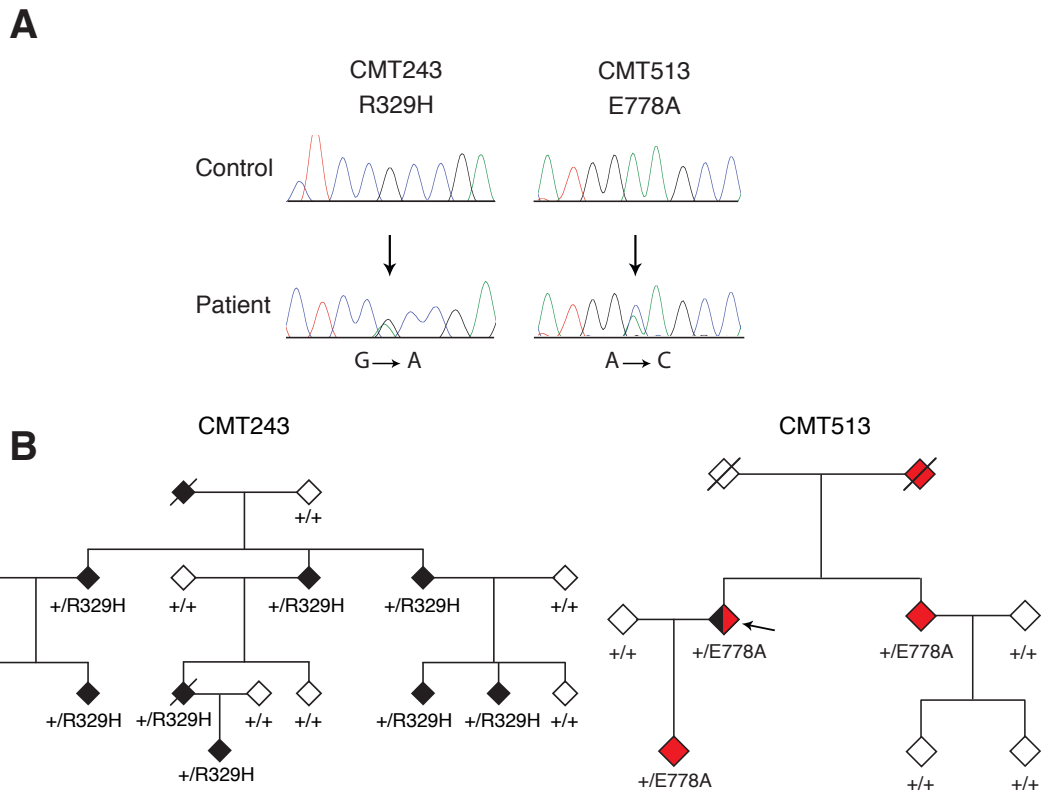

Figure 2.1 Validation and Segregation of *AARS* Variants. A: Chromatograms from control and affected ('Patient') individuals are shown for R329H (left) and E778A (right). The nucleotide changes for each mutation are depicted below the corresponding chromatogram. **B:** Genotyping was performed to determine the segregation of *AARS* variants with disease in families with CMT. Filled symbols represent affected individuals, with black indicating a diagnosis of CMT and red indicating a diagnosis of rippling muscles and cramps. Empty symbols indicate unaffected individuals. Where applicable, the individual's genotype is indicated with the amino-acid change or + (for a wild-type allele). Slashes indicate deceased individuals, the question mark indicates an unknown diagnosis, and the arrow indicates the proband in family CMT513. All individuals have been designated with a diamond symbol to protect identities.

θ=0). Affected individuals exhibited early-onset axonal neuropathy with variable sensorineural deafness. Progressive gait difficulty, foot drop, pes cavus, and hammer toes were also reported. Nerve conduction velocities were consistent with an intermediate CMT phenotype (classified as 25-45 m/s) and audiology showed mild to moderate high frequency sensory neural loss. Importantly, samples from affected individuals in CMT243 tested negative for mutations in other genes previously implicated in CMT disease, including *PMP22*, *MFN2, GDAP1*, and *EGR2*.

The E778A *AARS* variant (c.2333 A>C) was identified in CMT513, an Australian family including four members with autosomal dominant rippling muscles, and cramps (Fig 2.1). CMT513 also includes a proband affected with sporadic axonal CMT (Fig. 2.1; arrow). The E778A *AARS* variant segregates with rippling muscles, and cramps in all three affected family members, while the variant is absent in the remaining four unaffected family members genotyped. Affected individuals exhibited cramps at night with rippling and twitching muscles at rest. Conduction studies in the proband (Fig. 2.1B; arrow) showed a motor and sensory axonal neuropathy. Clinical examination revealed absent reflexes, wasting of the feet, and mild distal sensory loss in the lower limbs. DNA samples from affected CMT513 family members tested negative for *PMP22* gene mutations.

Rippling muscle disease, an autosomal dominant disorder characterized by mechanically triggered, electrically silent muscle contractions, is caused by missense mutations in the caveolin-3 (*CAV3*) gene (Betz *et al.*, 2001). Caveolins are expressed in skeletal and

smooth muscle tissue, glial cells, and peripheral nerves; and form flask-shaped invaginations of the plasma membrane (Lee *et al.*, 2008; Parton, 1996; Scherer *et al.*, 1996; Williams and Lisanti, 2004). Caveolins participate in the maintenance of plasma membrane integrity, vesicular trafficking, and in signal transduction pathways (Gazzerro *et al.*, 2010). We screened the proband from CMT513 for *CAV3* gene coding mutations by sequencing each *CAV3* coding exon. These analyses did not reveal any *CAV3* coding variants (data not shown). These data indicate that *CAV3* coding mutations are not responsible for the phenotype present in CMT513.

In addition to the above-mentioned variants, a third *AARS* variant [c.211A>T which predicts p.Asn71Tyr (N71Y)] was recently identified in a Taiwanese family with autosomal dominant axonal CMT disease (Lin *et al.*, 2011). The N71Y *AARS* variant segregates with CMT disease in all seven affected family members, while the variant is absent in three unaffected family members (data not shown). Thus, we also included N71Y *AARS* in our functional analyses (see Chapter 3).

R329H AARS is a Recurrent Allele

The R329H *AARS* variant has now been identified in three families with CMT disease; including the two French families identified by Latour, *et al.*, and the Australian family presented here (Latour *et al.*, 2010; McLaughlin *et al.*, 2012). These data suggest the R329H *AARS* variant is a recurrent mutation. We sought to determine whether the Australian family shares a haplotype with either of the two previously reported French families, which would indicate the R329H *AARS* mutation descended from a common

ancestor, or, if it is the result of multiple *de novo* mutations. We therefore performed haplotype analysis on individuals from family CMT243 using three microsatellite markers near the *AARS* locus: D16S3050, D16S397, and D16S3106. Importantly, these three microsatellite markers were previously evaluated in the two French families with R329H *AARS* mutations, allowing for a direct comparison of the three haplotypes. These studies revealed that each family carries different alleles at each marker tested indicating the R329H *AARS* mutation resides on three independent haplotypes in each of the three affected families, consistent with this variant resulting from multiple *de novo* mutations (Fig. 2.2A).

To assess the genetic mechanism of the recurrent R329H *AARS* mutation, we examined the DNA sequence surrounding the c.986 G>A *AARS* change. Interestingly, when the protein-coding DNA sequence is observed in the reverse-complemented state, the affected nucleotide (c.986G) is a cytosine within a CpG dinucleotide (Fig. 2.2B). It is estimated that ~80% of CpG cytosines are methylated to form 5-methylcytosine (5mC) in human cells (Ehrlich *et al.*, 1982). Importantly, 5mCs are known to be mutational "hotspots" that arise due to spontaneous deamination of 5mC to form thymine (Cooper and Youssoufian, 1988; Coulondre *et al.*, 1978; Selker and Stevens, 1985). If this event were to occur at the CpG dinucleotide indicated in Figure 2.2B, it would result in a c.986 G>A change on the opposite, coding strand of *AARS* exon 8, and would be predicted to result in an arginine to histidine change at amino acid position 329. To address this possibility, we evaluated the CpG dinucleotide content of the *AARS* locus using EMBOSS CpGPlot (Fig. 2.2C) (Rice *et al.*, 2000). In contrast to the remaining 19 *AARS*

Figure 2.2 R329H *AARS* is a Recurrent Mutation. A: Haplotype analysis was performed along chromosome 16 in family CMT243 and compared to the published data for the previously identified families with the R329H *AARS* mutation (Family 1 and Family 2). The three genotyped markers and *AARS* locus are indicated on the left, along with the alleles identified on each disease-associated haplotype (in base pairs). The distance between each locus is indicated in megabases (Mb). **B**: The codon affected by the R329H *AARS* variant harbors a CpG dinucleotide. A representative trace (in the reverse-complement orientation) of the region surrounding the R329H codon is shown. The CpG is indicated with a line and the affected cytosine is indicated with an arrow. **C**: The *AARS* locus was computationally evaluated for CpG dinucleotide content (see methods). Each *AARS* exon number is indicated along the top of the panel, with vertical white boxes representing coding exons and horizontal lines representing introns. Areas with at least 100 base pairs containing an observed/expected CpG dinucleotide ratio > 60% and GC content >50% are indicated in yellow. Note that *AARS* exon 8 is the only coding exon to meet these criteria. **D**: The methylation status of CpG dinucleotides in *AARS* exon 8 was evaluated via bisulfite ($NaHSO_3$) treated DNA sequencing analysis. The DNA sequence from ten representative clones harboring *AARS* exon 8 after bisulfite treatment are shown, with the genomic consensus sequence ('Genomic') provided along the top. Converted cytosines are indicated with black arrows and non-converted cytosines are indicated with red arrows. The CpG corresponding to R329H *AARS* is underlined. Note that all non-CpG cytosines are converted to thymines, while all CpG cytosines remain unchanged indicating that they are methylated. **E**: *AARS* exon 8 harbors multiple, methylated cytosines in CpG dinucleotides. A representation of bisulfite sequencing products of the seven CpGs (indicated along the top of the panel) residing in *AARS* exon 8 is shown for two control individuals (Control 1 and Control 2). Eighteen clones were analyzed for each control. Filled circles indicate methylated CpGs. The arrow indicates the affected CpG giving rise to R329H *AARS*.

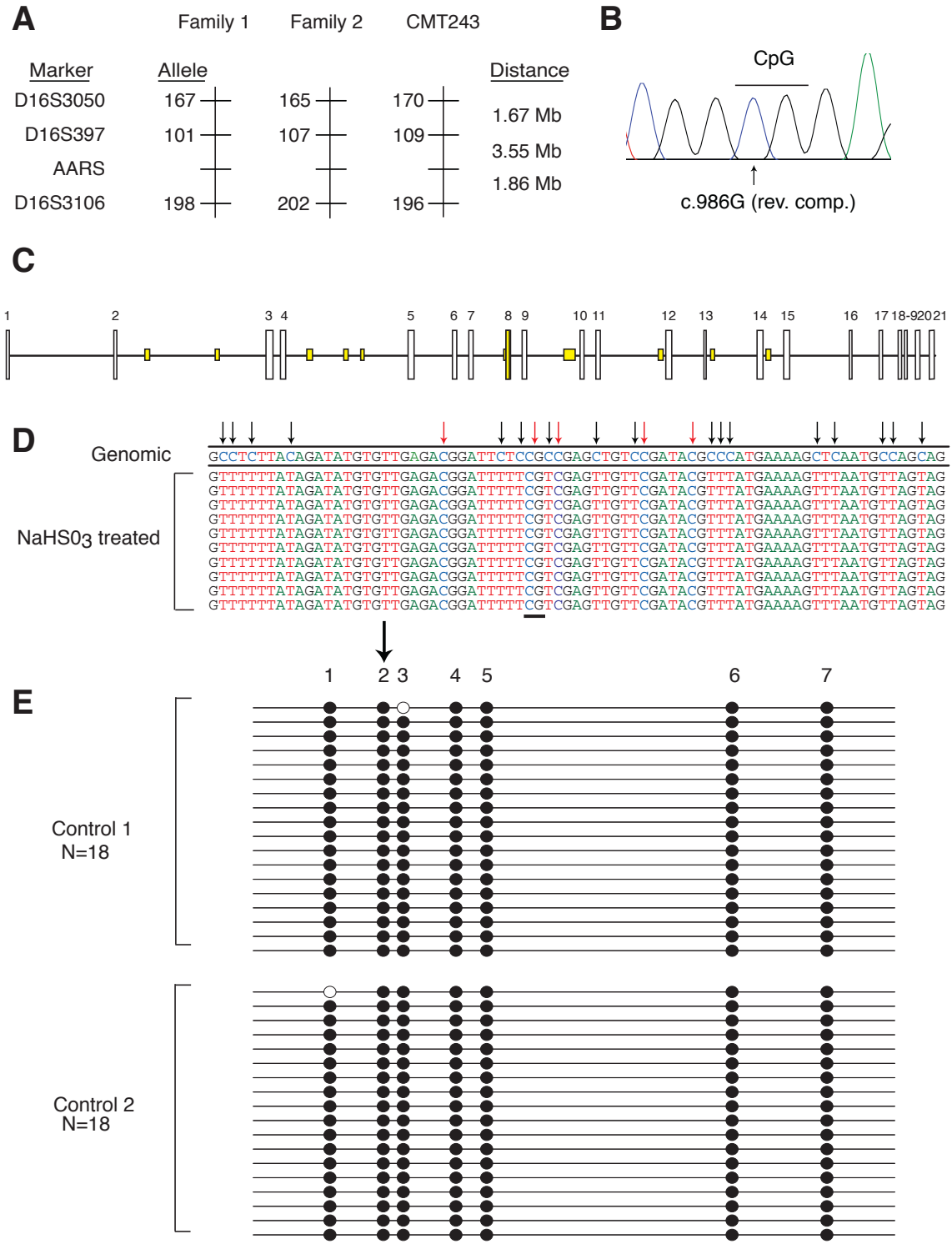
A
Family 1
Family 2
CMT243
Marker
Allele
Distance
D16S3050
D16S397
AARS
D16S3106
167
101
198
165
107
202
170
109
196
1.67 Mb
3.55 Mb
1.86 Mb
B
CpG
c.986G (rev. comp.)
C
1
2
3 4
5
6 7
8 9
10 11
12
13
14 15
16
17 18-9 20 21
D
Genomic
NaHS0$_3$ treated
GCCTCTTACAGATATGTGTTGAGACGGATTCTCCGCCGAGCTGTCCGATACGCCCATGAAAAGCTCAATGCCAGCAG
GTTTTTTATAGATATGTGTTGAGACGGATTTTTCGTCGAGTTGTTCGATACGTTTATGAAAAGTTTAATGTTAGTAG
E
1
2 3
4
5
6
7
Control 1
N=18
Control 2
N=18

coding exons, the exon encoding R329 (exon 8) has a an elevated CpG dinucleotide content (6.48%; Fig. 2.2C).

Sodium bisulfite DNA sequencing is a common approach to identify 5mCs in genomic DNA. Treatment of DNA with sodium bisulfite converts non-methylated cytosines to uracils, but leaves 5mCs unchanged (Frommer *et al.*, 1992). Sodium bisulfite-treated DNA can be amplified with strand-specific, bisulfite-specific primers flanking the region of interest, thereby leading to converted uracils being amplified as thymidines. After cloning and sequencing of amplified bisulfite-treated PCR products, methylated cytosines remain intact, while non-methylated cytosines appear as thymidines. To determine if the R329H *AARS* variant might be generated via methylation-mediated deamination of the identified CpG dinucleotide, we PCR-amplified the genomic region surrounding *AARS* exon 8 from two independent unaffected human DNA samples treated with sodium bisulfite. Subsequently, each DNA sample was subjected to TA-cloning, and eighteen resulting clones from each DNA sample were selected for DNA sequence analysis. Examination of the DNA sequencing data showed that >99% of non-CpG cytosines (Fig. 2.2D, black arrows) were converted to thymidine. In contrast, cytosines residing in CpG dinucleotides were largely unconverted and remained cytosines after sodium bisulfite treatment (Fig. 2.2D, red arrows). To predict the methylation status of each cytosine in *AARS* exon 8, the sequence data from each clone was analyzed with BiQ Analyzer software (Bock *et al.*, 2005). A total of 28 cytosines were analyzed, including 7 cytosines

residing in CpG dinucleotides. In 94% of the clones examined, all 7 CpG cytosines were methylated, including the mutated cytosine that gives rise to R329H *AARS* (Fig. 2.2E).

To ensure the validity of the above-mentioned data, we employed the BiQ Analyzer software to assess similar DNA sequencing data generated from PCR products encompassing *AARS* exon 7 and 9, as well as a third, unlinked and previously-characterized CpG island at the X-linked *SOX3* locus (Cotton *et al.*, 2009). More than 90% of the CpGs in *AARS* exon 7 are methylated, 11% of CpGs in *AARS* exon 9 are methylated, and the *SOX3* locus displayed the expected methylation patterns, with DNA isolated from a female individual containing higher levels of methylation than DNA isolated from a male individual (Fig. 2.3).

Because all of the CpGs contained within *AARS* exon 8 appear to be highly methlyated, we predicted the consequences of deamination of each 5mC within *AARS* exon 8 to determine if C>T transitions could give rise to additional pathogenic amino-acid changes. Because the transition could occur on either stand, there are 14 possible deamination consequences. Of these, 11 are predicted to affect the AARS amino-acid sequence, including 2 that would result in a stop codon (Table 2.2). Combined, these data support the notion that R329H *AARS* is a recurrent mutation generated via 5mC deamination of a CpG dinucleotide on the non-coding DNA strand at the *AARS* locus. Furthermore, *AARS* exon 8 is predicted to be a highly mutable region with potentially detrimental consequences, and should be closely scrutinized for mutations in patients with dominant axonal CMT.

Figure 2.3 Bisulfite Sequencing Analysis of *AARS* Exon 7, *AARS* Exon 9, and *SOX3* Exon 1. **A**: Evaluation of the methylation status of 5 CpGs in *AARS* exon 7. A representation of bisulfite sequencing products of *AARS* exon 7 is shown for two control individuals (Control 1 and Control 2). Seventeen and eighteen clones were analyzed for Control 1 and Control 2, respectively. Filled circles indicate methylated CpGs. **B**: Similar analyses as described in (**A**) for two CpG dinucleotides within *AARS* Exon 9. Eighteen and nineteen clones were evaluated for Control 1 and Control 2, respectively. **C**: Evaluation of the methylation status of 19 CpGs in a *SOX3* CpG island. The female control (19 clones evaluated) is denoted ♀, while the male control (18 clones evaluated) is denoted ♂.

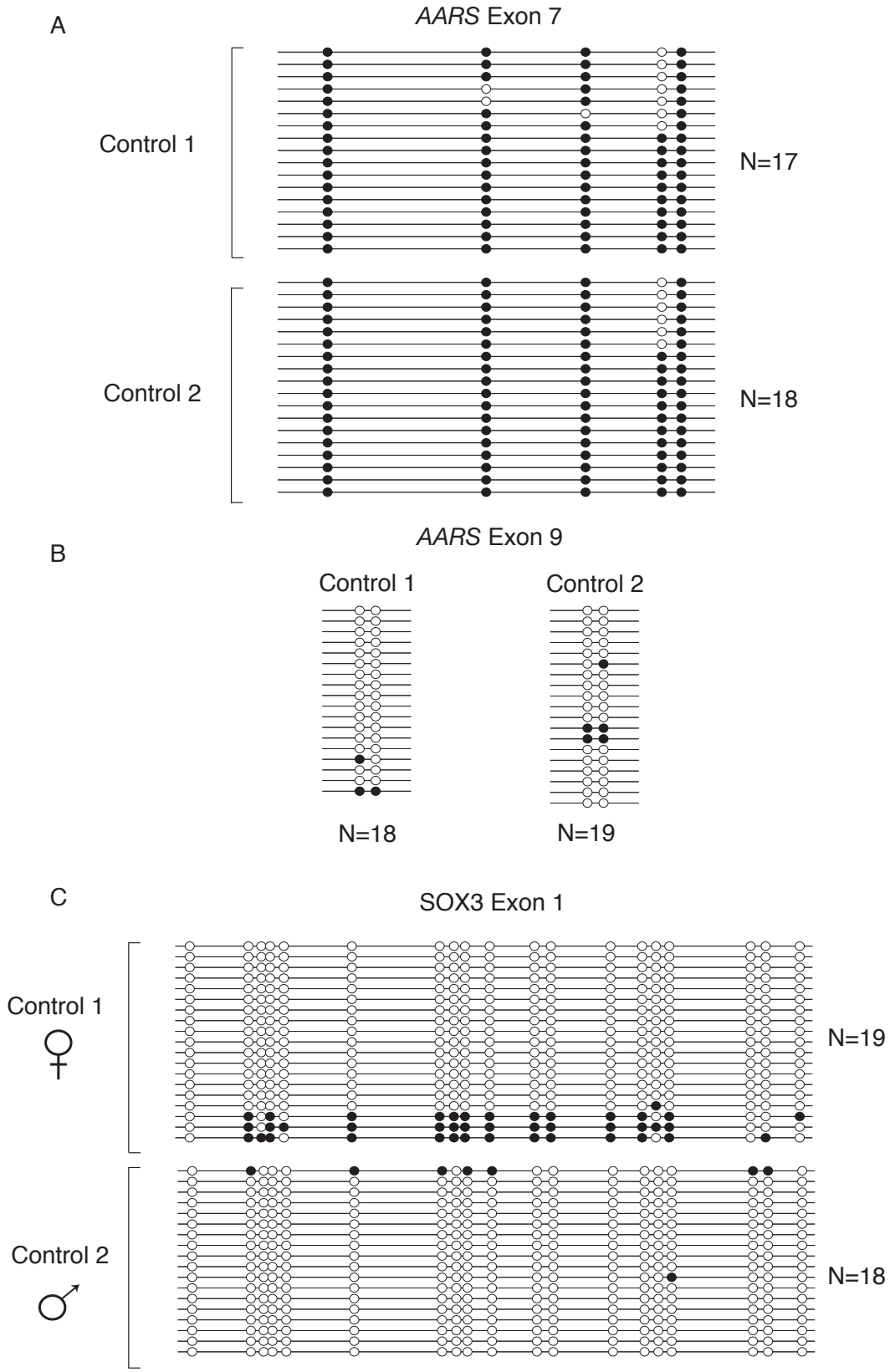
A
AARS Exon 7
Control 1
N=17
Control 2
N=18
B
AARS Exon 9
Control 1
Control 2
N=18
N=19
C
SOX3 Exon 1
Control 1
♀
N=19
Control 2
♂
N=18

Table 2.2 Predicted Consequences for Deaminated Methyl-CpGs in *AARS* Exon 8

CpG[a]	Affected Amino Acid	Predicted Change[d]
1[b]	R326	W
1[c]	R326	Q
2[b]	R329	C
2[c]	R329	H
3[b]	R330	Stop
3[c]	R330	Q
4[b]	R333	Stop
4[c]	R333	Q
5[c]	A335	T
6[b]	T348	M
7[c]	V354	I

[a]Numbers refer to the annotations presented in Figure 2.2E.
[b]CpG on coding strand
[c]CpG on non-coding strand

Lysyl-tRNA Synthetase (KARS) Gene Mutations in a Single Patient with CMTRIB

The I302M *KARS* variant (c.906C>G) was identified in the heterozygous state in patient BAB663 (Fig. 2.4A; BAB663). This patient's pedigree indicates an apparent autosomal dominant mode of inheritance (Fig. 2.4B; BAB663). Electrophysiological studies revealed that BAB663 exhibited normal motor nerve conduction velocities (MNCVs) in all nerves tested, accompanied by normal amplitudes of evoked nerve response (6 mV, 7mV, 8mV, 11mV, 7 mV, and 4mV in the left median, left ulnar, right median, right ulnar, left peroneal, and left post tibial nerves, respectively). Distal motor latencies were prolonged (7.2 ms in the right and left median nerve, 3.6 ms in the left ulnar nerve, 4.2 ms in the left ulnar nerve, 7.6 ms in the left peroneal nerve, and 5.8 ms in the left tibial nerve). Thus, this patient has a phenotype consistent with hereditary neuropathy with liability to pressure palsies (HNPP) (Li *et al.*, 2002). Interestingly, patient BAB663 also carries a heterozygous p.Arg238His mutation in the *GJB1* gene and the 1.4 Mb *PMP22* deletion. The *GJB1* variant and the *PMP22* deletion have previously been reported as pathogenic in CMTX1 and HNPP, respectively (Chance *et al.*, 1993; Nelis *et al.*, 1997). Given the HNPP diagnosis, the *PMP22* deletion should be considered the primary causal variant in BAB663, thereby decreasing the likelihood that the I302M *KARS* variant is associated with disease.

Two additional *KARS* variants, L133H and Y173SfsX7, were identified in a single patient with intermediate CMT, developmental delay, self-abusive behavior, dysmorphic features, and a vestibular Schwannoma (Fig. 2.4; BAB564). Patient BAB564 exhibited

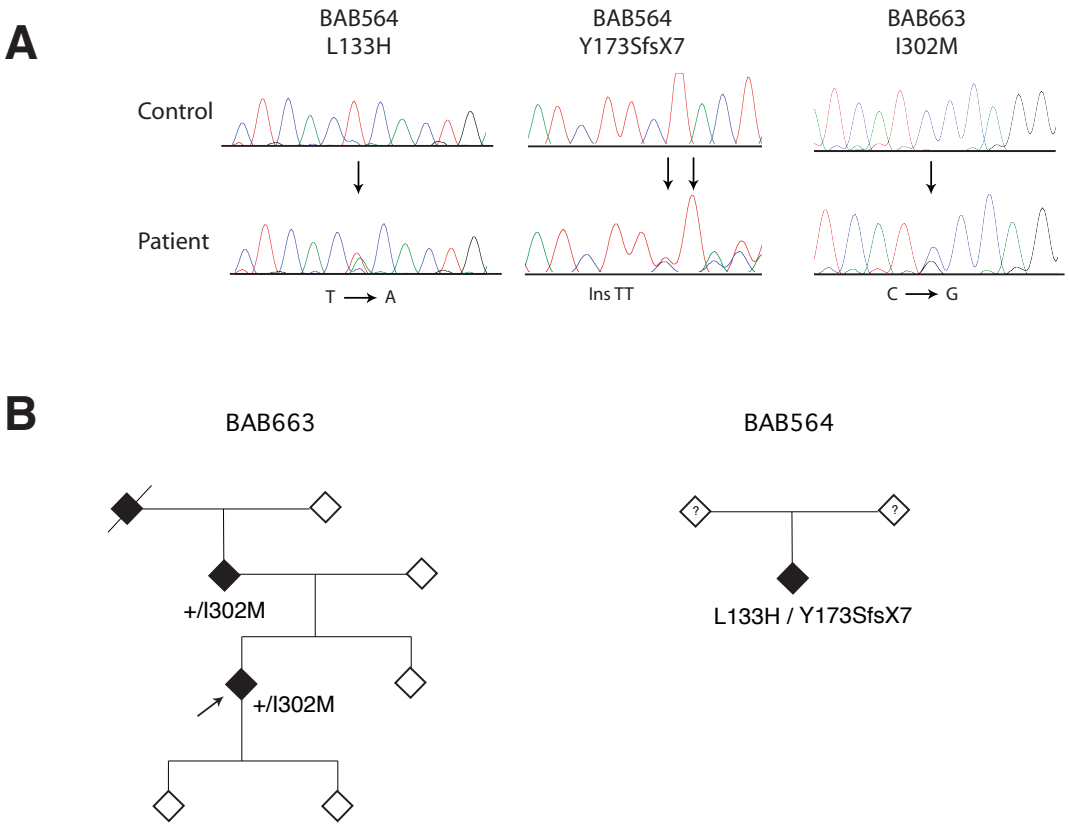

Figure 2.4 Validation and Segregation of *KARS* Variants. A: Chromatograms from control and affected ('Patient') individuals are shown for L133H (left), Y173SfsX7 (middle), and I302M (right). The nucleotide changes for each mutation are depicted below the corresponding chromatogram. **B:** Genotyping was performed to determine the segregation of *KARS* variants with disease in families with CMT. Filled symbols represent affected individuals, with black indicating a diagnosis of CMT disease. Empty symbols indicate unaffected individuals. Where applicable, the individual's genotype is indicated with the amino-acid change or + (for a wild-type allele). Slashes indicate deceased individuals, question marks indicate an unknown diagnosis, and the arrow indicates the proband in family BAB663. All individuals have been designated with a diamond symbol to protect identities.

MNCVs of 39.5 m/s and 30.6 m/s in the median and ulnar nerves, respectively. In addition, this patient displayed decreased amplitudes of evoked motor response in these nerves (0.5 mV).

Patient BAB564 is a Compound Heterozygyote for L133H and Y173SfsX7 KARS

Patient BAB564 is adopted, resulting in a lack of DNA samples or genetic information from either biological parent. To distinguish between a complex allele, where the patient harbors both L133H *KARS* and Y173SfsX7 *KARS* in *cis* (on the same allele), and compound heterozygosity, where each variant resides in *trans* (on separate alleles), we performed a more detailed molecular analysis of BAB564. The L133H variant resides on exon 3, while the Y173SfsX7 variant resides on exon 4, enabling us to amplify a ~3.7 Kb segment that spans both variants. After amplifying the ~3.7 Kb segment spanning both variants using genomic DNA from the patient, we cloned and sequenced ten individual clones. The L133H *KARS* variant was exclusively present in four clones, while the Y173SfsX7 variant was exclusively present in six clones (Fig. 2.5). Together, these data indicate that BAB564 is a compound heterozygote for L133H *KARS* and Y173SfsX7 *KARS*. Because BAB564 is adopted, these efforts helped to provide the hypothesis for a recessive mode of inheritance in this patient.

AARS and KARS Mutations Affect Highly Conserved Residues

To determine if the identified *AARS* and *KARS* variants reside at amino-acid residues important for enzyme function, we mapped each affected residue onto the linear protein sequence and determined if any variants reside within known AARS functional domains.

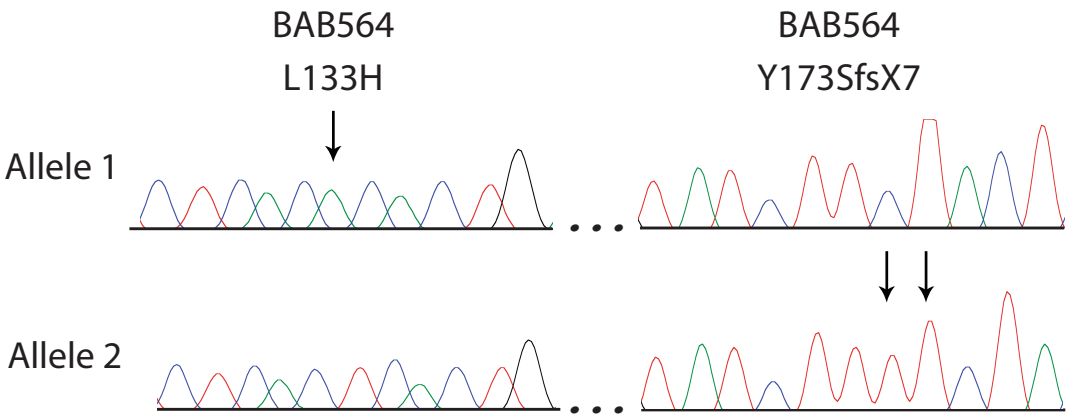

Figure 2.5 BAB564 is a Compound Heterozygote for L133H and Y173SfsX7 *KARS*. Chromatograms from allele-specific sequencing of a ~3.7 Kb PCR-generated genomic segment spanning the two *KARS* variants (L133H and Y173SfsX7) identified in patient BAB564. Arrows indicate the position of each mutation. Note that each variant was identified on separate alleles, indicating that this patient is a compound heterozygote.

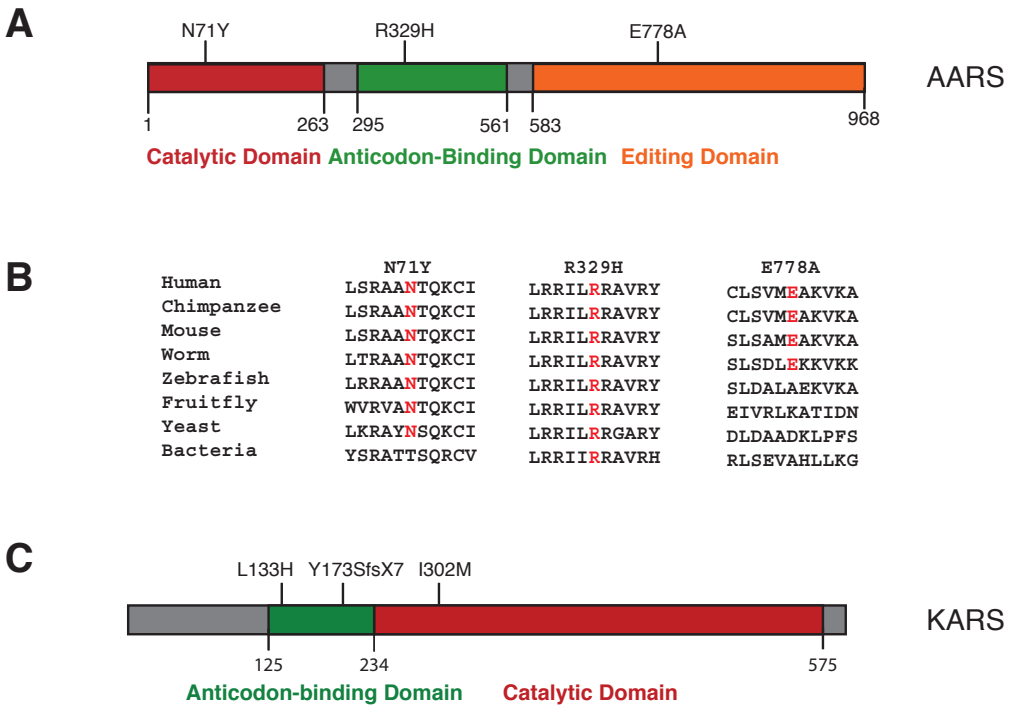

Figure 2.6 Localization and Conservation of AARS and KARS Variants. A, C: Each variant was mapped to the known functional domains of the appropriate protein. The catalytic domain is indicated in red, the anticodon-binding domain is indicated in green and the *AARS* editing domain is indicated in orange. The position of each domain along the protein is indicated below the cartoon. **B, D**: Multiple-species protein alignments were generated to assess the conservation of each affected amino-acid position. For each of the detected variants, the affected amino acid is shown along with the flanking protein sequence in multiple, evolutionarily diverse species (indicated on the left). Note that each specific amino-acid change is given at the top, with conservation indicated in red for each protein sequence.

Evaluation of the AARS protein sequence revealed asparagine 71 is located within the catalytic domain of the enzyme, arginine 329 resides within the tRNA-binding domain, and glutamic acid 778 is located in the editing domain of the protein (Fig. 2.6A). The evolutionary conservation of each affected AARS residue was assessed by aligning AARS protein orthologs from multiple species ranging from humans to bacteria. Asparagine 71 is conserved among all eight species analyzed with the exception of bacteria, while arginine 329 is conserved in all eight species analyzed, including yeast and bacteria (Fig. 2.6B). In contrast, glutamic acid 778 is not conserved among vertebrate species; note that an alanine is permissive in the zebrafish ortholog of AARS (Fig. 2.6B).

A similar analysis was performed for each *KARS* variant. Evaluation of the predicted domains in the linear KARS protein sequence revealed that leucine 133 and tyrosine 173 are located in the tRNA-binding domain, while isoleucine 302 is located within the catalytic domain of the enzyme (Fig. 2.6C). The evolutionary conservation of each affected KARS residue was also assessed (Fig 2.6D). Leucine 133 was conserved among all species analyzed, with the exception of yeast and bacteria. Isoleucine 302 was conserved among all species examined, including yeast and bacteria. Tyrosine 173 was conserved among all species analyzed with the exception of bacteria. Together, these analyses indicate that N71Y *AARS,* R329H *AARS*, L133H *KARS*, Y173SfsX7 *KARS*, and I302M *KARS* alter amino-acid residues that are conserved among evolutionarily diverse species, and reside within critical functional domains, suggesting these variants may impair enzyme function.

Discussion

Prior to the completion of this thesis, mutations in three genes encoding ARS enzymes were implicated in CMT disease (*AARS, GARS* and *YARS*) (Antonellis *et al.*, 2003; Jordanova *et al.*, 2006; Latour *et al.*, 2010). To determine the full extent of involvement of ARS genes in CMT disease, we set out to identify disease-associated ARS mutations in patients with CMT disease and no known disease causing mutation. Focusing on variants identified in the *AARS* and *KARS* genes, we utilized a combination of sequence confirmation, segregation analysis, LOD score calculation, healthy control screening, conservation analysis, long-range PCR, and bisulfite sequencing to determine if each variant is genetically implicated with disease.

We identified the R329H *AARS* variant in a large Australian pedigree with autosomal dominant axonal CMT disease. In 2010, Latour, *et al.* also identified the R329H *AARS* mutation in two French families with autosomal dominant axonal CMT disease, now referred to as CMT type 2N (CMT2N). Importantly, the phenotype of the affected patients described in the original French families is similar to the phenotype presented in affected members in the Australian family we identified with R329H *AARS* mutations (Latour *et al.*, 2010). Affected members of each of the families exhibited age of onset in the early 20's, MNCVs in the intermediate range, and a lower limb predominance of symptoms. The family we identified also exhibited variable sensorineural deafness; possibly broadening the range of symptoms physicians might associate with CMT2N. Deafness has also been described in other forms of CMT including those associated with *MPZ* (CMT1B), *PMP22* (CMT1E), *SH3TC2* (CMT4C), *NDRG1* (CMT4D), *GJB1*

(CMTX1), *PRPS1* (CMTX5), and *INF2* (CMTDIE) gene mutations (Boerkoel *et al.*, 2002; Boyer *et al.*, 2011; Colomer *et al.*, 2006; Kalaydjieva *et al.*, 2000; Kim *et al.*, 2005; Kim *et al.*, 2007; Kurihara *et al.*, 2004; Stojkovic *et al.*, 1999).

The mutagenic mechanism of the reccurent R329H *AARS* mutation was previously unknown. Our haplotype and bisulfite DNA sequence analyses suggest that R329H *AARS* is a recurrent mutation resulting from methylation-mediated deamination of a CpG dinucleotide and indicate that the prevalence of this mutation in CMT disease should be further investigated. Recurrent, methylation-mediated, disease-associated mutations have been described in other genes including the tumor suppressor protein p53 (*TP53)* gene, the phenylalanine hydroxylase (*PAH*) gene, and the methyl CpG binding protein 2 (*MECP2*) gene (Greenblatt *et al.*, 1994; Murphy *et al.*, 2006; Wan *et al.*, 1999). These findings often dictate mutation-specific screening of other, relevant patients with no known mutation. We also discovered that six additional CpGs in *AARS* exon 8 are methylated, suggesting that this exon has the capacity to be highly mutable. Combined, these data have important clinical implications. Our data suggesting the recurrent nature of the R329H *AARS* mutation indicate that all patients with axonal CMT disease and no known disease-causing mutation should be screened for the R329H *AARS* mutation. Furthermore, it may be prudent to thoroughly assess each of the remaining methylated CpGs in *AARS* exon 8 in similar patients to fully evaluate the *AARS* gene for CMT-associated mutations.

Our mutation screen of the *AARS* gene also identified the E778A *AARS* variant, which

segregates with dominant rippling muscle disease in a family including a proband with the additional phenotype of axonal CMT disease. Although E778A *AARS* was absent in over 950 chromosomes from neurologically normal control individuals, the affected residue is not well conserved. Moreover, the mutation resides in the editing domain of the AARS protein, which has previously been associated with a non-CMT phenotype in the *Aars*$^{sti/sti}$ mouse (Lee *et al.*, 2006) Together, these data weaken the argument for pathogenicity of the E778A *AARS* mutation. Because CMT513 is too small for linkage analysis, further functional studies must be performed to determine the pathogenicity of the E778A *AARS* variant (see Chapter 3).

Mutational analysis of the *KARS* gene led to the discovery of a I302M *KARS* variant in a heterozygous individual with clinical and electrophysiological evidence for hereditary neuropathy with liability to pressure palsies (HNPP). This patient also harbors the common 1.4 Mb deletion at the *PMP22* locus that causes HNPP. While I302M *KARS* resides at a residue within the catalytic core of the enzyme that is conserved between human and bacteria, the *PMP22* deletion should be considered the primary pathogenic mutation in BAB663. However, it will be important to determine if the if the R238H *GBJ1* and/or I302M *KARS* variants identified in this patient modify the clinical phenotype. Several recent studies suggest the potential for a more severe neuropathy phenotype associated with variants at more than one CMT locus (Chung *et al.*, 2005; Hodapp *et al.*, 2006; Meggouh *et al.*, 2005).

The L133H and Y173SfsX7 *KARS* variants were identified a compound heterozygous patient with intermediate CMT, developmental delay, self-abusive behavior, dysmorphic features, and a vestibular Schwannoma. The discovery of these variants led to the classification of a new form of CMT disease termed CMT recessive intermediate type B (CMTRIB; OMIM 613641). *KARS* encodes both cytoplasmic and mitochondrial forms of the KARS enzyme. Interestingly, this is the first report of a patient with compound heterozygous mutations in a bi-functional tRNA synthetase. Because no genetic information is available from either biological parent of the proband, functional studies will be required to determine if one or both of these variants is pathogenic (Chapter 3).

The studies outlined in this chapter have provided genetic evidence to implicate mutations in the *AARS* and *KARS* genes in patients with CMT2N and CMTRIB, respectively. These studies have broadened our understanding of the types of ARS genes involved in CMT disease. While *AARS* encodes a cytoplasm-specific tRNA synthetase, *KARS* encodes a bifunctional enzyme. Together, these data further implicate aminoacyl-tRNA synthetases that charge tRNAs in the cytoplasm with CMT disease. In addition, these studies also indicate that ARS-related CMT disease can be inherited in a dominant (for CMT2N *AARS* mutations) or recessive manner (for CMTRIB *KARS* mutations). Functional characterization of the *AARS* and *KARS* mutations presented here are required to obtain a better understanding of pathogenic mechanisms of CMT2N and CMTRIB at the molecular level. These studies will be described in the next chapter.

Aminoacyl-tRNA synthetases have emerged as the most commonly implicated gene family in CMT disease. The genetic implication of *AARS* and *KARS* variants in CMT disease warrants further studies into the additional unevaluated ARS variants identified in ARS genes. Moving forward, it will be imperative to genetically catalog and assess each of these variants to determine the full extent of involvement of ARS genes in CMT disease.

CHAPTER 3

Functional Evaluation of Disease-Associated Aminoacyl-tRNA Synthetase Mutations in Patients with Charcot-Marie-Tooth Disease

The data presented in this chapter were previously published in *The American Journal of Human Genetics* (Volume 87, Issue 4) and in *Human Mutation* (Volume 33, Issue 1) (McLaughlin *et al.*, 2012; McLaughlin *et al.*, 2010). All figures and tables are used with permission from Elsevier (License No. 2827080090840) and John Wiley and Sons (License No. 2822181011090). I performed all of the work presented, with the exception of biochemical analyses of wild-type and mutant AARS and KARS enzymes, which were performed by our collaborators Reiko Sakaguchi and Ya-Ming Hou at Thomas Jefferson University.

Introduction

The majority of disease-associated ARS mutations identified to date segregate with disease in a dominant fashion and lead to loss-of-function effects in various capacities including cellular localization, aminoacylation activity, and the ability to support yeast cell growth (Antonellis *et al.*, 2006; Froelich and First, 2011; Jordanova *et al.*, 2006; Nangle *et al.*, 2007; Storkebaum *et al.*, 2009; Xie *et al.*, 2007). Several *GARS* and *YARS* mutants display localization defects when expressed in neuronal cells. For example, wild-type *GARS* forms granular structures when tagged with enhanced green fluorescent

protein (EGFP) and expressed in MN-1 cells (Antonellis *et al.*, 2006). In contrast, EGFP-tagged L129P *GARS*, G420R *GARS*, H418R *GARS*, D500N *GARS*, and G526*R GARS* variants fail to form these granules when expressed in MN-1 cells, and instead localize diffusely throughout the cell body and neurite projections (Antonellis *et al.*, 2006). A similar mislocalization defect is observed when G41R *YARS* and E196K *YARS* expression is compared with wild-type *YARS* expression. While wild-type *YARS* tagged with EGFP is localized to granular structures in the distal portion of projecting neurons when expressed in N2a cells, G41R *YARS* and E196K *YARS* fail to form granules in neuronal projections when expressed in N2a cells (Jordanova *et al.*, 2006).

Two *in vitro* assays are utilized to evaluate aminoacylation activity of ARS enzymes. The pyrophosphate release assay monitors the pyrophosphate release that occurs during the activation step of the aminoacylation reaction (see Fig. 1.2), while substituting tritium (^{3}H) labeled amino-acids in the aminoacylation reaction allows monitoring of the production of ^{3}H-lableled aminoacylated tRNA, providing an assessment of the efficiency of both the activation and transfer steps. When the effect of *GARS* variants on aminoacylation activity was evaluated by monitoring the incorporation of [^{3}H]-glycine onto Gly-tRNA, L129P *GARS*, G240R *GARS*, H418R *GARS*, and G526R *GARS* resulted in reduced aminoacylation activity compared to wild-type *GARS* (Nangle *et al.*, 2007; Xie *et al.*, 2007). Similarly, G41R *YARS* and E196K *YARS* led to decreased activation of the amino-acid when evaluated via the pyrophosphate release assay, and G41R *YARS* and del153-156VKQV *YARS* led to reduced aminoacylation when evaluated by monitoring the incorporation of [^{3}H]-tyrosine into Tyr-tRNA (Froelich and First, 2011; Jordanova *et al.*, 2006; Storkebaum *et al.*, 2009).

Saccharomyces cerevisiae, a single celled organism known for being amenable to genetic manipulation, can be used to evaluate both loss-of-function and dominant-negative effects of ARS mutations. Loss-of-function can be evaluated by expressing ARS mutants in a haploid yeast strain where the endogenous ARS gene has been deleted. Yeast viability assays have identified loss-of-function effects resulting from L129P *GARS,* H418R *GARS,* G526R *GARS,* G41R *YARS*, and E196K *YARS* mutations (Antonellis *et al.*, 2006; Jordanova *et al.*, 2006). The *Saccharomyces cerevisiae* model system can also be utilized to assess for a dominant-negative effect by expressing ARS mutants in the presence of a wild-type allele. While none of the *GARS* mutants have been evaluated for a dominant-negative effect in yeast, both G41R *YARS* and E196K *YARS* display a dominant-negative effect when modeled in the yeast ortholog *TYS1* (Jordanova *et al.*, 2006).

All *GARS* and *YARS* mutations identified to date have led to loss-of-function effects. We sought to determine if the *AARS* and *KARS* variants we implicated with CMT disease in Chapter 2 also result in loss-of-function effects in localization, aminoacylation, and/or yeast viability assays. Based upon previous studies, loss-of-function ARS mutations are expected to lead to one or more of the following functional consequences: mislocalization following overexpression in neuronal cells, a reduction in aminoacylation activity, and/or the inability to support yeast cell growth. Together, these studies will establish if loss of aminoacylation activity is a major component to CMT disease pathology, and will aid in determining if other mechanisms, such as gain-of-function or loss of a non-canonical

function, should be pursued. Importantly, these studies may also reveal the molecular mechanism(s) by which heterozygosity for *AARS* mutations lead to CMT2N, while compound heterozygosity for *KARS* mutations lead to CMTRIB.

Materials and Methods

cDNA Cloning and Mutagenesis

DNA constructs for aminoacylation and yeast complementation assays were generated using Gateway cloning technology (Invitrogen Carlsbad, CA). The human *AARS* open reading frame (minus the stop codon) and the *Saccharomyces cerevisiae* alanyl-tRNA synthetase (*ALA1)* locus (including the open reading frame and 628 base pairs of proximal promoter sequence) were PCR amplified using human cDNA and *Saccharomyces cerevisiae* genomic DNA, respectively. Likewise, cytoplasmic and mitochondrial forms of the human *KARS* open reading frame (minus the stop codon) and the *Saccharomyces cerevisiae* lysyl-tRNA synthetase *(KRS1)* locus (including the open reading frame and 500 base pairs of proximal promoter sequence) were PCR amplified using human coding DNA (cDNA) and *Saccharomyces cerevisiae* genomic DNA, respectively. Each primer was designed to include flanking Gateway *att*B1 (forward) and *att*B2 (reverse) sequences (Appendix A6). Subsequently, purified PCR products containing each gene were recombined into the pDONR221 vector via BP reaction according to the manufacturer's protocols (Invitrogen, Carlsbad, CA). The coding sequences of the resulting entry clones were sequence verified. Mutagenesis was performed using the QuikChange II XL Site-Directed Mutagenesis Kit (Agilent, Santa Clara, CA) and the appropriate mutation-bearing oligonucleotides (Appendix A7).

Subsequently, each human entry clone was recombined with a gateway-compatible pSMT3 destination vector (for aminoacylation assays), a gateway-compatible pDsRed2-N1 vector (for localization studies), or a gateway-compatible pEGFP-N2 vector (for localization studies). Each yeast entry clone was recombined with gateway-compatible pRS315 and pRS316 destination vectors for use in yeast complementation assays (ATCC, Manassas, VA). Subcloning was achieved via an LR reaction, according to the manufacturer's instructions (Invitrogen, Carlsbad, CA). Each resulting expression construct was analyzed by restriction enzyme digestion with *Bsr*GI (New England Biosystems, Ipswich, MA) to confirm the presence of an appropriately-sized insert.

Cell Culture and Differentiation

The mouse motor neuron cell line MN-1 (Salazar-Grueso *et al.*, 1991) was cultured in Dulbecco's modified eagle medium (DMEM) supplemented with 10% fetal bovine serum (FBS), 100 U/ml penicillin, 50 μg/ml streptomycin, and 2mM L-glutamine and grown at 37°C in 5% CO_2 (Invitrogen, Carlsbad, CA). For assays requiring differentiation, cultured cells were counted using the Countess Automated Cell Counter (Invitrogen Carlsbad, CA) and ~1.25 X 10^5 cells were placed into each well of a four-well polystyrene tissue culture treated glass slide (BD Biosciences, Sparks, MD). MN-1 cells were differentiated by the addition of 2 nM glial cell line-derived neurotrophic factor (GDNF) and 833 pM GDNF receptor α-1 (GFR α-1; both from R&D Systems) to the culture medium and incubation for 48 h (Paratcha *et al.*, 2001).

AARS Antibody and DAPI Staining

For AARS localization studies, mouse MN-1 cells were cultured at 37°C for 48 hours in differentiation medium (see above). Cells were fixed in 4% paraformaldehyde, permeabilized in 0.2% Triton X-100 in 1X phosphate buffered saline (PBS) for 5 min, washed in 1X PBS, and incubated in blocking solution containing 10% normal goat serum in 1X PBS with 0.1% sodium azide for 30 min. Cells were then incubated in 10 μg/ml anti-AARS (B23) (sc-130683, Santa Cruz Biotechnology, Santa Cruz, CA) in blocking solution for 60 min. After three washes in 1X PBS, cells were incubated in 1:2000 Alexa Fluor 488 goat anti—rabbit IgG (Invitrogen, Carlsbad, CA) for 60 minutes. Cells were washed three times in 1X PBS, the well apparatus was removed, and slides were coated with ProLong anti-fade reagent (Invitrogen, Carlsbad CA), covered, and sealed with nail polish. All incubation and wash steps were performed at room temperature. For KARS localization studies, the cells were stained with 4',6-diamidino-2-phenylindole (DAPI) prior to imaging. Cells fixed with 4% paraformaldehyde, washed 3X with 1X PBS, and incubated for 5 min with 300nM DAPI. After incubation, cells were washed 3X with 1X PBS, the well apparatus was removed, and slides were treated and sealed as described above.

MN-1 Transfections

Also for AARS localization studies, constructs expressing either wild-type or mutant AARS tagged with DsRed (described above) were transfected into MN-1 cells. For cytoplasmic KARS localization studies, constructs expressing either wild-type or mutant cytoplasmic KARS tagged with EGFP were transfected in MN-1 cells. Assays evaluating the localization of mitochondrial KARS were performed by cotransfecting constructs

expressing either wild-type or mutant mitochondrial KARS tagged with EGFP along with a construct expressing mito-DsRed (DsRed2 fused to the mitochondrial targeting sequence from subunit VIII of human cytochrome *c* oxidase (Rizzuto *et al.*, 1995)). For each transfection reaction, 6-μl of Lipofectamine 2000 and 250-μl of OptiMEM I minimal growth medium (Invitrogen, Carlsbad, CA) were combined and incubated at room temperature for 10 min. Purified plasmid DNA (4 μg) was diluted in 250-μl of OptiMEM I, combined with the above Lipofectamine–OptiMEM I mixture, and incubated at room temperature for 20 min. The entire transfection cocktail was then added to ~1.25 X 10^5 MN-1 cells (if subsequently differentiated) or ~2.5 X 10^5 MN-1 cells (if not differentiated) in a 15 ml conical tube. After a 2 h incubation at 37°C, the transfection reaction was centrifuged at 2000 r.p.m. for 2 minutes and the cells were resuspended in 250-μl normal growth medium (see above). Cells to be differentiated were allowed to recover for 24 h at 37°C, washed with 1X PBS, and subsequently incubated with differentiation medium (see above). After 48 h, cells were fixed as described above.

Microscopy and Image Analysis

Microscopic images were obtained using the Olympus FluoView FV500/IX Laser Scanning Confocal Microscope using Olympus Fluoview image software at the University of Michigan Microscopy and Image Analysis Core.

Aminoacylation Assays

All wild-type and mutant AARS and KARS open reading frames (ORFs) were cloned in-frame with the SMT3 protein (N-terminus) to improve solubility for expression in *E. coli.* Control experiments indicate the presence of the SMT3 protein has no effect on the aminoacylation activity of these enzymes (Mossessova and Lima, 2000). Wild-type and mutant ORFs were also cloned with an in-frame His-tag on the C-terminus to allow for affinity purification through a metal resin. For AARS aminoacylation assays, protein expression was achieved in *E. coli* strain Rosetta 2 (DE3) pLysS and purification with the nickel affinity resin was achieved according to the manufacturer's protocol (Novagen, Darmstadt, Germany). The T7 transcript of human $tRNA^{Ala}$ was prepared and purified as previously described (Hou *et al.*, 1993), heat-denatured at 85°C for 3 min, and annealed at 37°C for 20 min before use. Steady-state aminoacylation assays were monitored at 37°C in 50 mM HEPES (pH 7.5), 20 mM KCl, 10 mM $MgCl_2$, 4 mM DTT, 2 mM ATP, and 50 mM alanine with a trace of [^{3}H]-alanine (Perkin Elmer, Waltham, MA) at a specific activity of 3,693 dpm/pmole. The reaction was initiated by mixing AARS enzyme (20-600 nM) with varying concentrations of annealed tRNA (0.3-20 mM). A similar reaction protocol was followed for KARS aminoacylation assays with the following exceptions: KARS constructs were expressed in the BL21(DE3) pRIL *E. coli* strain, $tRNA^{Lys}$ was substituted for $tRNA^{Ala}$, 50 mM lysine was substituted for 50 mM alanine, [^{3}H]-lysine was substituted for [^{3}H]-alanine, and the reaction was initiated by mixing KARS enzyme with various concentrations of annealed tRNA. Aliquots of each reaction mixture were spotted on filter paper, quenched by 5% TCA, washed, and measured for radioactivity by a liquid scintillation counter (Beckman LS6000SC). The amount of radioactivity retained on the filter paper was corrected for quenching effects to

reveal the amount of synthesis of either Ala-tRNA^{Ala} or Lys-tRNA^{Lys}. Steady-state kinetics was determined by fitting the initial rate of aminoacylation as a function of tRNA concentration to the Michaelis-Menten equation.

AARS Editing Assays

The substrate Ser-tRNA^{Ala} for analysis of post-transfer editing was prepared by ^{32}P-labeling of the A76 nucleotide in the transcript of human tRNA^{Ala} with the CCA enzyme (Shitivelband and Hou, 2005), followed by aminoacylation with chemically synthesized Ser-DBE, using the dFx flexizyme (Murakami *et al.*, 2006). Deacylation assays were performed in 50 mM HEPES (pH 7.5), 20 mM KCl, 4 mM DTT, and 10 mM $MgCl_2$ at 37 °C, using 5 nM of an AARS enzyme and 20 mM of Ser-tRNA^{Ala}. At the indicated time points, aliquots of a deacylation reaction were removed and mixed with S1 nuclease for 30 min to digest the tRNA in the aliquots to a 5'-phosphate mononucleotide. The aliquots were processed via thin layer chromatography (TLC) in 0.55 M acetic acid / 0.1 M NH_4Cl for 30 min to separate [^{32}P]-seryl-AMP from [^{32}P]-AMP. Quantification of the two products by a phosphorimager and analysis of the ratio of [Ser-AMP] *versus* [AMP] determined the amount of Ser-tRNA^{Ala} remaining after the editing reaction.

Yeast Viability Assays

For *ALA1* yeast viability assays, a commercially available diploid heterozygous *ala1*Δ yeast strain (MATa/α, his3Δ1/his3Δ1, leu2Δ0/leu2Δ0, LYS2/lys2Δ0, met15Δ0/MET15, ura3Δ0/ura3Δ0; Open Biosystems, Huntsville, AL), created by replacing the *ALA1* locus with a KAN^R cassette, was transformed with a *URA3*-bearing pRS316 vector containing

wild-type *ALA1* (see above). For *KRS1* yeast viability assays, a commercially available diploid heterozygous *krs1*Δ yeast strain [MATa/α his3Δ1/his3Δ1 leu2Δ0/leu2Δ0 LYS2/lys2Δ0 met15Δ0/MET15 ura3Δ0/ura3Δ0; Open Biosystems, Huntsville, AL), created by replacing the *KRS1* locus with a KAN^R cassette, was transformed with a *URA3*-bearing pRS316 vector containing wild-type *KRS1* (see above). Lithium acetate transformations were performed using yeast cells grown in the exponential phase after treatment with 0.1M lithium acetate overnight. Subsequently, the cells were collected, resuspended in 0.1M lithium acetetate, and boiled following the addition of 200 ng vector DNA and 5-ul 10 mg/ml salmon sperm DNA (Invitrogen, Carlsbad, CA). After boiling, the cells were treated with 67% (w/v) polyethylene glycol (PEG; Hampton Research, Aliso Viejo, CA) in 0.1M lithium acetate and allowed to incubate at 30°C for 30 minutes. Following a heat shock at 42°C for 15 minutes, the transformed cells were collected and grown on yeast medium lacking uracil (Teknova, Hollister, CA). Subsequently, sporulation and tetrad dissections (see below) were performed to obtain a haploid *ala1*Δ strain that carries the wild-type *ALA1* pRS316 maintenance vector (*ALA1* KO + *ALA1*/*URA3*) in the case of *ALA1* tetrad dissections or a haploid *krs1*Δ strain that carries the wild-type *KRS1* pRS316 maintenance vector (*KRS1* KO + *KRS1/URA3*) in the case of *KRS1* tetrad dissections. Tetrad dissections were performed by patching the transformed diploid strain twice onto pre-sporulation plates [(5% D-glucose (Fisher Scientific, Hampton, NH), 3% nutrient broth (Becton, Dickinson and Company, Franklin Lakes, NJ), 1% yeast extract (Acros Organics, Waltham, MA), and 2% agar (Teknova, Hollister, CA)]. Several microliters of cells were then transferred into 2 mLs of supplemented liquid sporulation medium [(1% potassium acetate (Fisher Scientific,

Hampton, NH), 0.005% zinc acetate (Fisher Scientific, Hampton, NH), 1X Ura supplement (MP Biomedicals, Solon, OH), 1X His supplement (MP Biomedicals, Solon, OH), and 1X Leu supplement (MP Biomedicals, Solon, OH)] and incubated for 5 days at 25°C followed by 3 days at 30°C. Sporulated strains were dissected using a MSM 400 dissection microscope (Singer Instruments, Somerset UK), and plated on yeast extract, peptone, and dextrose (YPD) plates (Becton, Dickinson and Company, Franklin Lakes, NJ). Resulting spores were individually patched onto solid growth medium containing geneticin (G418) or 0.1% 5-fluoroorotic acid (5-FOA), or media lacking uracil to confirm the presence of the KAN^R cassette and the experimental vector, and to ensure the absence of the maintenance vector (Teknova, Hollister, CA).

Two spores that grew on G418 and yeast medium lacking uracil yet did not grow on 5-FOA medium were selected for use in the yeast viability assays. For *ALA1* studies, two resulting haploid *ALA1* KO + *ALA1*/*URA3* strains bearing a wild-type pRS316 maintenance vector were transformed with *LEU2*-containing pRS315 constructs harboring wild-type or mutant *ALA1* (described above) and grown on medium lacking uracil and leucine (Teknova, Hollister, CA). For *KRS1* studies, two resulting haploid *KRS1* KO + *KRS1/URA3* strains bearing a wild-type pRS316 maintenance vector were then transformed with *LEU2*-containing pRS315 constructs harboring wild-type or mutant *KRS1* (described above) and grown on medium lacking uracil and leucine (Teknova, Hollister, CA). For each transformation, at least 9 colonies were selected for additional analysis. Each colony was diluted in 100-µl H_2O, then further diluted 1:10 (for *ALA1* studies) or 1:10 and 1:50 (for *KRS1* studies) and spotted on growth medium

containing 0.1% 5-FOA (Teknova, Hollister, CA), incubated for 3 days at 30°C. Growth was assessed by visual inspection. Because 5-FOA is toxic to yeast cells bearing a functional *URA3* allele, only cells that spontaneously lost the *URA3* maintenance plasmid and for which the *LEU2* test plasmid could complement the chromosomal *ala1*Δ or *krs1*Δ allele were expected to grow.

Yeast Growth Curve Assays

ALA1 and *KRS1* growth curve assays testing for a loss-of-function effect were performed using strains that survived 5-FOA treatment (see above). *ALA1* growth curve assays testing for a dominant-negative effect were performed using strains containing the *URA3*-containing pRS316 maintenance vector harboring wild-type *ALA1* and the *LEU2*-containing pRS315 constructs harboring wild-type or mutant *ALA1*. Similar assays testing for a dominant-negative effect were performed by over-expressing wild-type and R329H *ALA1* using vectors containing a strong, constitutively active *ADH1* promoter. *KRS1* growth curve assays testing for a dominant-negative effect were performed using strains containing the *URA3*-containing pRS316 vector harboring wild-type *KRS1* and the *LEU2*-containing pRS315 constructs harboring wild-type or mutant *KRS1*. Three transformants from each strain were inoculated medium lacking leucine (for loss-of-function assays; Teknova, Hollister, CA) or medium lacking leucine and uracil (for dominant-negative assays; Teknova, Hollister, CA) and incubated shaking overnight at 30°C. Each culture was initially normalized at time (t)=0 to OD_{600}=0.01 and further incubated at 30°C for the reminder of the assay. OD_{600} readings were recorded, as indicated, using the NanoDrop 1000 spectrophotometer (Thermo Scientific, Wilmington,

DE). Growth curves were created using the average measurements of three independent cultures.

Results

Mutant AARS and KARS Proteins do not Lead to Overt Mislocalization

Many *GARS* and *YARS* mutations lead to localization defects when overexpressed in neuronal cell lines (Antonellis *et al.*, 2006; Jordanova *et al.*, 2006). To determine if *AARS* and *KARS* mutations result in a similar mislocalization effect, we performed localization studies in the mouse motor neuron cell line MN-1 (Salazar-Grueso *et al.*, 1991). We first examined the endogenous localization of the AARS protein in the MN-1 cell line after differentiation and staining with an anti-AARS antibody. Confocal microscopy revealed diffuse localization throughout the cell and nucleus, extending into the neurite projections (Fig. 3.1A-B). Notably, this localization pattern is in contrast to the distinct granular staining pattern of the endogenous GARS and YARS proteins (Antonellis *et al.*, 2006; Jordanova *et al.*, 2006). Subsequently, we assessed the localization of each AARS protein variant by transfecting constructs expressing wild-type *AARS*, N71Y *AARS*, R329H *AARS*, or E778A *AARS* with a C-terminal DsRed tag in MN-1 cells, and examining the localization pattern after differentiation via confocal microscopy. Similar to wild-type AARS, N71Y AARS, R329H AARS, and E778A AARS proteins were localized diffusely throughout the cell body and neurite projections (Fig. 3.1C-F; arrows). These data indicate that disease-associated AARS variants do not grossly mislocalize in differentiated neurons, at the resolution of confocal microscopy.

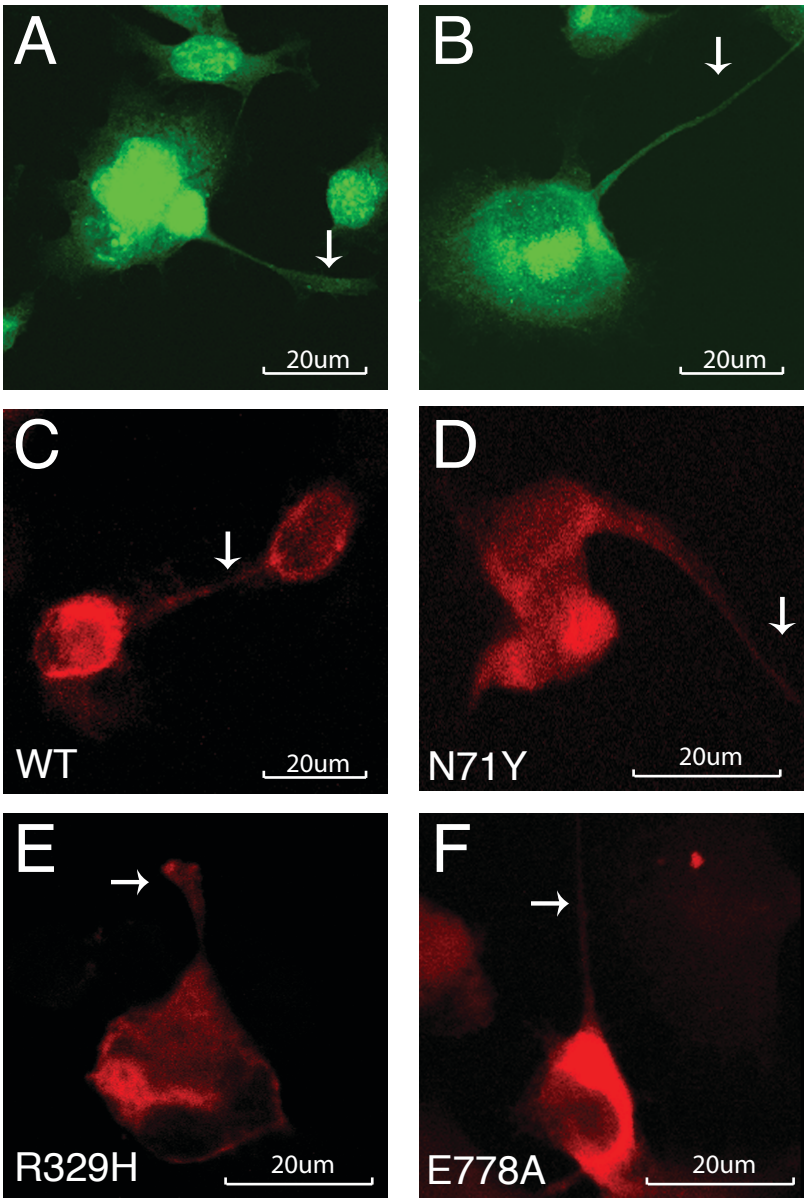

Figure 3.1 Evaluation of AARS Localization in Differentiated MN-1 cells. **A, B**: Differentiated MN-1 cells were stained with α-AARS and visualized via confocal microscopy. Endogenous AARS protein is localized diffusely throughout the cell body, nucleus, and neurite projections (arrows). **C**: Wild-type AARS with a C-terminal DsRed tag was transfected into MN-1 cells. After differentiation, localization was analyzed via confocal microscopy. Wild-type AARS is localized diffusely throughout the cell body and neurite projection (arrow). **D-F**: Similar analyses as described in (**C**) for N71Y AARS, R329H AARS, and E778A AARS, respectively. Similar to wild-type AARS, each AARS variant is also localized diffusely throughout the cell body and neurite projections (arrows). The scale bar shown represents 20 um.

The *KARS* gene utilizes an alternative splicing mechanism to encode cytoplasmic and mitochondrial forms of the KARS enzyme (Tolkunova *et al.*, 2000). We therefore evaluated each variant using both the cytoplasmic (cytoKARS) and mitochondrial forms (mitoKARS) of the KARS protein. Localization studies analyzing cytoKARS protein variants were performed by transfecting constructs expressing the cytoplasmic form of wild-type *KARS*, L133H *KARS*, or I302M *KARS* with a C-terminal EGFP tag in MN-1 cells, and examining the localization pattern via confocal microscopy. Similar to wild-type cytoKARS, both L133H cytoKARS and I302M cytoKARS localized diffusely throughout the cytoplasm. Mitochondrial KARS protein variants were assessed as described above, after co-transfection with a construct to express mito-DsRed, which allows visualization of mitochondria. As expected, wild-type mitoKARS localized specifically to the mitochondria, as evidenced by complete merging of the EGFP and DsRed signals (Fig. 3.2). Both L133H mitoKARS and I302M mitoKARS showed a mitochondrial localization pattern similar to wild-type mitoKARS (Fig. 3.2). Together, these data indicate that disease-associated KARS variants do not grossly mislocalize in cultured neurons at the resolution of confocal microscopy.

Mutant AARS and KARS Proteins Impair Aminoacylation Activity

Because many *GARS* and *YARS* mutations lead to a reduction in aminoacylation activity, we chose to monitor the effect of each *AARS* and *KARS* mutation on charging capacity (Froelich and First, 2011; Jordanova *et al.*, 2006; Nangle *et al.*, 2007; Storkebaum *et al.*, 2009; Xie *et al.*, 2007). AARS catalyzes the aminoacylation of $tRNA^{Ala}$ in the cytoplasm via a two-step aminoacylation reaction (Lodish, 2008). The *AARS* mutations described in

Figure 3.2 Localization of Cytoplasmic and Mitochondrial KARS Proteins in MN-1 Cells. Top row: Constructs expressing cytoplasmic forms of wild-type, L133H, or I302M KARS with a C-terminal EGFP tag were transfected into MN-1 cells, stained with DAPI (to visualize the nuclei) and visualized via confocal microscopy after merging EGFP and DAPI images. Similar to wild-type KARS, L133H KARS and I302M KARS are localized diffusely throughout the cytoplasm. Bottoms rows: Constructs expressing mitochondrial forms of wild-type, L133H, or I302M KARS with a C-terminal EGFP tag were co-transfected into MN-1 cells along with Mito-DsRed (to visualize mitochondria), stained with DAPI (to visualize the nuclei) and visualized via confocal microscopy after merging EGFP, DAPI, and DsRed images. Similar to wild-type KARS, L133H KARS and I302M KARS are localized to the mitochondria. The scale bar shown represents 30 um for the cytoplasmic images and 20 um for the mitochondrial images.

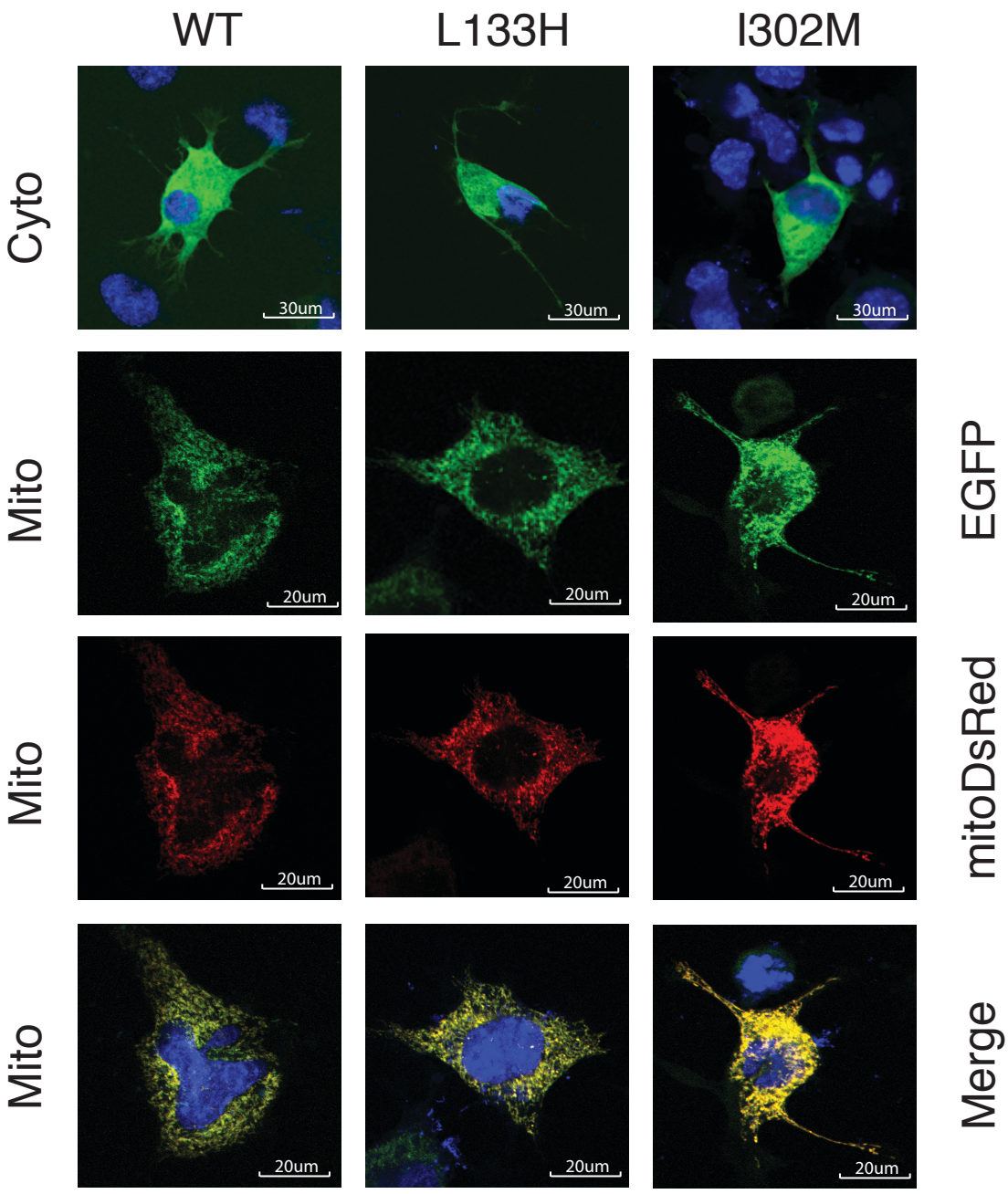
WT
L133H
I302M
Cyto
Mito
Mito
Mito
EGFP
mitoDsRed
Merge
30um
20um

Chapter 2 have not been tested for an effect on aminoacylation activity, however when the analogous amino-acid to arginine 329 AARS is mutated to an alanine in *E. coli*, a ~700-fold reduction in bacterial alaS aminoacylation activity is observed (Ribas de Pouplana *et al.*, 1998). Substitution for a histidine at this position was never tested. We therefore tested the ability of each human AARS protein variant to catalyze the aminoacylation reaction *in vitro*. Human cytoplasmic $tRNA^{Ala}$ was synthesized via *in vitro* transcription and used as a substrate for aminoacylation in the presence of tritium-labeled alanine. Analyses of the catalytic efficiency (k_{cat}/K_m) of aminoacylation revealed that N71Y AARS and R329H AARS impaired enzyme activity, resulting in a 4,130-fold and 50-fold decrease in catalytic efficiency compared to wild-type AARS, respectively (Fig. 3.3 and Table 3.1). In contrast, E778A AARS showed catalytic activity similar to the wild-type enzyme (Fig. 3.3). Thus, the N71Y *AARS* and R329H *AARS* alleles encode enzyme subunits with reduced charging capacity *in vitro*.

Because E778A AARS resides within the editing-domain of the AARS enzyme, we sought to determine if E778A AARS results in a loss of editing function. We utilized mis-charged Ser-$tRNA^{Ala}$ as a substrate for post-transfer editing in the presence of wild-type AARS or E778A AARS and measured the ability of each enzyme to hydrolyze the incorrectly charged aminoacyl-tRNA. Analysis of E778A AARS editing activity revealed Ser-$tRNA^{Ala}$ hydrolysis comparable to that of the wild-type AARS enzyme (Fig. 3.4). This is in contrast to the reduced editing activity observed for A734E AARS, an enzyme modeling the previously-described editing-defective $Aars^{sti/sti}$ mutation that causes ataxia and Purkinje cell loss in affected mice, but not peripheral neuropathy (Fig. 3.4) (Lee et

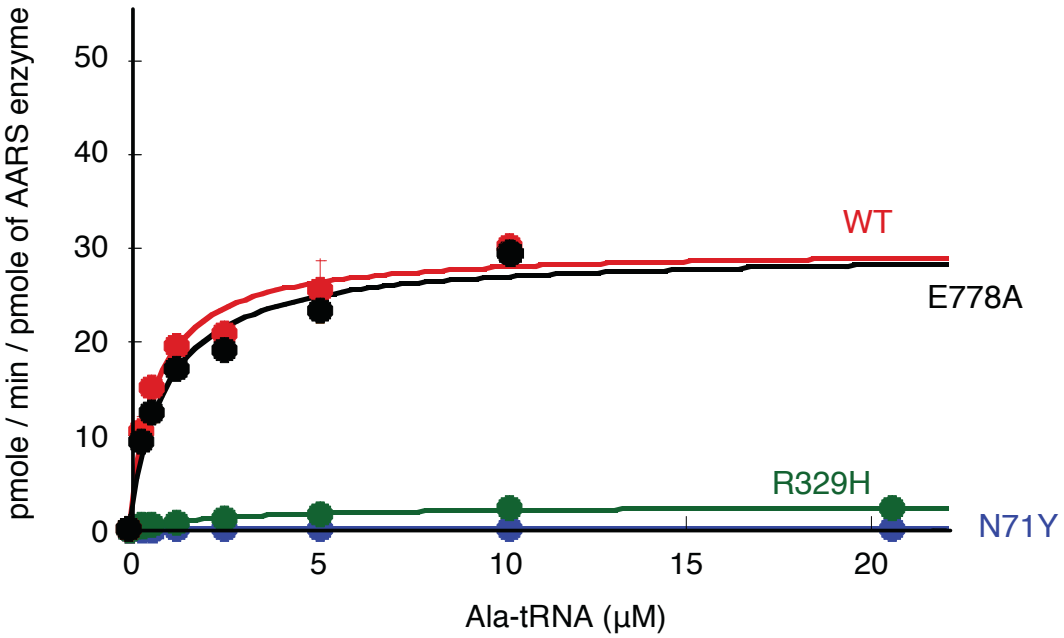

Figure 3.3 Aminoacylation Activities of Variant AARS Enzymes. Aminoacylation of $tRNA^{Ala}$ with alanine by AARS enzymes. Analysis of the rate of aminoacylation (pmole/min/pmole of enzyme) as a function of tRNA concentration for the wild-type AARS enzyme (red) and the mutants N71Y (blue), and R329H (green), and E778A (black) after fitting the data to the Michaelis-Menten equation. Values represent the average of two independent experiments, and error bars indicate the standard deviation. This work was performed by Reiko Sakaguchi and Ya-Ming Hou at Thomas Jefferson University.

Table 3.1 Aminoacylation Kinetics of AARS Protein Variants

Enzyme	K_m **(mM)**	k_{cat}**(s^{-1})**	k_{cat} **/** K_m **(mM^{-1}s^{-1})**	**Ratio to WT**
Wild-type AARS	0.70 ± 0.21	0.54 ± 0.04	0.81 ± 0.19	1
N71Y AARS	2.9 ± 0.7	0.0006 ± 0.0004	0.0002 ± 0.0001	1/4130
R329H AARS	3.0 ± 0.2	0.047 ± 0.0001	0.016 ± 0.001	1/50
T562I AARS	1.3 ± 0.3	1.13 ± 0.002	0.89 ± 0.19	1/0.9
E778A AARS	0.89 ± 0.08	0.53 ± 0.001	0.60 ± 0.05	1/1.4

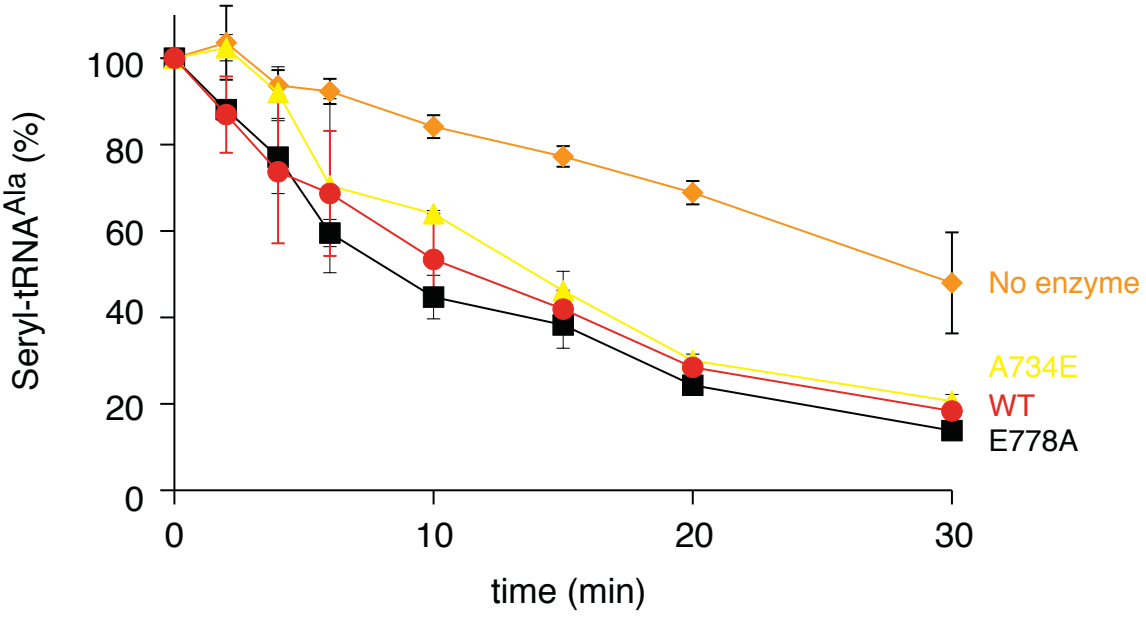

Figure 3.4 Effect of *AARS* Variants on Editing Activity. Deacylation of the incorrectly charged Ser-tRNA^{Ala} by the wild-type (red), E778A (black), and the previously-described A734E (yellow) AARS enzymes is plotted over time. The uncatalyzed deacylation (the no-enzyme reaction, indicated in orange) was run in parallel as a control for background hydrolysis. Values represent the average of two independent experiments, and error bars indicate the standard deviation. This work was performed by Reiko Sakaguchi and Ya-Ming Hou at Thomas Jefferson University.

al., 2006; Stum *et al.*, 2011). These data indicate that E778A *AARS* does not lead to diminished editing activity *in vitro*.

KARS is a bifunctional ARS enzyme that catalyzes the aminoacylation of $tRNA^{Lys}$ in the cytoplasm and mitochondria. We investigated the ability of each cytoplasmic KARS variant to catalyze the aminoacylation reaction *in vitro*. Human $tRNA^{Lys}$ was synthesized by *in vitro* transcription and used as the substrate for aminoacylation. Analysis of the catalytic efficiency (k_{cat}/K_m) of aminoacylation showed that the T623S KARS (modeling a common polymorphism) and I302M KARS variants maintain normal catalytic activity, indicating that these variants do not negatively affect aminoacylation (Table 3.2). In contrast, L133H KARS impairs enzyme activity, resulting in a ~94% reduction in the catalytic efficiency of aminoacylation relative to the wild-type KARS enzyme (Table 3.2 and Figure 3.5).

Mutant AARS and KARS Proteins do not Allow Cell Growth when Modeled in the S. cerevisiae Orthologs

Several *GARS* and *YARS* mutations have resulted in the inability to support yeast cell growth when modeled in their respective yeast orthologs (Antonellis *et al.*, 2006; Jordanova *et al.*, 2006). To further assess for mutation-associated defects in AARS enzyme function, we modeled each *AARS* variant in the S*accharomyces cerevisiae* ortholog *ALA1* (Table 3.3) and determined the ability of each *ALA1* variant to complement the deletion of the endogenous *ALA1* gene. Using tetrad dissections, we created a haploid yeast strain, with the endogenous *ALA1* gene deleted (*ala1*Δ), and

Table 3.2 Aminoacylation Kinetics of KARS Protein Variants

Enzyme	K_m (μM)	k_{cat} (s^{-1})	k_{cat}/K_m ($s^{-1}\mu M^{-1}$)	**Relative Activity**
Wild-type KARS	1.8 ± 0.9	1.4 ± 0.1	0.8	1
L133H KARS	5.8 ± 2.4	0.3 ± 0.3	0.05	0.06
I302M KARS	2.1 ± 0.8	2.7 ± 1.6	1.3	1.6
T623S KARS	3.5 ± 0.1	4.0 ± 0.7	1.1	1.4

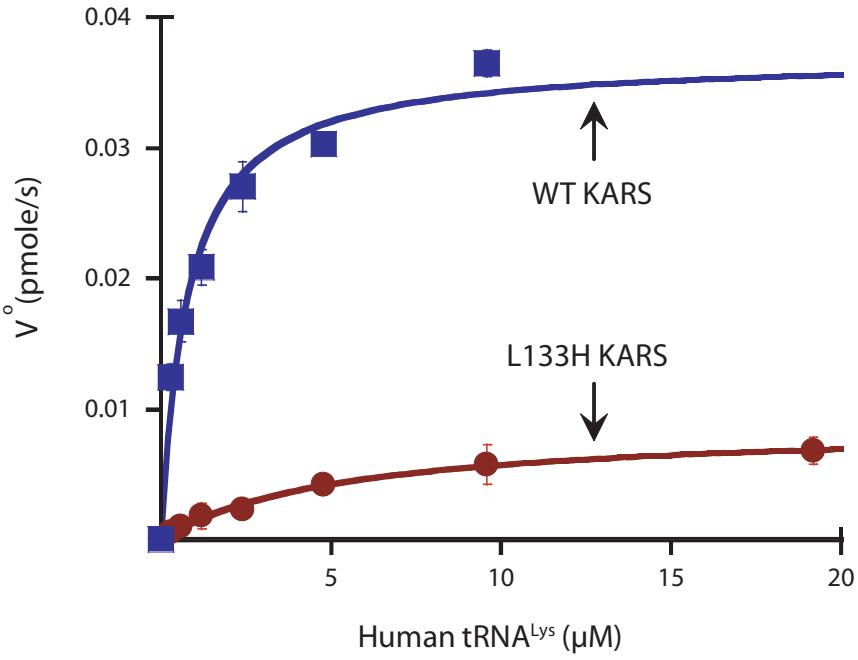

Figure 3.5 Effect of L133H *KARS* on Aminoacylation Activity. Aminoacylation of $tRNA^{Lys}$ with lysine by KARS enzymes. Analysis of the rate of aminoacylation (pmole/min/pmole of enzyme) as a function of tRNA concentration for the wild-type KARS enzyme (blue) and L133H KARS (red) after fitting the data to the Michaelis-Menten equation. Values represent the average of two independent experiments, and error bars indicate the standard deviation. This work was performed by Reiko Sakaguchi and Ya-Ming Hou at Thomas Jefferson University.

Table 3.3 Human *AARS* Variants Modeled in the Yeast Ortholog *ALA1*

Human *AARS*[1]	Yeast *ALA1*[2]
N71Y	N75Y
R329H	R329H
E778A	D771A

[1]Amino-acid coordinates correspond to GenBank accession number NP_001596.2
[2]Amino-acid coordinates correspond to GenBank accession number NP_014980.1

viability maintained via addition of a wild-type copy of *ALA1* on a *URA3*-bearing plasmid (pRS316). Experimental (wild-type and mutant) *ALA1* alleles were generated on a *LEU2*-bearing vector (pRS315) and transformed into the strain described above. The ability of each *ALA1* variant to rescue the *ala1*Δ strain was evaluated by analysis of growth on solid media containing 5-fluoroorotic acid (5-FOA). The *URA3* gene product is toxic in the presence of 5-FOA and allows selection of yeast strains in which the maintenance allele has been spontaneously lost (Boeke *et al.*, 1987). Therefore, 5-FOA selection allows analysis of the effect of the experimental alleles on yeast viability. Two experimental vectors were prepared for each mutant and five colonies from each transfection assay were evaluated. An insert-free pRS315 construct was unable to rescue the *ala1*Δ allele, whereas wild-type *ALA1* was able to fully complement the *ala1*Δ allele (Fig. 3.6). These data are consistent with *ALA1* being an essential gene, and the wild-type experimental *ALA1* vector harboring a functional allele, respectively. The E778A *ALA1* allele allowed growth in a manner consistent with wild-type *ALA1*. In contrast, N71Y *ALA1* and R329H *ALA1* were unable to rescue the *ala1*Δ allele. To determine if the E778A *ALA1* variant results in a more subtle loss-of-function effect, we evaluated the growth of the E778A *ALA11* haploid strain in liquid media lacking leucine (to select for the *LEU2*-bearing pRS315 vector expressing E778A *ALA1*) by measuring the optical density at 600 nm ($O.D._{600}$) over a 24 hour period. These studies failed to reveal an overt growth defect in the E778A *ALA1* strain compared to the wild-type *ALA1* strain (Fig. 3.7). Combined, these data indicate that N71Y AARS and R329H AARS enzymes display reduced functional activity when modeled in the *S. cerevisiae* ortholog *ALA1*.

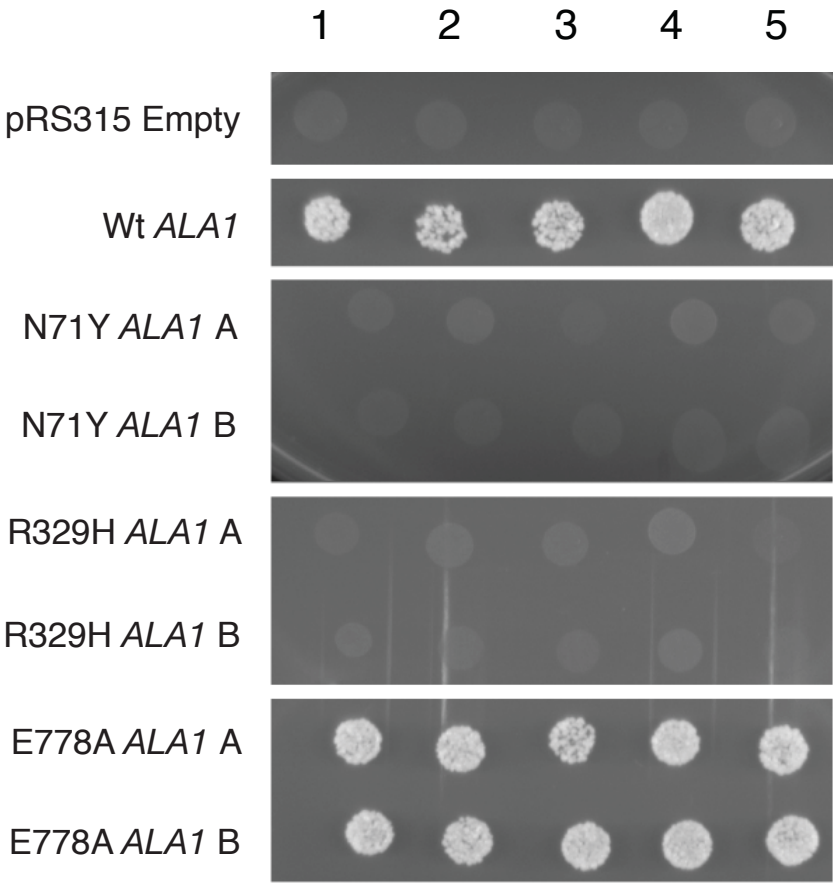

Figure 3.6 Genetic Complementation of *ALA1* Deletion in *S. cerevisiae*. Five representative cultures of each yeast strain (indicated along the top of the figure) were inoculated and grown on solid growth medium containing 5-FOA. Each strain was previously transfected with a vector containing no insert (pRS315 Empty), wild-type *ALA1* (Wt *ALA1*), or the indicated mutant form of *ALA1* that modeled a human *AARS* mutation (see Table 3.3). Two independently generated mutant-bearing constructs were analyzed (indicated as 'A' and 'B' on the left side of the panel). Before inoculating on 5-FOA-containing medium, each strain was resuspended in 100-µL water, then diluted 1:10.

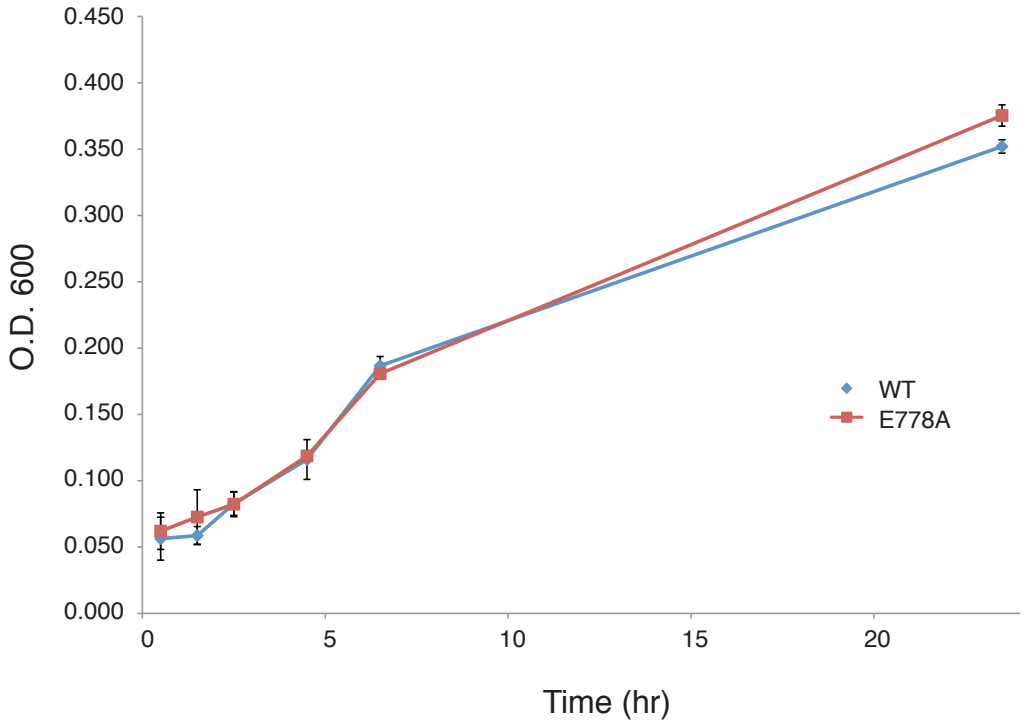

Figure 3.7 Growth Curve Analysis of the E778A *ALA1* Haploid Strain. Wild-type and E778A *ALA1* stains were inoculated in liquid growth media lacking leucine and allowed to incubate overnight. Each strain was subsequently diluted to O.D.600=0.05 at time=0. Growth measurements for the wild-type strain (depicted in blue) and for the E778A *ALA1* strain (depicted in red) were taken at each time point, as indicated. Error bars represent the standard deviation of three separate measurements.

Disease-associated *YARS* variants demonstrate a dominant-negative effect when modeled in the yeast ortholog *TYS1* (Jordanova *et al.*, 2006). To test N71Y *ALA1*, R329H *ALA1*, and E778A *ALA1* for a dominant-negative effect, we performed growth curve analysis on the respective haploid yeast strains (described above) in media lacking leucine and uracil, before selection on 5-FOA (*i.e.*, strains that harbor two *ALA1* expression constructs: either two wild-type *ALA1* constructs, or one wild-type *ALA1* construct and one mutant *ALA1* construct) (Fig. 3.8). Similar experiments were performed on strains expressing the R329H *ALA1* variant from a strong yeast promoter (*ADH1*) (Fig. 3.9). No differences were seen in growth patterns between strains expressing a mutant *ALA1* variant and those expressing wild-type *ALA1* in either experiment. Therefore, ALA1 mutant enzymes do not appear to exert a dominant-negative effect on the wild-type enzyme.

To assess *KARS* mutations for loss-of-function defects *in vivo*, we modeled each *KARS* variant in the yeast ortholog (*KRS1*; Table 3.4) and determined the effect on yeast cell viability. A haploid yeast strain with the endogenous *KRS1* gene deleted (*krs1*Δ), and viability maintained via transformation with a wild-type copy of *KRS1* on a *URA3*-bearing vector (pRS316), was created using tetrad dissection. Experimental alleles were generated on a *LEU2*-bearing vector (pRS315), transformed into the above strain, and viability was assessed by analysis of yeast growth on 5-FOA media. The wild-type *KRS1* vector supported yeast growth, while an insert-free pRS315 construct did not, consistent with our experimental vector harboring a functional *KRS1* allele, and with *KRS1* being an essential gene, respectively (Fig. 3.10). The L133H *KRS1* and I302M *KRS1* variants allowed growth in a manner consistent with wild-type *KRS1*. In contrast, the Y173SfsX7

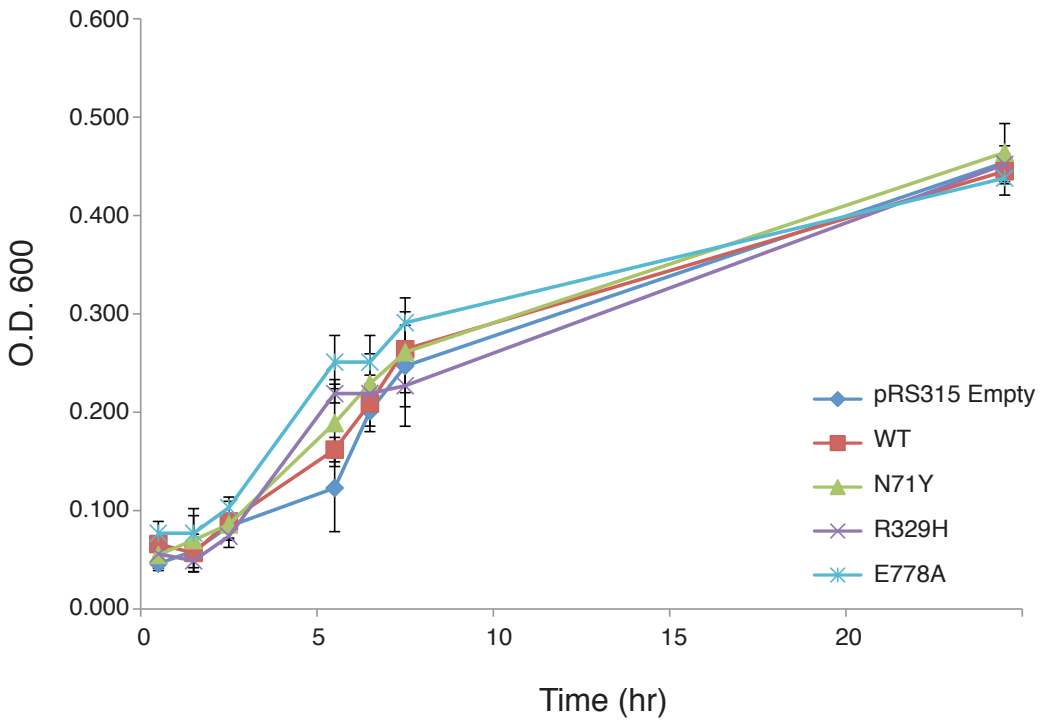

Figure 3.8 Growth Curve Analyses Monitoring the Effect of Expressing *ALA1* Variants in the Presence of Wild-Type *ALA1*. Haploid yeast strains (containing a wild-type *ALA1* allele on a pRS315 vector) expressing the indicated allele, were inoculated in liquid growth media, allowed to incubate overnight and diluted to O.D.600=0.05 at t=0. Growth measurements for strains containing the empty vector (depicted in blue), the wild-type strain (depicted in red), the N71Y strain (depicted in green), the R329H strain (depicted in lavender), and the E778A *ALA1* strain (depicted in aqua) were taken at each time point, as indicated. Error bars represent the standard deviation of three separate measurements.

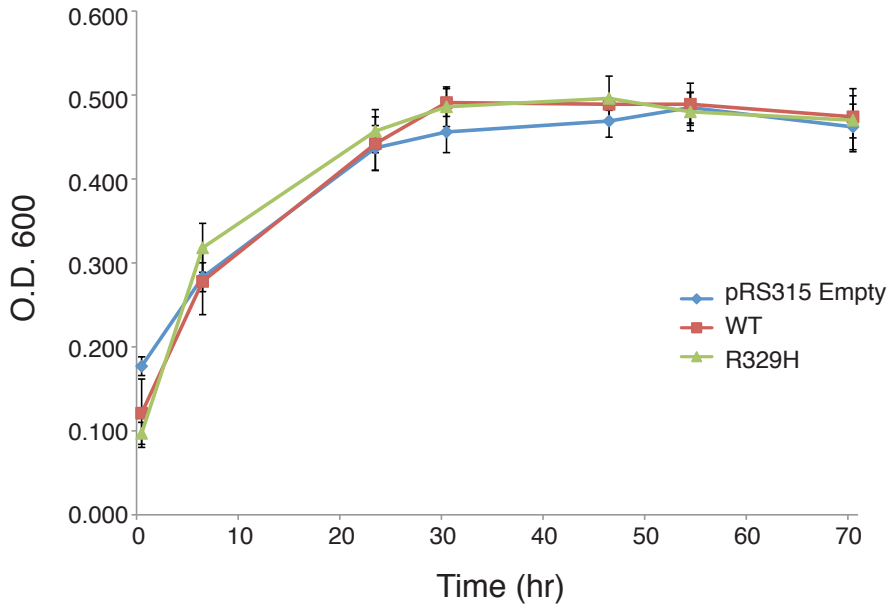

Figure 3.9 Growth Curve Analyses Monitoring the Effect of Overexpressing R329H *ALA1* in the Presence of Wild-Type *ALA1*. Haploid yeast strains (containing a wild-type *ALA1* allele on a pRS315 vector) overexpressing the indicated allele, were inoculated in liquid growth media, allowed to incubate overnight and diluted to O.D.600=0.100 at t=0. Growth measurements for strains containing the empty vector (depicted in blue), overexpressing the wild-type allele (depicted in red), or overexpressing the R329H allele (depicted in green) were taken at each time point, as indicated. Error bars represent the standard deviation of three separate measurements.

Table 3.4 Human *KARS* Variants Modeled in the Yeast Ortholog *KRS1*

Human *KARS*[1]	Yeast *KRS1*[2]
L133H	N103H
Y173SfsX7	H146FfsX12
I302M	I277M

[1]Amino-acid coordinates correspond to GenBank accession number NP_001123561.1
[2]Amino-acid coordinates correspond to GenBank accession number NP_010322

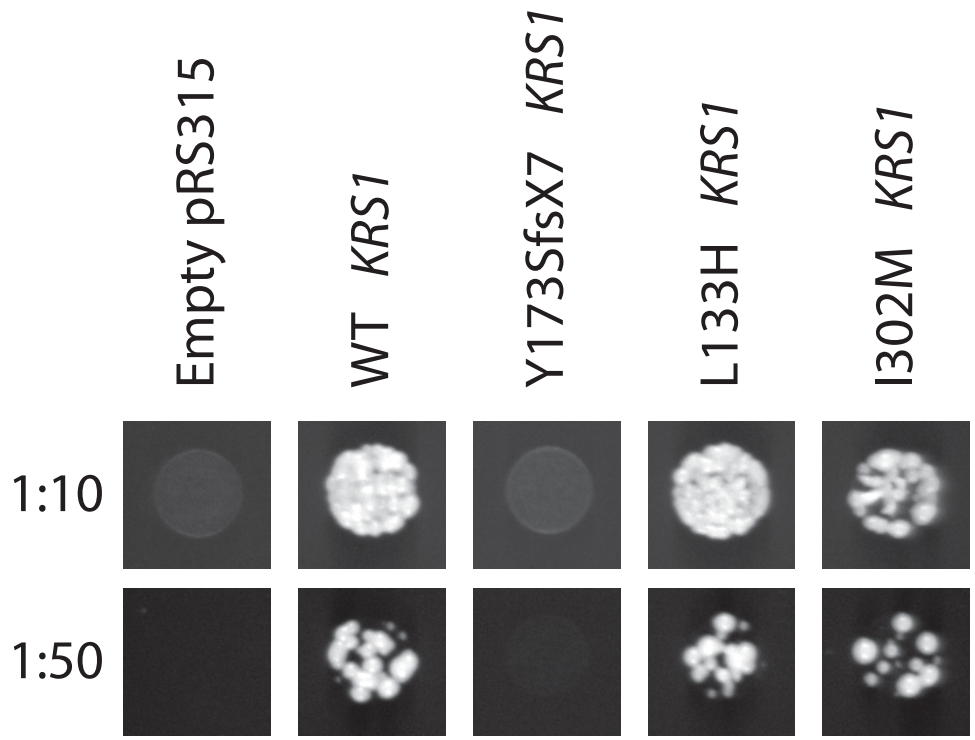

Figure 3.10 Genetic Complementation of *KRS1* Deletion in *S. cerevisiae*.
Representative cultures of the indicated yeast strains were inoculated and grown on solid growth medium containing 5-FOA. Each strain was previously transfected with a vector containing no insert (pRS315), wild-type *KRS1* (WT *KRS1*), or the indicated mutant form of *KRS1* that modeled a human *KARS* mutation (see Table 3.4). Before inoculating on 5-FOA-containing medium, each strain was resuspended in 100-μL water then diluted 1:10 or 1:50 in water.

KRS1 allele did not complement the *krs1*Δ allele (Fig. 3.10). To determine if L133H *KRS1* or I302M *KRS1* result in a subtle loss-of-function effect, we evaluated the L133H *KRS1* and I302M *KRS1* haploid strains by measuring the growth ($O.D._{600}$) of each strain in liquid medium lacking leucine, over a period of 72 hours. These studies did not reveal an overt growth defect for either L133H *KRS1* or I302M *KRS1,* when compared to the wild-type *KRS1* strain (Fig. 3.11). Together, these data suggest that Y173SfsX7 *KARS* is a null allele when modeled in the yeast ortholog *KRS1*.

To determine if the L133H *KRS1*, Y173SfsX7 *KRS1*, and I302M *KRS1* alleles elicit a dominant-negative effect on the endogenous *KRS1* allele, we performed growth curve analyses on the respective haploid yeast strains (described above) in liquid growth medium lacking uracil and leucine, before selection on 5-FOA (*i.e.*, strains that harbor two *KRS1* expression constructs: two wild-type *KRS1* construct, or one wild-type *KRS1* construct and one mutant *KRS1* construct) (Fig. 3.12). No differences in growth rates between strains expressing a mutant *KRS1* variant and those expressing wild-type *KRS1* were observed. These data suggest that KRS1 mutant enzymes do not exert a dominant-negative effect on the wild-type KRS1 enzyme.

Discussion

This chapter describes the functional consequences of *AARS* and *KARS* mutations identified in patients with CMT disease. Here, we present functional data implicating the N71Y *AARS* and R329H *AARS* mutations in CMT2N, and the L133H *KARS* and Y173SfsX7 *KARS* mutations in CMTRIB. We established that the N71Y *AARS*, R329H

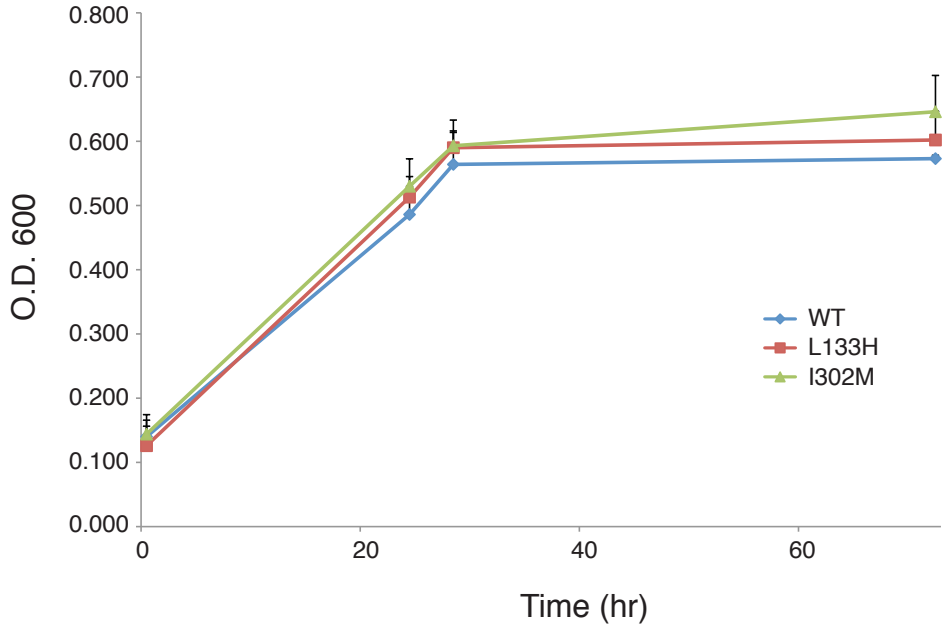

Figure 3.11 Growth Curve Analysis of *KRS1* Haploid Strains. Wild-type, L133H, and I302M haploid *KRS1* stains were inoculated in liquid growth media, allowed to incubate overnight and diluted to O.D.600=0.100 at time=0. Growth measurements for the wild-type strain (depicted in blue), the L133H *KRS1* strain (depicted in red), and the I302M *KRS1* strain were taken at each time point, as indicated. Error bars represent the standard deviation of three separate measurements.

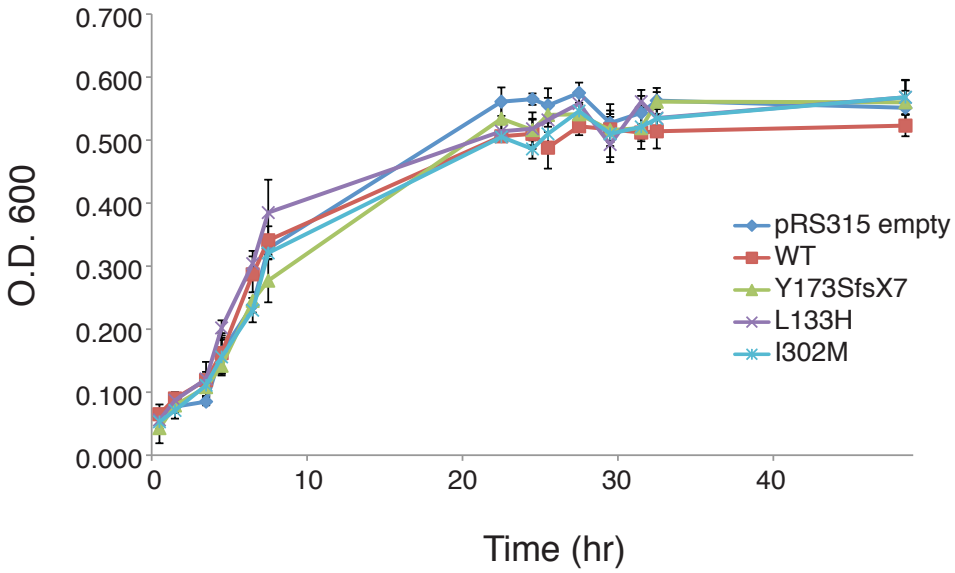

Figure 3.12 Growth Curve Analyses Monitoring the Effect of Expressing *KRS1* Variants in the Presence of Wild-Type *KRS1*. Haploid yeast strains (containing a wild-type *KRS1* allele on a pRS315 vector) expressing the indicated allele, were inoculated in liquid growth media, allowed to incubate overnight and diluted to O.D.600=0.05 at time=0. Growth measurements for strains containing the empty vector (depicted in blue), the wild-type strain (depicted in red), the Y173SfsX7 strain (depicted in green), the L133H strain (depicted in lavender), and the I302M *KRS1* strain (depicted in aqua) were taken at each time point, as indicated. Error bars represent the standard deviation of three separate measurements.

AARS, and L133H *KARS* mutations result in impaired tRNA charging activity *in vitro*. While these mutations result in loss of tRNA charging activity, it is important to note that the aminoacylation assay employed here tests the ability of mutant ARS homodimers to perform tRNA charging function, as wild-type monomers are not included in the aminoacylation reaciton. In order to determine if wild-type:mutant ARS heterodimers are able to effectively charge tRNA, sequential immunoprecipitation of wild-type and mutant subunits prior to performing the aminoacylation assay is required . These studies will provide a more accurate assessment of the effect of ARS mutations on the aminoacylation activity of wild-type:mutant heterodimers in patients with dominant CMT disease. We were also able to determine that the N71Y *AARS*, R329H *AARS*, and Y173SfsX7 *KARS* mutations result in the inability to support yeast cell growth. The yeast viability assay allows for the interrogation of loss-of-function and dominant-negative effects on yeast growth *in vivo.* While the yeast viability assay is an excellent model for determining the effect of ARS mutations in the presence or absence of a wild-type copy of the ARS gene in question, this assay is unable to aid in the determination of the effects of ARS mutations on axons. The evaluation of ARS mutations in a multicellular model system with a well-defined neuronal system is required to fully understand the effects of ARS mutations on peripheral nerve axons (see Chapter 4). We did not identify mislocalization defects for any of the ARS mutations analyzed following overexpression of each mutant ARS protein in the MN-1 cell line. We do not find it surprising that localization defects were not detected in this assay, as each disease-associated ARS mutation we identified resulted in a loss-of-function characteristic in aminoacylation

and/or yeast viability assays. While none of the mutant ARS enzymes evaluated here result in localization defects, it remains unclear if mutant ARS enzymes mislocalize or accumulate after several decades of life. Evaluation of the localization of ARS enzymes in nerve biopsies from patients with CMT disease in the fourth or fifth decade of life or in the nerves of aged animals from an appropriate model system will be required to fully evaluate the effect of each disease-associated ARS mutation on localization. Together, the functional data evaluating the effect of ARS mutations on localization, aminoacylation, and yeast viability provide further evidence towards the critical role ARS enzymes play in peripheral nerve health.

The data presented in this chapter also provide evidence for genotype-phenotype correlations in ARS-related CMT disease. While patients with missense, loss-of-function *AARS* mutations display dominant axonal CMT disease with the classical CMT phenotype (along with variable deafness), the patient with missense and frameshift loss-of-function *KARS* mutations is affected with recessive intermediate CMT disease along with developmental delay, self-abusive behavior, dysmorphic features, and a vestibular Schwannoma. Together, these data indicate that patients compound heterozygous for ARS mutations may have a more severe clinical phenotype compared to patients heterozygous for ARS mutations. This may be due to a more dramatic loss of aminoacylation activity in patients compound heterozygous for ARS mutations. Further mutation screens will be required to determine if additional patients exist with homozygous or compound heterozygous ARS mutations, and if these patients exhibit more severe phenotypes.

To date, four ARS genes have been implicated in CMT disease with an axonal pathology (*GARS, YARS, AARS,* and *KARS*) (Antonellis *et al.*, 2003; Jordanova *et al.*, 2006; Latour *et al.*, 2010; McLaughlin *et al.*, 2010). The encoded enzymes are either bifunctional (GARS and KARS charge tRNA in the cytoplasm and mitochondria), or charge tRNA specifically in the cytoplasm (YARS and AARS). In the case of *AARS*, *GARS*, and *YARS*, the phenotypes are autosomal dominant and the mutations are either missense or in-frame deletions. In the case of *KARS*, the phenotype appears autosomal recessive and the mutations identified include a missense change and frame-shift mutation. Each disease-associated ARS mutation identified to date has been associated with a loss-of-function, as observed by impaired tRNA charging, the inability to complement deletion of the corresponding yeast ortholog, and/or abnormal localization of the ARS enzyme (with the exception of E71G *GARS*) (Antonellis *et al.*, 2006; Froelich and First, 2011; Jordanova *et al.*, 2006; McLaughlin *et al.*, 2012; McLaughlin *et al.*, 2010; Nangle *et al.*, 2007; Storkebaum *et al.*, 2009; Xie *et al.*, 2007). Importantly, these loss-of-function characteristics have not been observed upon analysis of non-pathogenic ARS variants (McLaughlin *et al.*, 2012; McLaughlin *et al.*, 2010). Combined, these observations suggest that there is an impaired tRNA charging component to the pathophysiology of ARS-related CMT disease. It is possible that ARS mutations lead to a reduction in aminoacylation activity at a level that breaches a threshold required by peripheral neurons, particularly those with long axons.

The data presented herein are consistent with two molecular mechanisms by which an aminoacylation threshold could be breached in peripheral nerve axons: a dominant-negative effect, in which mutant ARS monomers dimerize with, and antagonize wild-type ARS monomers, and a severe loss of aminoacylation activity, caused by loss-of-function and null mutations working in concert within the same patient. A dominant-negative effect could be the pathogenic mechanism resulting from *AARS, GARS*, and *YARS* mutations. The presence of wild-type and mutant ARS monomers in a single patient would lead to three species of ARS dimers, including wild-type:wild-type, wild-type:mutant, and mutant:mutant. In the event that the wild-type:mutant, and mutant:mutant dimers are non-functional, a dominant-negative effect could reduce charging capacity to ≤33% to that of wild-type. A dominant-negative effect is supported by findings that: (1) the majority of ARS-related CMT phenotypes are dominant; (2) most ARS mutations are missense amino-acid changes; (3) all ARS enzymes implicated in CMT dsease to date act as oligomers; and (4) haploinsufficiency of *Gars* does not cause axonopathy in a *Gars* mouse model (Antonellis *et al.*, 2003; Jordanova *et al.*, 2006; Latour *et al.*, 2010; McLaughlin *et al.*, 2012; McLaughlin *et al.*, 2010; Seburn *et al.*, 2006). The presence of loss-of-function and null mutations in a single patient illustrates another genetic mechanism by which ARS mutations may lead to a breach in the required level of aminoacylation activity in PNS axons. BAB564, a compound heterozygous patient with loss-of-function and null mutations, is predicted to suffer from a severe depletion of Lys-tRNA^{Lys}. These two mutations may mimic a dominant-negative effect by severely reducing aminoacylation activity at the enzymatic level. Together, *GARS,*

YARS, AARS, and *KARS* mutations indicate that breaching an aminoacylation threshold required by peripheral neurons may be a central component to ARS-related CMT disease.

While the data presented here provide *in vitro* and *in vivo* evidence that defective tRNA charging may be a central component to ARS-related peripheral neuropathy, we cannot rule out toxic gain-of-function, abnormal axonal transport, a loss of a yet undiscovered neuronal-specific secondary function, or interplay between these various pathogenic mechanisms. Moving forward, it will be important to further interrogate the functional effects of *GARS, YARS, KARS,* and *AARS* mutations, especially in the context of the axon, to aid in the determination of the precise molecular pathology by which these mutations lead to CMT disease. The next chapter of this thesis focuses on the determining the effect of expressing a mutant ARS enzyme in the neurons of a multi-cellular model system.

CHAPTER 4

A *C. elegans* Model System for Assessing ARS-Mediated Neurotoxicity

The data presented in this chapter is currently being prepared for a future manuscript and has not been published. Without exception, the author performed all of the work presented in this chapter. Asim Beg provided worm strains, laboratory supplies, technical assistance, and instruction for all of the assays in this chapter.

Introduction

This thesis highlights the role of aminoacyl-tRNA synthetase (ARS) gene mutations in patients with CMT disease. Mutational analyses of the 37 genes encoding ARS enzymes continue to produce potentially novel variants with unknown pathogenic consequences. Many of these variants occur in sporadic cases, or in families where limited genetic information is available, making it difficult to implicate these variants on a genetic basis. Furthermore, the localization, aminoacylation, and yeast viability assays we currently employ to assess for aminoacylation defects are not capable of determining the effect of ARS mutations in the context of the axon, which is problematic given that each disease-associated ARS mutation discovered to date results in an axonal CMT phenotype. Together, these obstacles present the need for a rapid, tractable, *in vivo* model system capable of distinguishing between pathogenic and non-pathogenic variants in axons. Creation of this model system will aid in the evaluation of the pathogenicity of newly

identified ARS variants, and will provide a platform for discovering proteins and pathways involved in ARS-related peripheral neuropathy.

Here, we utilize a *Caenorhabditis elegans* model system as a resource for studying the pathogenicity of ARS mutations in neurons. The *C. elegans* model system possesses several noteworthy features including: a short, definitive life-span; the ability to express transgenes in single or multiple copies; a well characterized, non-myelinated neuronal system allowing for specific interrogation of axonal defects; and the ability to synchronize a population of worms to definitive developmental stages for the purpose of teasing out developmental versus degenerative deficits.

To validate the use of *C. elegans* as model system for evaluating ARS-related peripheral neuropathy, we chose to create a worm model assessing the R329H *AARS* mutation and the G931S *AARS* polymorphism in the *C. elegans* ortholog *ars-2*. The R329H *AARS* mutation is the most common CMT-associated ARS mutation identified to date, having been discovered in three unrelated families with CMT2N (Chapter 2), and results in loss-of-function defects in both aminoacylation and yeast viability assays (Chapter 3) (Latour *et al.*, 2010; McLaughlin *et al.*, 2012). The G931S *AARS* variant is a common polymorphism, present at a frequency of 0.0099 in the NINDS cohort (see Table 2.1), that fully supports yeast cell growth (data not shown). Because Arg329 and Gly931 are conserved in *C. elegans,* we utilized the *C. elegans* ortholog *ars-2* to create transgenic worm strains overexpressing either wild-type *ars-2*, R329H *ars-2,* or G931S *ars*-2 in GFP-positive γ-aminobutyric acid (GABA)ergic neurons.

The GABAergic nervous system consists of 26 GABAergic neurons, including 19 inhibitory (D-type) GABA motor neurons that project commissural axons from neuronal cell bodies on the ventral side of the worm to the dorsal nerve cord. The D-type GABA neurons are composed of 6 DD and 13 VD motor neurons, which innervate the dorsal and ventral body wall muscles in the adult worm, respectively. The D-type GABA motor neurons are required for proper locomotor function; when acetylcholine (ACh) release results in contraction of the body wall muscle on one side of the worm, GABA release results in relaxation on the other side of the worm, allowing the worm to bend. The *C. elegans* nervous system allows for simplified interrogation of morphological defects and motor nerve function, and has previously been used to evaluate other neurodegenerative disorders including Parkinson's diseases, Alzheimer's disease, amyotrophic lateral sclerosis and Huntington's disease (Calahorro and Ruiz-Rubio, 2011; Dimitriadi and Hart, 2010).

To assess for neurotoxic effects associated with R329H *ars-2*, we will visualize the GABAergic neuron morphology of each strain in adult and developing worms, and determine the effect of each *ars-2* allele on thrashing behavior. Based upon the dominant inheritance pattern identified in patients with CMT2N, and the fact that most patients affected with CMT2N report clinical symptoms in their mid-20's, we expect R329H *ars-2* to act in a dominant manner over endogenous *ars-2* alleles, and to result in a degenerative defect in GABAergic commissural axons; that is, we expect commissural axons to form normally during development and subsequently degenerate in older, adult

worms. We also hypothesize that overexpression of R329H *ars-2* will result in deficits in GABA motor neuron activity, leading to a reduction in thrashing behavior.

The creation of a *C. elegans* model system for assessing the toxicity of ARS mutations in neurons will allow us to monitor the morphological and motor consequences of ARS mutations in GABA commissural axons. This model organism will be validated using pathogenic and non-pathogenic ARS variants and will aid in determining the pathogenicity of potentially novel ARS variants identified in patients with CMT disease in the future. Importantly, this model system will also provide a platform for further investigation of the overarching functional mechanisms of ARS-related peripheral neuropathy.

Materials and Methods

cDNA Cloning and Mutagenesis

The *C. elegans ars-2* coding region was PCR amplified using L4 *C. elegans* cDNA and PCR primers containing flanking *att*B1 (forward) and *att*B2 (reverse) sequences to allow cloning into the pDONR221 vector using BP clonase (Invitrogen, Carlsbad, CA) (Appendix A8). Mutant and polymorphic clones were generated using the Quickchange II XL mutagenesis kit (Agilent, Santa Clara, CA) along with appropriate mutation bearing oligonucleotides (Appendix A9). Subsequently, the *ars-2* locus was subcloned into a gateway-compatible vector downstream of the glutamic acid decarboxylase gene (*unc-25*) promoter and upstream of the nucampholin gene (*let-858)* termination signal (Jin *et al.*, 1999). All constructs were verified by fully sequencing the open reading frame.

Propagation and Maintenance of Worm Strains

All *C. elegans* strains were maintained on nematode growth medium (NGM) agar [3g NaCl, 17g bacto-agar, 2.5g bacto-peptone, and 1mL cholesterol in 1L H_2O]. NGM plates were seeded with 500-µl OP50 bacteria and allowed to grow overnight at room temperature before use. The *oxIs-12* strain, which expresses GFP under the direction of the GABA vesicular transporter gene (*unc-47)* promoter [P*unc-47*::GFP], was used as the parental strain for all experiments in this chapter (McIntire *et al.*, 1997). The *oxIs-12* strain was routinely maintained by chunking, the process of removing a chunk of agar from an exhausted plate of worms and placing it on a new seeded NGM plate. Experimental worm strains were selected with the use of a co-injected pharyngeal marker which expresses mCherry under the direction of the myosin-3 gene (*myo-3)* promoter [P*myo-3*::mCherry]. P*myo-3*::mCherry expression is limited to the pharynx, and therefore does not compromise interrogation of GABAergic motor neurons. Maintenance of experimental strains was achieved by alternating chunking with the enrichment of P*myo-3*::mCherry-positive worms (*i.e.,* worms with a red pharynx). Experimental strains were enriched by transferring 10-20 positive worms to new plates and allowing the worms to produce offspring.

Microinjection

A Koehler illuminated Leica DMI6000B microscope (Leica Microsystems Inc., Buffalo Grove, IL) fitted with a N_2 gas controlled micromanipulator set at 30 psi was used for all microinjection procedures. A 10-µl injection mixture consisting of 1µg of either wild-

type, R329H, or G931S P*unc25*::*ars-2*::T*let858* and 25ng of P*myo3*::mCherry was prepared and loaded into a glass capillary needle. The needle was loaded onto the micromanipulator and broken to allow flow through the needle. Young adult *oxIs-12* worms were immobilized in halocarbon oil on a dried 2% agarose bed. The injection needle, positioned at a 45° angle towards the syncytial gonad arm of the worm, was used to penetrate the gonad and deliver the DNA solution until the gonad became flooded with the DNA mixture. The needle was subsequently removed and a drop of M9 buffer [5.8 grams Na_2HPO_4, 3 grams KH_2PO_4, 0.5 grams NaCl, and 1 gram of NH_4Cl in 1L H_2O] was placed on top of the worm. The worm was removed from the buffer and placed onto a 60 mm seeded NGM agarose plate and allowed to recover for 1 hour. Each injected F_0 worm was then placed on a separate 35 mm seeded NGM plate and allowed to give rise to F_1 progeny. The F_1 progeny were scored for the presence of a red pharynx, indicating successful transmission of the P*myo3*::mCherry marker. Positive F_1 progeny were placed on separate 35 mm seeded NGM plates and allowed to give rise to F_2 progeny. Two positive F_2 worms were used to generate stable transgenic lines for each genotype.

Synchronization and Aging of Worms

Synchronization of worms was achieved via the addition of 2 mL M9 buffer to a plate of worms at ~50% capacity. After gently swirling the plate, all worms were discarded by aspirating the M9 buffer from the plate. Any remaining worms were removed using a sterile pick. This process leaves only embryos behind, which are then allowed to develop further. Synchronization was used to generate worms at three larval stages: larval stage 1 (L1), larval stage 2 (L2), and larval stage 3 (L3). L1 worms were allowed to develop 9

hours after synchronization, L2 worms were allowed to develop 21 hours after synchronization, and L3 worms were allowed to develop 29 hours after synchronization. Before the gonads are completely developed, at larval stage 4 (L4), the vulva appears as a distinct white crescent moon shape and is devoid of oocytes. Therefore, L4 worms were chosen by the absence of eggs in the gonad. One-day-old (1D) adult worms were generated by allowing L4 worms to develop for ~24 hours, while four-day-old (4D) adult worms were generated by allowing L4 worms to develop for ~96 hours.

Confocal Microscopy and Image Analysis

Representative confocal images of each worm strain were obtained using a Nikon A1R-A1 confocal microscope (Leica Microsystems Inc., Buffalo Grove, IL) to produce a series of z-stack images for each worm. Each series of images was used to create a maximum z-stack projection using Image J software (Abramoff *et al.*, 2004).

GABA Neuron Phenotyping

The *oxIs-12* and experimental strains were scrutinized for gross morphological defects by analyzing GFP-positive GABA neurons in each strain using a Leica DMI6000B microscope (Leica Microsystems Inc., Buffalo Grove, IL). Morphological defects were defined as failure of the commissural axon to reach the dorsal nerve cord, horizontal branching of the commissural axon, and discontinuation of the GABAergic dorsal nerve cord.

Thrash Assays

Well-fed worms of the desired stage were placed into 80-µl room temperature M9 buffer in individual wells of a 96-well microtiter plate containing 100-µl solidified 1% agar at the bottom of each well. Each worm was allowed to equilibrate in the buffer for 2 minutes followed by 2 minutes of imaging. Worms were filmed using a 2 Megapixel Leica DFC340 FX camera attached to a Leica M165 C microscope (Leica Microsystems Inc., Buffalo Grove, IL), which captured 8-bit resolution images at 1 frame ms^{-1} using Leica Application Suite Advanced Fluorescence imaging software. Movies were stored in audio video interleave (AVI) format and analyzed at ½X speed using QuickTime Player. A thrash was counted anytime the head of the worm crossed the mid-line axis. Excel was used to record the number of thrashes during each two-minute period, and these counts were used to obtain a mean one-minute thrash count. The Student's t-test was used to determine if there was a mean difference in the number of thrashes amongst genotypes.

Results

R329H ars-2 Leads to Morphological Defects in GABAeric Motor Neurons

As outlined in the introduction, the *C. elegans* GABA nervous system consists of 26 GABA neurons, including 19 inhibitory (D-type) GABA motor neurons (Figure 4.1). The D-type GABA commissural axons project from neuronal cell bodies, located on the ventral side of the worm, to the dorsal nerve cord, and are composed of 6 DD and 13 VD motor neurons, which innervate the dorsal and ventral body wall muscles in the adult worm, respectively (Figure 4.1).

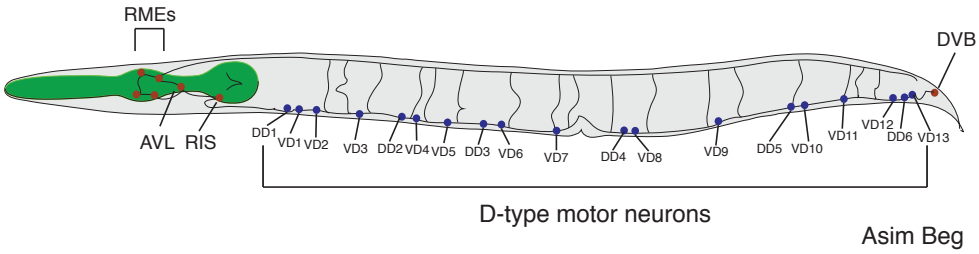

Figure 4.1 The *C. elegans* GABA Nervous System. A schematic drawing of the 26 GABAergic neurons. The pharynx is depicted in green with the anterior side of the worm facing left and the dorsal side of the worm facing up. The non-inhibitory GABA neuronal cell bodies are depicted in orange (4 RMEs, AVL, RIS, and DVB) while the 19 inhibitory (D-type) GABA neuronal cell bodies are depicted in blue with their commissural axons projecting ventral to dorsal.

We sought to determine if overexpression of R329H *ars-2* in *C. elegans* GABAergic motor neurons would have an effect on the morphology of D-type commissural axons. Therefore, we cloned wild-type *ars-2*, R329H *ars-2*, and G931S *ars-2* (a non-pathogenic variant with a frequency of 0.0099 in the NINDS cohort; see Table 2.1) downstream of the glutamic acid decarboxylase gene (*unc-25*) promoter and injected each construct into *oxIs-12* worms (Table 4.1) (Jin *et al.*, 1999). The *oxIs-12* strain is a *C. elegans* strain with an integrated transgene that expresses GFP under the control of the GABA vesicular transporter gene (*unc-47)* promoter, allowing for visualization of all GABA neurons and their commissures (McIntire *et al.*, 1997). We analyzed all 19 D-type motor neurons, along with the dorsal and ventral nerve cords in each strain, to assess for gross morphological abnormalities using fluorescence microscopy. Overexpression of wild-type *ars-2* and G931S *ars-2* resulted in GABAergic neuronal morphology comparable to *oxIs-12* worms (Figure 4.2). Specifically, the dorsal and ventral nerve cords were both intact and each D-type GABA commissural axon projected from its neuronal cell body on the ventral side of the worm and spanned to the dorsal nerve cord. In contrast, overexpression of R329H *ars-2* led to significant GABA motor neuron morphological defects including failure to reach the dorsal nerve cord, horizontal branching, and discontinuation of the GABAergic dorsal nerve cord (Figures 4.2 and 4.3). To quantify the percentage of R329H *ars-2* worms that exhibited these defects, we imaged 100 worms from each genotype at larval stage 4 (L4), one-day-old adult (1D), and four-day-old adult (4D) developmental stages. While ≥30% of R329H *ars-2* worms displayed abnormal GABA motor neuron morphological phenotypes at all stages examined, *oxIs-12*, wild-type *ars-2*, and G931S *ars-2* worms rarely displayed any morphological defects

Table 4.1 Human *AARS* Variants Modeled in the *C. elegans* Ortholog *ars-2*

Human *AARS*[1]	*C. elegans ars-2*[2]
R329H	R329H
G931S	G935S

[1]Amino-acid coordinates correspond to GenBank accession number NP_001596.2
[2]Amino-acid coordinates correspond to GenBank accession number NP_491281.1

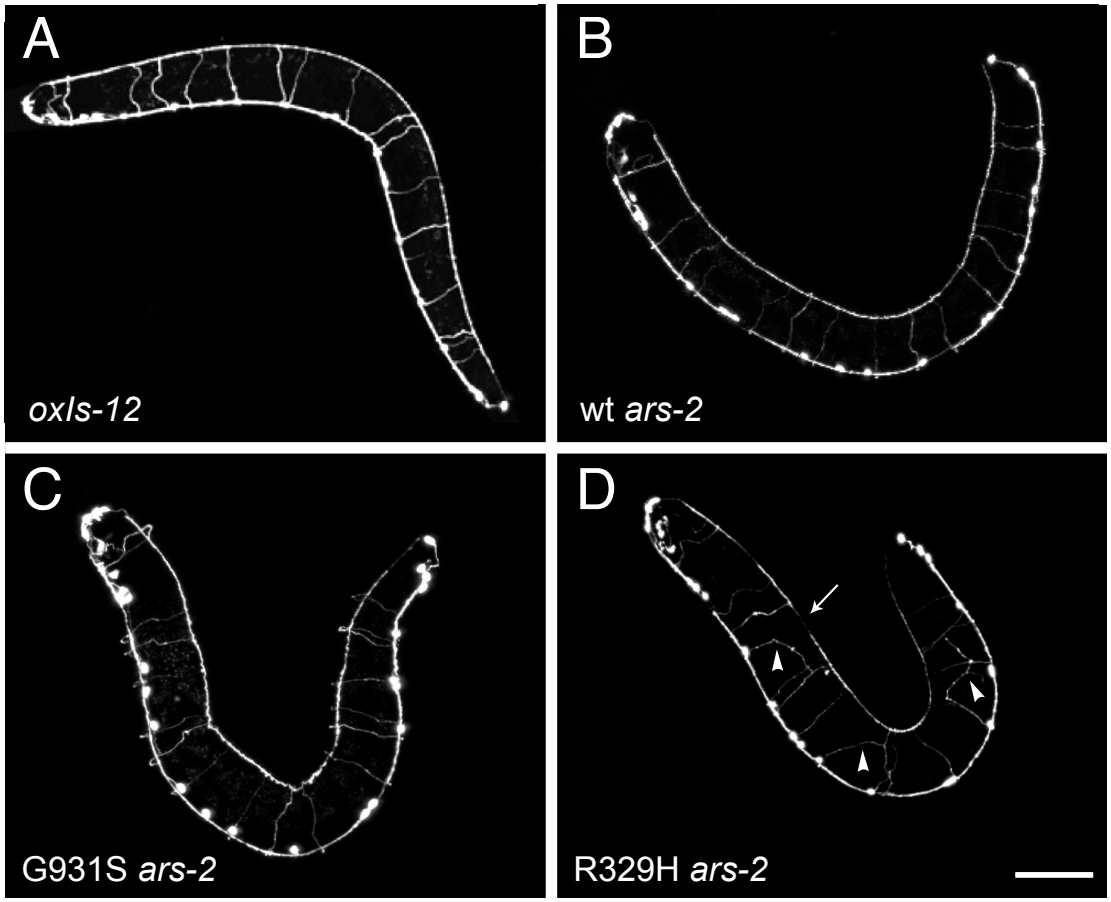

Figure 4.2 Phenotyping of P*unc-25::ars-2::*T*let-858* Worms. Confocal images of representative animals from each strain are depicted with the anterior side of the worm facing left and the dorsal side of the worm facing up. **A:** Control *oxIs-12* (P*unc*-47::GFP) animals display a stereotypical pattern featuring prominent neuronal cell bodies along the ventral nerve cord projecting GABA commissural neurons to the dorsal spinal cord. Overexpression of each *ars-2* variant, under control of the *unc-25* promoter, was performed in an *oxIs12* background. **B, C:** Animals expressing both wild-type *ars-2* and G931S *ars-2* display neuronal processes similar to *oxIs-12* worms. **D:** Conversely, expression of R329H *ars-2* leads to abnormal axonal branching (arrowheads) and thinning of the dorsal nerve cord (arrow). The scale bar represents 100 μm.

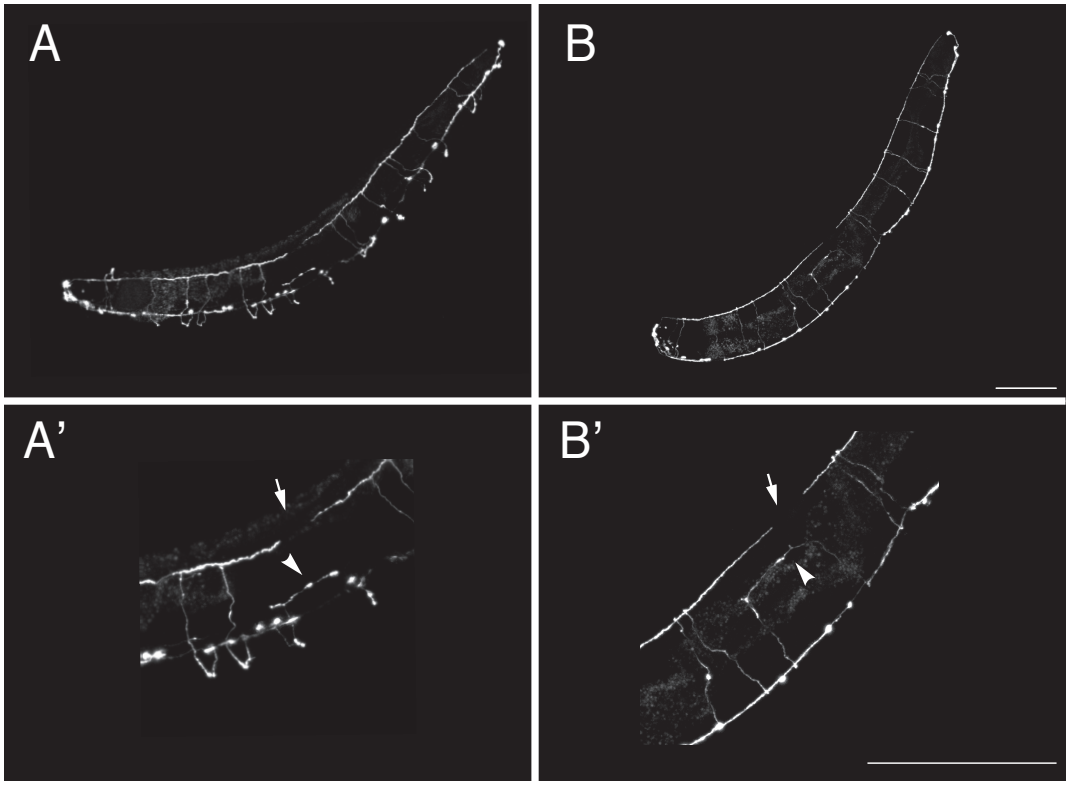

Figure 4.3 R329H *ars-2* Overexpression Leads to Abnormal GABAergic Axon Morphology. Confocal images of P*unc-25::*R329H.*ars-2::*T*let-858* animals are depicted with the anterior side of the worm facing left and the dorsal side of the worm facing up. **A, B:** Worms overexpressing R329H *ars-2* frequently display abnormal commissural axonal phenotypes denoted by horizontal axonal branching (arrowheads) and discontinuation of the dorsal nerve cord (arrows). Scale bars represent 100 μm.

Table 4.2 Abnormal GABAeric Neuronal Morphology

	Developmental Stage		
Genotype	L4	1D	4D
oxIs-12	0/100	0/100	2/100
wt *ars-2*	1/100	3/100	1/100
R329H *ars-2*	30/100	33/100	35/100
G931S *ars-2*	0/100	0/100	1/100

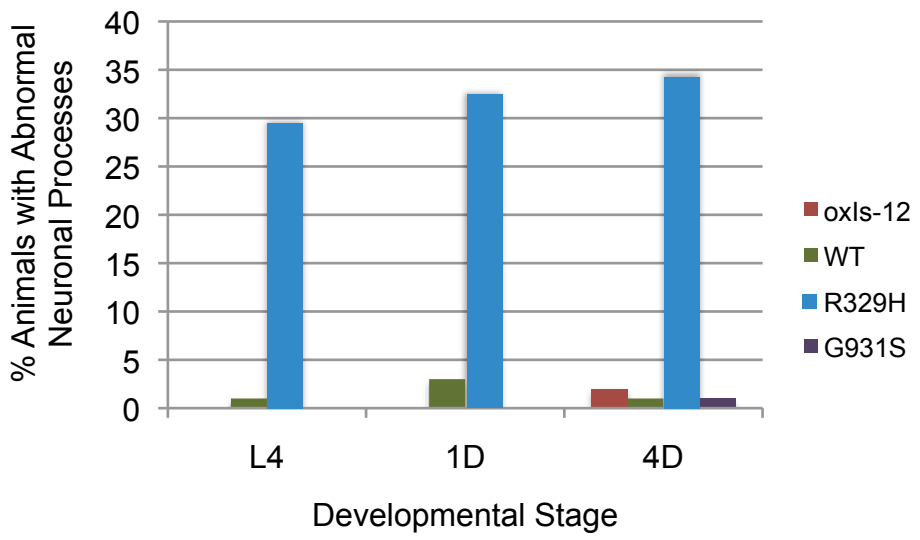

Figure 4.4 Quantification of Abnormal GABAergic Phenotypes. A total of 100 worms from each developmental stage were scored for the presence of abnormal GABAergic axon morphology and percentages of worms with abnormal GABAergic processes were calculated. While *oxIs-12*, wild-type (WT) *ars-2*, and G931S *ars-2* worms rarely presented abnormal phenotypes, ~30-35% of R329H *ars-2* worms displayed abnormal GABA commissural axons at larval stage 4 (L4), one day adult (1D), and four day adult (4D) developmental stages.

(Table 4.2 and Figure 4.4). These data indicate that R329H *ars-2* has a dominant neurotoxic effect on axonal morphology.

R329H ars-2-Induced Morphological Defects Appear During GABA Neuron Remodeling

Degeneration of peripheral nerve axons is a cardinal sign of axonal CMT disease, and often leads to subsequent muscle weakness and wasting. We sought to determine if the abnormal GABAergic neuronal morphology we discovered in the R329H *ars-2* worms is the result of a developmental defect (where the commissural axons fail to form correctly during development) or a degenerative defect (where the commissural axons form normal synapses but then degenerate). The first D-type motor neurons to form in the worm are the 6 DD neurons, which appear embryonically (McIntire *et al.*, 1993b). During larval stage L1, 14 VD neurons develop and the 6DD neurons innervate the ventral body wall muscles (Jin *et al.*, 1994; White *et al.*, 1978). While the 14 VD synaptic outputs remain unchanged throughout the life of the animal, the 6 DD neurons undergo a dramatic remodeling of synaptic outputs to innervate dorsal body wall muscles during larval stage L2 to adult, allowing the DD and VD motor neurons to adopt opposite synaptic outputs in the adult worm (Hallam and Jin, 1998; Petersen *et al.*, 2011; White *et al.*, 1978).

To determine if the abnormal GABAergic neuronal morphology is a result of a developmental or a degenerative defect, we analyzed 100 worms from each larval stage (L1-L4). The *oxIs-12*, wild-type *ars-2*, and G931S *ars-2* worms failed to show overt morphological abnormalities at any larval stage. That is, each strain had 6 normally developed DD neurons at larval stage L1, and 19 normally developed D-type neurons at

Table 4.3 Abnormal GABAergic Axon Morphology at Larval Stages

	Developmental Stage			
Genotype	L1	L2	L3	L4
wt *ars-2*	0/100	0/100	0/100	1/100
R329H *ars-2*	0/100	0/100	13/100	30/100
G931S *ars-2*	0/100	0/100	0/100	0/100

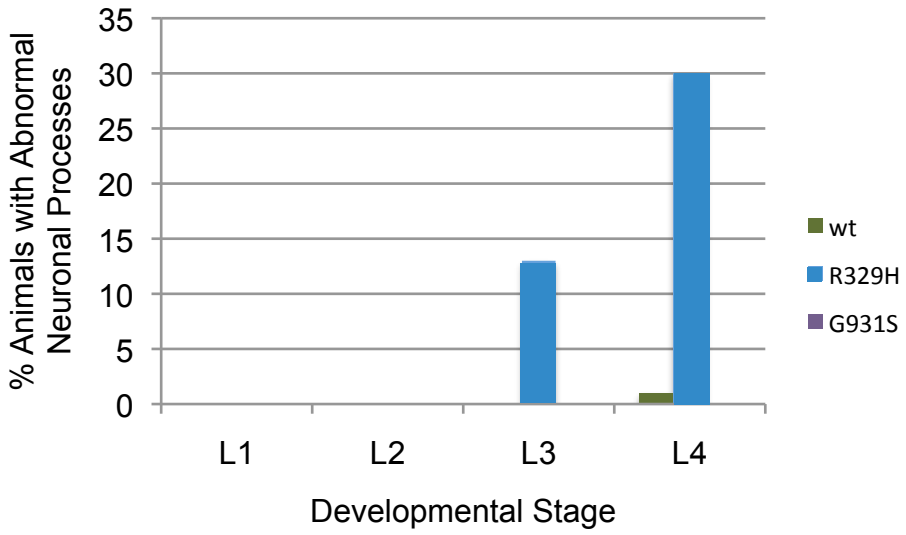

Figure 4.5 Quantification of Abnormal GABAergic Axon Morphology in Larval Stage Worms. A total of 100 worms from each developmental stage were scored for the presence of abnormal GABAergic axon morphology and percentages of worms with abnormal GABAergic processes were calculated. Wild-type (WT) *ars-2* and G931S *ars-2* worms rarely presented abnormal axon morphology at larval stages L1-L4. Conversely, abnormal axonal morphology began to appear at larval stage L3 in R329H *ars-2* worms, and reached 30% by larval stage L4.

larval stage L2 (Table 4.3 and Figure 4.5). While the R329H *ars-2* worms correctly formed 6DD neurons by larval stage L1, and 19 D-type neurons by larval stage L2, we began to notice the same morphological abnormalities we identified in adult R329H *ars-2* worms at larval stage L3, with 13% of worms being affected (Table 4.3 and Figure 4.5). By larval stage L4, these morphological defects were present in 30% of the worms affected (Table 4.3 and Figure 4.5).

Interestingly, the R329H *ars-2* morphological abnormalities seem to appear during the time when the 6DD neurons undergo remodeling, a process in which the DD neurons remove their synaptic outputs from the ventral body wall muscles in order to innervate the dorsal body wall muscles, suggesting the 6DD neurons undergo degeneration during the remodeling process. However, upon further analysis of the affected GABA neurons, we were able to conclude that the DD and VD GABA neurons are equally affected, making it unlikely that the 6 DD neurons are exclusively undergoing degeneration (data not shown). Given these data, it is difficult to distinguish between a pure developmental phenotype and a degenerative phenotype in the R329H *ars-2* worms at this time.

R329H ars-2 Worms Display Normal Motor Neuron Function

In *C. elegans*, locomotion is achieved via sinusoidal body movements, made possible by the reciprocal inhibition of ventral and dorsal body wall muscles (McIntire *et al.*, 1993a). During reciprocal inhibition, acetylcholine (ACh) release results in contraction of the body wall muscle on one side of the worm and stimulates GABA release on the other side of the worm, leading to relaxation. This process occurs in a reciprocal fashion

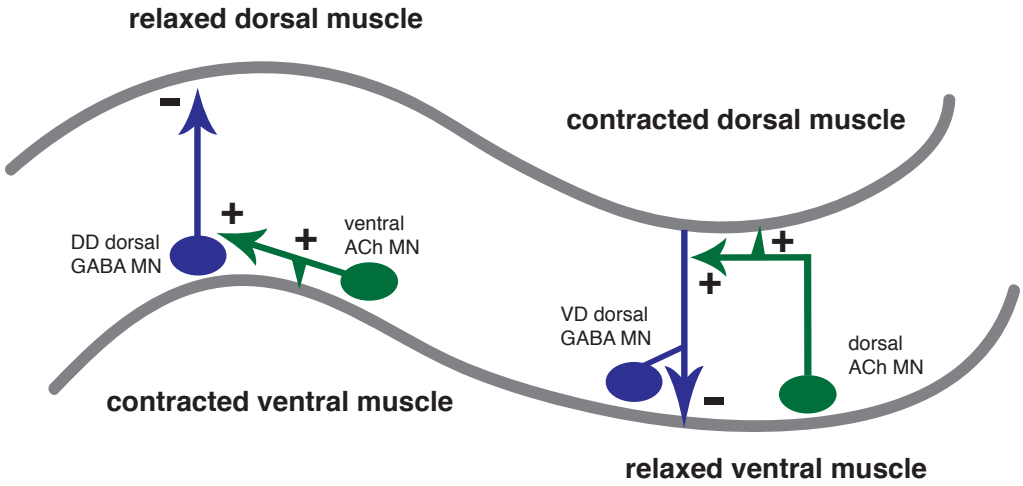

Figure 4.6 Reciprocal Inhibition. The classical sinusoidal movement of *C. elegans* is achieved by reciprocal inhibition of the body wall muscles and is facilitated by GABA (blue) and ACh (green) motor neurons. The DD and VD GABA motor neurons synapse to the dorsal and ventral body wall muscles, respectively. In addition to forming a synapse with the ventral and dorsal body wall muscles, the cholinergic motor neurons also send inputs to the GABAergic motor neurons. ACh release leads to contraction of the body wall muscle on one side of the worm and stimulates GABA release on the other side of the worm, leading to relaxation. This process occurs in a reciprocal fashion contralaterally, causing the body to bend. Adapted from: Schuske, *et al.*, 2004.

contralaterally, causing the body to bend (Figure 4.6). The thrash assay, which measures the number of thrashes (*i.e.,* the number of times the head of the worm crosses the mid-line axis) a worm completes over a period of time when placed in a drop of liquid, is often used as a proxy for evaluating motor function in *C. elegans* (Tsalik and Hobert, 2003). Because thrashing requires reciprocal inhibition, it is also a direct test of the function of GABAergic motor neurons.

We utilized the thrash assay to evaluate GABA motor neuron function in 15 worms from each genotype at L4, one-day-old (1D) adult, and four-day-old (4D) adult stages. We counted the number of thrashes over two-minute time intervals and obtained mean one-minute thrash counts for each worm. We did not identify a statistically significant difference between the mean number of thrashes in wild-type *ars-2* and G931S *ars-2* worms at any stage (Figure 4.7). However, there was a noticeable trend towards reduced thrashing rates for R329H *ars-2* worms at all stages examined, and there was a statistically significant difference in the mean number of thrashes between wild-type *ars-2* and R329H *ars-2* worms at the one-day-old adult stage (Figure 4.7).

While evaluating the thrashing data, we noticed that the standard errors of the mean number of thrashes for R329H *ars-2* worms were elevated when compared to the standard errors of the other genotypes (Figure 4.8). Therefore, we questioned whether the R329H *ars-2* worms consisted of two distinct thrashing populations, corresponding to worms that had phenotypically abnormal GABAergic neurons ("affected" worms) and worms that had phenotypically normal GABAergic neurons ("unaffected" worms). We

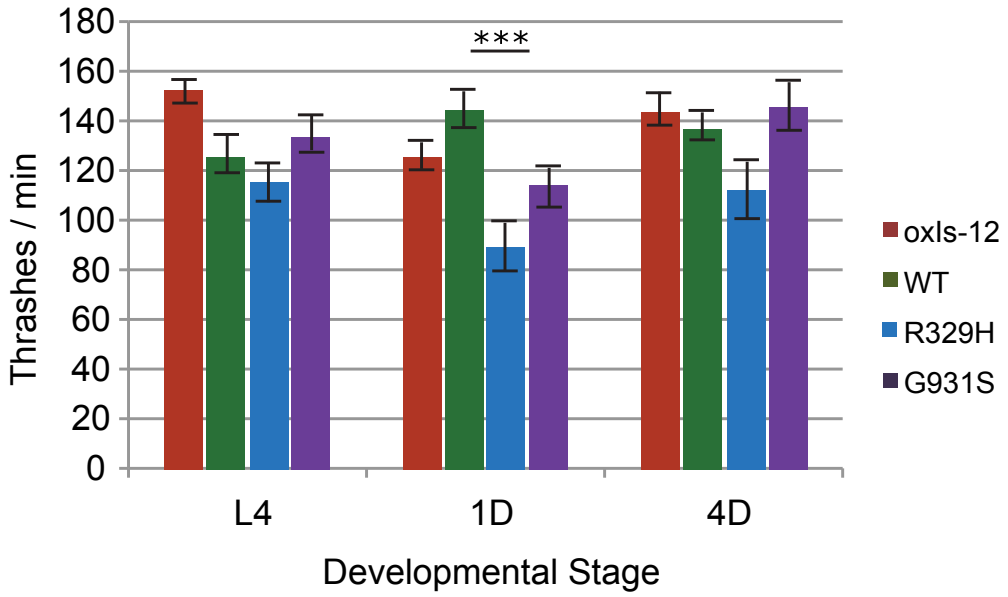

Figure 4.7 Analysis of Thrashing Behavior in *ars-2* Transgenic Worms. Fifteen worms from each genotype and each developmental stage were analyzed for thrashing behavior. The developmental stage assayed is indicated below each series of data in the column chart. Motor function is significantly reduced in R329H *ars-2* 1-day-old adult worms, but not at any other stage. Error bars indicate ± S.E.M., $^{***}P < 0.001$.

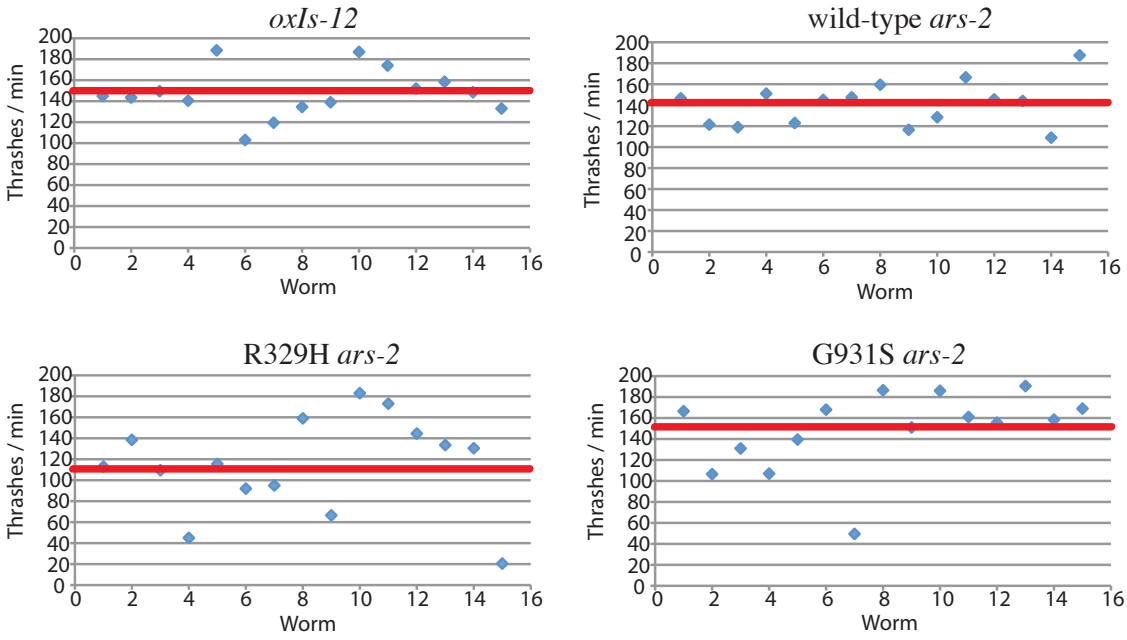

Figure 4.8 Scatter Plots for Thrash Counts in 4-Day-Old Adult Worms. Thrash counts for each of 15 4-day-old adult worms are depicted for each genotype in the form of light blue diamonds. The red line denotes the mean thrash count for each genotype. Unlike thrash counts for oxIs-*12*, wild-type *ars-2*, and G931S *ars-2* worms, thrash counts for R329H *ars*-2 worms show substantial scatter around the mean.

hypothesized that the abnormal GABAergic neuronal architecture in the affected R329H *ars-2* worms led to reduced thrashing rates, while R329H *ars-2* worms with normal GABAergic neuronal morphology exhibited thrashing rates compared to that of wild-type *ars-2* worms. To test this hypothesis, we repeated the thrashing experiment in four-day-old R329H *ars-2* adult worms and separated the worms into two groups: affected and unaffected. While the mean number of thrashes was reduced in affected R329H *ars-2* worms compared to all other genotypes, there was not a statistically significant difference between the mean number of thrashes in affected R329H *ars-2* worms and wild-type *ars-2* worms (Figure 4.9). Furthermore, there was no difference in the mean number of thrashes between affected R329H *ars-2* worms and unaffected R329H *ars-2* worms (Figure 4.9). Together, these data indicate that GABAergic motor neuron function is not severely affected in R329H *ars-2* worms.

Discussion

Described here is the creation of a *C. elegans* model system of R329H *AARS*-related peripheral neuropathy. Overexpression of R329H *ars-2*, but not wild-type *ars-2* or G931S *ars-2*, leads to overt morphological GABAergic neuronal phenotypes including failure of axonal commissures to reach the dorsal nerve cord, horizontal branching of axonal commissures, and discontinuation of the GABAergic dorsal nerve cord. These data indicate that R329H *ars-2* is dominantly toxic to GABAergic axons *in vivo*. While these morphological abnormalities do not result in a statistically significant reduction of thrashing behavior in aged R329H *ars-2* worms, we did notice that there was an overall reduction in the mean number of thrashes in R329H *ars-2* worms at all developmental

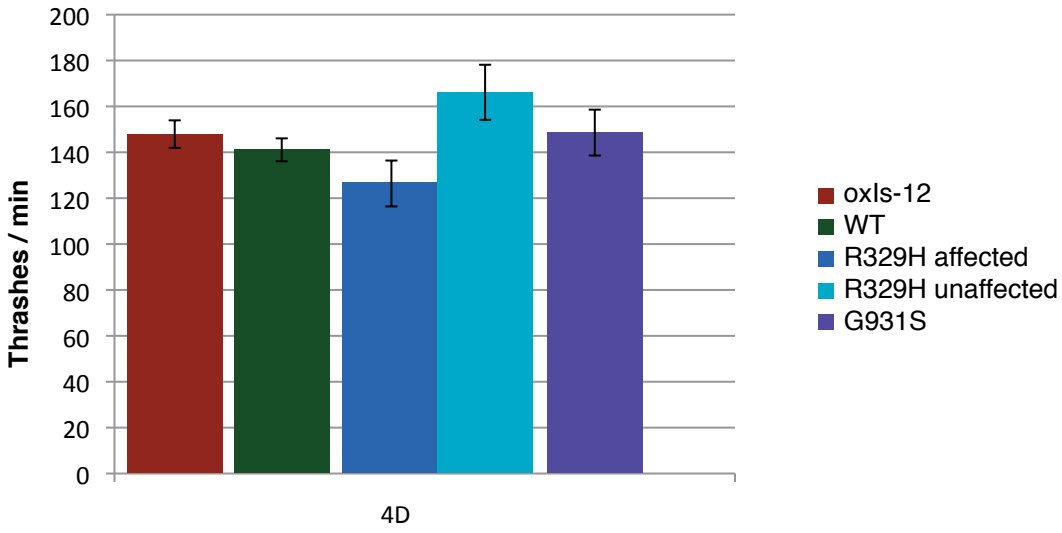

Figure 4.9 Analysis of Thrashing Behavior in 4-day-Old Adult Affected and Unaffected R329H *ars-2* Transgenic Worms. Fifteen worms from each genotype and each developmental stage were analyzed for thrashing behavior. R329H *ars-2* worms were further divided into two categories: affected (*e.g.* worms with abnormal neuronal morphology) and unaffected (*e.g.* worms with normal neuronal morphology) worms. Motor function is not significantly reduced in either the unaffected or affected R329H *ars-2* strains. Error bars indicate ± S.E.M..

stages examined. Although not quantifiable, we also noticed that if the R329H *ars-2* worms, in particular, were not routinely enriched, the strains would rapidly cease to yield positive progeny, indicating that the R329H *ars-2* transgene could be slightly unstable or that it imparts some level of lethality.

Patients with CMT2N exhibit a neurodegenerative phenotype characterized by progressive muscle weakness and wasting and diminished deep tendon reflexes (Latour *et al.*, 2010; Lin *et al.*, 2011; McLaughlin *et al.*, 2012). While we weren't able to unequivocally determine whether the morphological defects we discovered in the R329H *ars-2* GABAergic motor neurons occur in response to a developmental or degenerative defect, we were able to confirm that these defects appear at larval stage L3 and are maximal by larval stage L4. Moving forward, it will be important to further investigate developmental versus neurodegenerative involvement in the R329H *ars-2* worms. Time-lapse studies of GABAergic neurons, monitoring the extension of the growth cone from larval stage L2 to larval stage L4, may help determine if the commissural neurons form normally during development. In addition, laser ablation of single GABAergic neurons in R329H *ars-2* worms, followed by time-lapse imaging, will allow for interrogation of neuronal regeneration after axonal damage. Together, these experiments will help to tease out whether R329H *ars-2* results in a developmental defect, a neurodegenerative defect, or a combination of both.

The R329H *ars-2* worm model was created to aid in the assessment of the pathogenicity of novel ARS variants in patients with CMT disease. Importantly, we were able to

confirm that this model system is able to distinguish between pathogenic and non-pathogenic variants affecting amino acids conserved between human and worm. This worm model was recently utilized to evaluate a p.Arg137Gln (R137Q) histidyl-tRNA synthetase (*HARS*) gene mutation in the *C. elegans* ortholog *hars-1*. Like the R329H *ars-2* worms, worms overexpressing R137Q *hars-1* exhibited overt GABAergic neuronal abnormalities including failure of GABAergic commissures to reach the dorsal nerve cord, axonal beading, and discontinuation of the GABAergic dorsal nerve cord (Vester, *et al.* In Preparation). Moreover, while larval stage L4 and one-day-old adult worms displayed thrashing behavior comparable to wild-type *hars-1* worms, four-day-old adult worms exhibited a statistically significant difference in the mean number of thrashes (Vester, *et al.* In Preparation). These data suggest that R137Q *hars-1* results in progressive deterioration of motor neuron function and further highlights the utility of the *C. elegans* model system in determining the pathogenicity of novel ARS alleles.

In addition to utilizing the *C. elegans* model to evaluate novel ARS mutations, it will also be prudent to further characterize this model and use it as a platform for interrogating other aspects of ARS-related peripheral neuropathy. The *C. elegans* model employed in this chapter was created using extensive overexpression of *ars-2* alleles specifically in GABAergic motor neurons. It would be interesting to determine the effect of expressing R329H *ars-2* in a larger subset of neurons. For example, the vesicular acetylcholine transporter gene (*unc-17)* promoter could be utilized to overexpress R329H *ars-2* in the 120 acetylcholinergic neurons (Alfonso *et al.*, 1993). It would also be interesting to create a model that accurately represents heterozygosity for a mutant R329H *ars-2* allele. For

example, insertion of a single copy of R329H *ars-2* into an *ars-2*$^{+/-}$ worm would effectively create a heterozygous R329H *ars-2* worm. Worm strains with increasing copies of R329H *ars-2* could then be generated to see if increased dosage of the mutant allele leads to more severe morphological and functional phenotypes. Finally, performing enhancer and/or suppressor screens may aid in the identification of other genes and/or pathways involved in ARS-related peripheral neuropathy.

In summary, *C. elegans* has proven to be a relevant model system for evaluating the effect of ARS mutations in GABAergic neurons. Utilizing the disease-associated R329H *ars-2* mutation, we have demonstrated that a mutant ARS enzyme can lead to morphological defects in GABA motor neurons. This *C. elegans* model system created here will allow for the interrogation of ARS variants of unknown pathogenicity, and may serve as a platform for dissecting the functional mechanism(s) of ARS-related peripheral neuropathy in the future.

CHAPTER 5

Summary, Future Directions, and Discussion

Summary of Dissertation Findings

In this concluding chapter I will summarize the important findings of my thesis work and explain how these results demonstrate the vital role aminoacyl-tRNA synthetases play in peripheral nerve health and maintenance. Prior to this dissertation, mutations in two genes encoding ARS enzymes were implicated in peripheral neuropathy, leading us to consider all ARS genes as potential candidates for CMT disease (Antonellis *et al.*, 2003; Jordanova *et al.*, 2006). Here, we present the genetic and functional evaluation of mutations discovered in the alanyl-tRNA synthetase (*AARS)* and lysyl-tRNA synthetase (*KARS)* genes in patients with CMT2N and CMTRIB, respectively. CMT2N is characterized by age of onset in the early 20's, MNCVs in the intermediate range, progressive gait difficulty, foot drop, pes cavus, hammer toes, and variable sensorineural deafness. Conversely, the patient we identified with CMTRIB exhibited MNCVs in the intermediate range, developmental delay, self-abusive behavior, dysmorphic features, and a vestibular Schwannoma. We discovered the N71Y *AARS* and R329H *AARS* mutations in two patients with CMT2N (McLaughlin *et al.*, 2012). We determined that the R329H *AARS* mutation likely results from deamination of a methylated CpG dinucleotide. In addition, we identified the L133H *KARS* and Y173SfsX7 *KARS* mutations in a compound heterozygous patient with CMTRIB (McLaughlin *et al.*, 2010). Each of the mutations

affect conserved amino-acid residues and is absent in neurologically normal control populations. While none of the mutations lead to overt mislocalization when expressed in cultured neuronal cells, the N71Y *AARS,* R329H *AARS*, and L133H *KARS* mutations all lead to impaired aminoacylation activity *in vitro*, and the N71Y *AARS,* R329H *AARS*, and Y173SfsX7 *KARS* mutations lead to severe growth defects when modeled in their respective *S. cerevisiae* orthologs (McLaughlin *et al.*, 2012; McLaughlin *et al.*, 2010). Together, these data further highlight the important role of ARS enzymes in peripheral neurons and support the continuing study of this class of enzymes in patients with peripheral neuropathy.

Ongoing mutational analyses of the 37 genes encoding ARS enzymes continue to produce potentially novel variants with unknown pathogenic consequences. To develop a platform for assessing these novel ARS variants, we created a *C. elegans* model system assessing the most common ARS mutation identified to date (R329H *AARS*) in the *AARS* ortholog *ars-2.* We discovered that overexpression of R329H *ars-2* in GABAergic motor neurons leads to overt morphological defects at larval stage L3 and beyond. In contrast overexpression of either wild-type *ars-2* or G931S *ars-2* failed to elicit any distinct morphological phenotypes. While the morphological defects observed in the R329H *ars-2* worms are quite severe, these worms appear to have normal motor function. The *C. elegans* model system created here will serve as a platform for assessing novel ARS variants and we hope that further interrogation of this model system will provide additional mechanistic insights into ARS-related peripheral neuropathy.

Advances in the Field of ARS-Related Peripheral Neuropathy

The thesis work presented herein has yielded several significant advances towards the current understanding of ARS-related peripheral neuropathy. In addition to the implication of the *GARS* and *YARS* genes in axonal CMT disease, we were able to implicate two additional ARS genes in inherited peripheral neuropathy. First, we utilized functional analyses to confirm the pathogenicity of the R329H *AARS* mutation previously identified in two families with CMT2N, and we also implicated an additional *AARS* mutation, N71Y *AARS,* in a Taiwanese family with CMT2N (Latour *et al.*, 2010; McLaughlin *et al.*, 2012). Second, we discovered mutations in the lysyl-tRNA synthetase (*KARS*) gene in a single compound heterozygous patient with intermediate CMT disease and additional non-neurological sequelae (McLaughlin *et al.*, 2012). These studies led to the creation of a new subtype of CMT disease termed CMT recessive intermediate type B (CMTRIB; OMIM 613641). The discovery of additional ARS genes implicated in CMT disease has improved our understanding of the types of genes mutated in axonal CMT disease and serves to highlight the important role ARS enzymes play in peripheral nerve health.

Our functional analyses have also provided key insights towards the mechanistic link between ARS gene mutations and inherited peripheral neuropathy. All of the disease-associated mutations we identified resulted in a loss-of-function effect in aminoacylation and/or yeast viability assays (McLaughlin *et al.*, 2012; McLaughlin *et al.*, 2010). These data suggest loss of tRNA charging function is a principal component to ARS-related peripheral neuropathy. A worm model, created by overexpressing R329H *ars-2* in a

worm with two intact copies of wild-type *ars-2,* argues against a model based solely upon haploinsufficiency, and suggests that a dominant-negative effect, where mutant ARS monomers antagonize wild-type ARS monomers, or gain-of-function effects, should be closely examined. These pathogenic mechanisms will be discussed in the next section.

Pathogenic Mechanisms of ARS Mutations

In this section of my thesis I will provide a final review of the current molecular pathologies being considered in ARS-related CMT disease, taking into consideration the culmination of data gleaned from this thesis and from previous studies on disease-associated ARS mutations. Here, I will argue that ARS mutations may lead to disease via diverse pathogenic mechanisms and suggest experiments for further interrogating these various pathogenic mechanisms and uncovering additional pathogenic mechanisms.

The data presented in this thesis, along with previously published data and ongoing studies in our lab and in collaborating laboratories, have resulted in a cumulative total of six genes encoding an ARS enzyme being implicated in CMT disease. These include alanyl-tRNA synthetase (*AARS),* glycyl-tRNA synthetase (*GARS*), histidyl-tRNA synthetase (*HARS*), lysyl-tRNA synthetase (*KARS*), methionyl-tRNA synthetase (*MARS*), and tyrosyl-tRNA synthetase (*YARS*). Disease-associated ARS mutations lead to dominant CMT disease (with the exception of *KARS* mutations in CMTRIB) and have been shown to result in various functional consequences including reduced aminoacylation activity, the inability to support yeast cell growth, improper cellular localization, and/or toxicity to neurons (Antonellis *et al.*, 2003; Antonellis *et al.*, 2006;

Chihara, *et al.,* 2007; Froelich, *et al*., 2011; Jordanova *et al.*, 2006; McLaughlin *et al.*, 2010; McLaughlin *et al.*, 2012; Nangle *et al.*, 2007; Storkebaum, *et al*., 2009; Xie *et al*., 2007). These data highlight the many ways disease-associated ARS mutations can perturb ARS function, and argue that several pathogenic mechanisms, including loss of tRNA charging activity and gain-of-function effects, could give rise to CMT disease pathology. Moving forward, it will be important to further interrogate the mechanisms by which ARS mutations may lead to reduced aminoacylation activity, and to explore the secondary affects of reduced tRNA charging function. It will also be critical to begin to explore various gain-of-function possibilities. Together, these studies will provide further mechanistic insights into the etiology of ARS-related CMT disease and may aid in the development of treatments and therapies for these diseases.

While it is clear that loss of tRNA charging function plays an important role in ARS-related peripheral neuropathy, the pathogenic mechanism by which dominant, loss-of-function ARS mutations lead to CMT disease remains elusive. Data obtained from a *Gars* mouse model argue against a simple haploinsufficiency mechanism, whereby the reduction of ARS enzyme function to ~50% leads to disease pathology. The $Gars^{XM256/+}$ mouse, a heterozygous null mouse created by inserting a gene-trap in the second intron of the *Gars* gene, lacks the axonal loss and neuromuscular junction (NMJ) defects commonly associated with mouse models of CMT2D (Seburn *et al.*, 2006). These data implore us to consider more complicated molecular mechanisms by which ARS mutations might lead to a reduction in aminoacylation activity that could breach axonal requirements. One possibility is a dominant-negative effect, in which mutant ARS

monomers dimerize with, and antagonize wild-type ARS monomers. A dominant-negative effect could reduce charging capacity to <<<50% to that of wild-type given that wild-type:mutant, and mutant:mutant dimers are non-functional (Figure 5.1). The majority of mutant:mutant ARS homodimers evaluated to date appear to be nonfunctional based upon previously-performed *in vitro* aminoacylation assays (Froelich and First, 2011; Jordanova *et al.*, 2006; McLaughlin *et al.*, 2012; McLaughlin *et al.*, 2010; Nangle *et al.*, 2007; Storkebaum *et al.*, 2009; Xie *et al.*, 2007); however, the effect of mutant ARS subunits on wild-type ARS subunits in a wild-type:mutant heterodimer, has not been fully evaluated. There are two central requirements for a dominant negative effect to occur; wild-type and mutant subunits must dimerize, and wild-type:mutant heterodimers must result in reduced charging capacity. To determine if wild-type and mutant monomers are capable of heterodimerizing, wild-type and mutant ARS monomers can be differentially-tagged and expressed in a neuronal cell line. Following co-immunoprecipitation of wild-type:mutant heterodimers using an antibody against one tag, western blot analyses using antibodies against the second tag can be performed. If wild-type and mutant subunits are capable of heterodimerizing, a dominant-negative effect on enzyme function can then be evaluated using a similar differential tagging strategy. Differentially tagged monomers can be immunoprecipitated sequentially to ensure the presence of a wild-type:mutant heterodimers, and these dimers can subsequently be utilized in an *in vitro* aminoacylation reaction to determine if wild-type:mutant heterodimers display reduced aminoacylation activity compared to wild-type:wild-type homodimers. The discovery of a dominant-negative effect could account for the fact that *Gars*$^{XM256/+}$ mice are phenotypically normal, while dominant mutations in several ARS

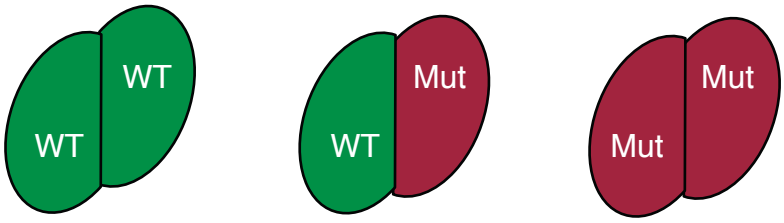

Figure 5.1 Depiction of a Dominant-Negative Effect on ARS Enzyme Activity. Several aminoacyl-tRNA synthetase enzymes function as dimers. Wild-type ARS monomers are depicted in green and mutant ARS monomers are depited in red. Below each dimer, the total charging capacity (in the event of a dominant-negative effect) provided by each dimer is depicted. In the event that wild-type:mutant, and mutant:mutant dimers are non-functional, a dominant-negative effect could reduce charging capacity to <<<50% to that of wild-type.

genes lead to peripheral neuropathy.

The majority of disease-associated ARS mutations identified to date result in a loss of tRNA charging activity. Moving forward, it will be important to explore the secondary effects of reduced aminoacylation activity. In the context of long, terminally differentiated neurons, a deficiency in aminoacylation activity could result in a reduction of charged tRNA and subsequent deprivation of proteins critical for axonal function, resulting in the degeneration of peripheral nerve axons. For example, ARS mutations may lead to shortages in proteins important for axonal transport (including KIF1B, RAB7, and DYNC1H1), cytoskeletal integrity (including DNM2, NEFL, HSPB1), or mitochondrial dynamics (including MFN2, GDAP1) (see Figure 1.1). To determine if reduced aminoacylation leads to a reduction in proteins important for axonal health and maintenance, the effect of ARS mutations on axonal protein levels can be monitored by comparing expression of the above-mentioned proteins in sciatic nerves from wild-type mice with sciatic nerves from *Gars*$^{C201R/C201R}$ mice. *Gars*$^{C201R/C201R}$ mice, created using N-ethyl-N-nitrosourea (ENU) mutagenesis, are homozygous for C201R *Gars* mutations and exhibit a 60% reduction in aminoacylation activity compared to wild-type littermates (Achilli *et al.*, 2009). If ARS mutations have an effect on axonal protein synthesis, we would expect reduced overall axonal protein levels in *Gars*$^{C201R/C201R}$ sciatic nerves when compared to protein levels in wild-type sciatic nerves, and we might expect specific reduction of proteins important for axonal transport, cytoskeletal integrity, and mitochondrial dynamics. The determination of the molecular mechanism by which ARS mutations lead to reduced charging capacity and the exploration of the functional

consequences of reduced aminoacylation activity in axons will provide further insight into the etiology of ARS-related peripheral neuropathy associated with loss-of-function ARS mutations.

While loss-of-function effects of disease-associated ARS mutations have been extensively studied, possible gain-of-function consequences of ARS mutations remain relatively unexplored. Interestingly, *Gars*$^{P234KY/+}$ mice display a CMT-like phenotype despite the fact that P234KY *Gars* does not lead to reduced aminoacylation activity *in vitro*. Moreover, overexpression of wild-type human *GARS* does not rescue axonal loss or NMJ defects in *Gars*$^{P234KY/+}$ mice (Motley *et al.*, 2011). These data suggest that gain-of-function mechanisms in collaboration with, or independent of, loss-of-function mechanisms should also be considered. An oft-overlooked consequence of reduced aminoacylation activity imparted by loss-of-function ARS mutations, is that reduction in aminoacylation activity would almost certainly lead to increased cellular pools of uncharged tRNA. These large pools of non-acylated tRNA have the propensity to be problematic to neurons in several ways: (1) excessive amounts of uncharged tRNA could be inherently toxic to neurons; (2) uncharged tRNAs could hijack non-cognate ARSs and undergo mischarging; and (3) uncharged tRNAs may compete with the entry of charged tRNAs into the A site of the 40S ribosome. Excessive amounts of uncharged tRNA may impart toxicity to neurons by triggering neuronal cellular stress responses and/or apoptosis. To test this hypothesis, differentiated neurons can be treated with increasing amounts of non-acylated or α-hydroxy-treated tRNA (where the tRNA is ligated with a hydroxyl group) and the effect on cellular stress response proteins and apoptotic markers

such as heat shock proteins (Hsp10, Hsp27, Hsp70, Hsp60, Hsp90), caspase-3, and caspase-7 can be evaluated (Beere, 2001; Owczarek *et al.*, 2008). If uncharged tRNAs evoke cellular stress response pathways and prompt apoptosis, we would expect to observe a decrease in Hsp27, Hsp70, Hsp90, caspase-3, and casepase-7 levels; along with an increase in Hsp10 and Hsp60 levels in cells treated with non-acylated tRNA or α-hydroxy-treated tRNA. Large groups of uncharged tRNAs may also impart toxicity by aberrantly sequestering ribonucleic acid (RNA)-binding proteins (RBPs), as demonstrated in fragile X tremor ataxia syndrome (FXTAS), where a (CCG)n expansion of 70 to 500 base pairs in the 5' untranslated region (UTR) of the fragile X mental retardation (*FMR1)* gene leads to nuclear *FMR1* RNA foci and sequestration of RBPs (Jin *et al.*, 2007; Sofola *et al.*, 2007). It would be interesting to determine if uncharged tRNAs are able to form foci in the neurons of individuals affected with CMT disease, and to determine if these tRNAs are able to bind with cellular RBPs, especially when present in excessive amounts. While mutant ARS enzymes are not predicted to participate in mischarging themselves (see (Stum *et al.*, 2011)), there is a possibility that uncharged non-cognate tRNAs can compete with cognate tRNAs for other ARS enzymes, a situation that may result in mischarging. To determine if uncharged tRNAs undergo mischarging when present in large quantities, aminoacylation assays can be performed with an ARS and its cognate tRNA while adding increasing amounts of non-cognate tRNA and determine if the non-cognate tRNA is acylated. This would allow us to determine whether a threshold exists where non-cognate tRNAs are able to compete with cognate tRNAs in the aminoacylation reaction. Finally, it is possible that uncharged tRNAs compete with charged-tRNAs for entry onto the 40S ribosomal A site, causing

translational pausing or otherwise slowing elongation. The ribosomal A site is the point of entry for the majority of aminoacyl-tRNAs, with the exception of Met-tRNA^{Met}, which enters at the P site (Alberts *et al.*, 2008). We could monitor the effects of uncharged tRNAs on protein translation by adding increasing amounts of uncharged tRNA or α-hydroxy-treated tRNA to differentiated neurons and measuring initiation factor EIF2α phosphorylation and elongation factor eEF2 phosphorylation (Carlberg *et al.*, 1990; Rowlands *et al.*, 1988). If uncharged tRNAs cause translational pausing, we would expect increased cellular levels of phosphorylated EIF2α and phosphorylated eEF2.

Mutant ARS enzymes may also impart gain-of-function effects independent of reduced aminoacylation activity. One possibility is that disease-associated mutations in ARS enzymes result in shunting of the aminoacylation reaction to produce diadenosine tetraphosphate (Ap4A), instead of aminoacyl-tRNA (Figure 5.2) Ap4A has proven to be a signaling molecule affecting many diverse cellular functions including transcriptional activation, cell division, and apoptosis (Nishimura *et al.*, 1997; Schulze-Lohoff *et al.*, 1995; Vartanian *et al.*, 1997). It is possible that mutant ARSs enzymes lead to increased production of Ap4A, resulting in aberrant neuronal signaling. It would be interesting to determine if mutant ARS enzymes result in increased Ap4A production *in vitro*, when compared to Ap4A production of wild-type enzymes. Another possibility is that mutant ARS enzymes indiscriminately bind to other cellular RNAs, leading to aberrant RNA stabilization, splicing, and/or transport. Interestingly, mutations in several genes involved in RNA processing have recently been implicated in amyotrophic lateral sclerosis (ALS) including the TAR DNA-binding protein (*TARDBP*) gene and the fused in sarcoma

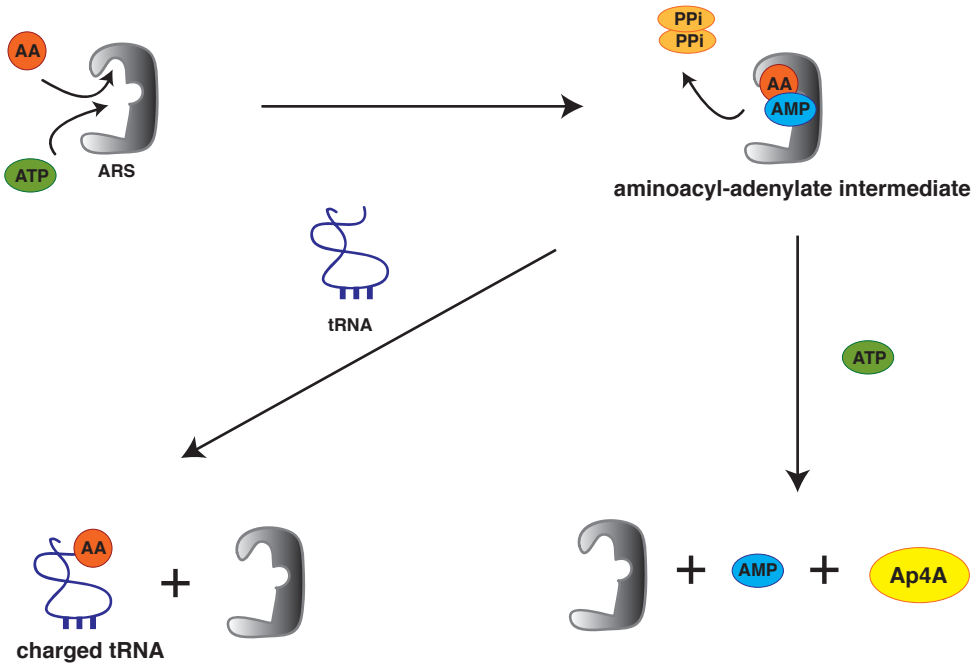

Figure 5.2 Synthesis of Ap4A by Aminoacyl-tRNA Synthetases. The ARS binds the amino-acid and an adenosine-5'-triphosphate (ATP) molecule to form an aminoacyl-adenylate intermediate, resulting in the release of two pyrophosphate molecules (PPi). In the enzyme-bound reaction, the ARS binds the tRNA via its anticodon-binding domain and the amino acid is transferred onto the tRNA. The aminoacyl-adenylate intermediate can also be attacked by an ATP molecule, resulting in the release of an AMP molecule and the formation of adenosine tetraphosphate (Ap4A).

(*FUS*) gene (Kwiatkowski *et al.*, 2009; Sreedharan *et al.*, 2008). Immunoprecipitation of wild-type and mutant ARS proteins followed by comparative RNA sequencing would allow us to determine if mutant ARS proteins are acting in a promiscuous manner.

Moving forward, it will be important to continue to explore the various molecular mechanism(s) by which mutations in ARS genes may lead to peripheral neuropathy. It will be essential to keep an open mind with respect to assessing the various functional mechanisms presented here, as it is possible that there are various mechanisms by which ARS mutations lead to disease pathology, or that one or more mechanisms are working in concert with each other to contribute to disease pathology. It is only through a complete understanding of the pathogenic mechanisms of ARS-related peripheral neuropathy that we can begin to develop therapies and treatments for patients with CMT disease.

Biomedical Implications and Discussion

This dissertation further highlights the importance of aminoacyl-tRNA synthetases in peripheral nerve health and maintenance, and specifically implicates loss-of-function mutations in the *AARS* and *KARS* genes in patients with inherited peripheral neuropathy. Given that a cumulative total of six ARS genes have been implicated in CMT disease thus far, we believe it is critical to genetically and functionally characterize every ARS mutation identified in patients with CMT disease in order to obtain a more complete understanding of the breadth of genes and pathogenic mutations involved in ARS-related peripheral neuropathy. Moving forward, it may also be prudent to screen for mutations in genes belonging to the aminoacyl-tRNA synthetase-interacting multifunctional protein

(AIMP) complex along with other genes involved in the translational machinery to determine if similar perturbations in protein translation lead to disease (Park *et al.*, 2010).

The discovery of disease-associated mutations in multiple ARS genes emphasizes the importance of protein synthesis in peripheral nerve axons, and highlights protein synthesis as an emerging mechanism of axonal CMT disease. While protein translation is required in every cell type, neurons, especially those with long, terminally differentiated axons, may have stricter translational requirements, and therefore may be more susceptible to mutations in genes encoding ARS enzymes. We hope that continuing studies exploring ARS-related peripheral neuropathies will yield further mechanistic insights into the etiology of these diseases, and serve as a basis for the design of therapies and treatments for these disorders.

APPENDICES

Appendix A. Oligonucleotide Primers (5' to 3')

Appendix A1. AARS and KARS Resequencing Primers

Exon	Forward Primer	Reverse Primer	Size (bp)
AARS Exon 2	GACTTTCAATTCCCTTAATTTTCC	TTTTATCTGGGCTCTGCTGC	276
AARS Exon 3	CCACCTGACATCACTTGCAC	AGAACCCAGTTCCCAGTGTG	315
AARS Exon 4	TCATACTAAATAGATTTTGGTTTGGC	TCATAAAACCCCACTCTGGC	280
AARS Exon 5	CAAGTCTGGGCAGAACTCTTG	GCTACACAGCTCCGAGTTCC	324
AARS Exon 6	TTTTAACCAGCAGGGACTGG	TTAAGAGTACAGCCTGGAAAACTC	279
AARS Exon 7	CTTTCTGCTAATGCTCCTCAATCC	AGCAACACTCAATCTCACACAC	346
AARS Exon 8	TTTGGGTAGGATTCCAAGGG	CACTCCATCCCTCTTAACGG	246
AARS Exon 9	GCAGGGAACAGTCTCTGGC	AAAGGGCTTGTCTTTCCCAG	272
AARS Exon 10	CATGGAAAAGGGGCTGTC	TGGAAGGAAACTCATGCTCAG	264
AARS Exon 11	TCCAGTCCTTTGGAGTCCC	GAGAAACAATCTTTCAAATACCCC	284
AARS Exon 12	AGAAGGAGTGAAAAGGTCATTG	ACTGTGGGGCAAAAGCAG	313
AARS Exon 13	TGCTCCTTAATATTGGTTATGTCTG	AGTTGCATCCCTCACAATCC	1080
AARS Exon 14	GGGGAGCAGATAACGAGGAG	GTGGACAGACAGTGACGGTG	335
AARS Exon 15	GTCGTACCGCACCTCCAG	TTGGTCCAGCCTAAGACCTAC	320
AARS Exon 16	CTTGTCCGCTAGTGTGACCC	GCAGACTGGGCTCCTCTTG	245
AARS Exon 17	TCCGCAGCTGCTCAGAC	CTGAAGACGGGGCATGTTTC	254
AARS Exon 18-19	ACCCTGACATCCCAGCAAG	CACATGTCAGCCACCAGAG	444
AARS Exon 20	GGCTGCAAATGCTCACAC	GTACACACACAGGCCTCAGC	253
AARS Exon 21	ATTCCTCCCTCAATCCCATC	GGCTCTTTAAAGGTCCCAAG	339
KARS Exon 1	GCACCTTGACCTGGAAATTAAC	CTTCCCAGCCCAGACTCTC	181
KARS Exon 2	CACCACATCTCTGTGTTTCCC	GGCTTAACGGAAAATGAACC	281

KARS Exon 3	GCTAGGGGCAGAACATAGAGG	CAAAGAATCTGCCAGAAGCC	298
KARS Exon 4	CAGAATACTGCCCTCTGCTAGG	AAGACCAACCCAGACCTTCC	339
KARS Exon 5	CACTGATACCATAAAATGACTTCTGG	TCAGCCTATTGCTGTGTTGC	221
KARS Exon 6-7	GGTTCCAGAGGAGACCAGTG	AGGCAAGGGAGAGGAGGAG	559
KARS Exon 8	ATGCAAAGCATGGTCTGTCC	CCCATCTAGCCAGTGGTATTC	258
KARS Exon 9-10	CCAGCCTGACCAATACAGAG	AATGCAAAAGTTAGGGCAGG	842
KARS Exon 11	TGAATTTGATTGGGTCAGAGC	TGCAGAAATGAACTCTCCCC	294
KARS Exon 12	GGGCTGGGACGATCAAATAC	ACCCAGCAGAAAGACCACC	254
KARS Exon 13	CAAAATTTAGCTCATTAGGGGC	GGCTGGTATTTCCTGGTGAG	242
KARS Exon 14	CACCTCGGAGCCTGGTAAC	CCAACACAATGCAGCTTCC	282
KARS Exon 15	AACAGAGGCAAGAGGAATGG	TCAAATGGAAAGCAGCACAC	282

Appendix A2. Locus-Specific PCR Primers for NINDS Control Genotyping

Primer	**Sequence**
R329H *AARS*_F	ACGTTGGATGCGTTGGGGACTAGTTTTTGC
R329H *AARS*_R	ACGTTGGATGTTTTCATGGGCGTATCGGAC
T562I *AARS*_F	ACGTTGGATGATGTGTAGCACATACCCTCC
T562I *AARS*_R	ACGTTGGATGTCTTCCTTGACCCCTCTTAG
R729W *AARS*_F	ACGTTGGATGCACAAAAGCTCCTGCATGAC
R729W *AARS*_R	ACGTTGGATGCCAGGGCCTCTTTCACTATG
E778A *AARS*_F	ACGTTGGATGTCAGGAAAGCAGAGAGCTTG
E778A *AARS*_F	ACGTTGGATGCTTGTTTGGAGCAGTCTGAG
G931S *AARS*_F	ACGTTGGATGAGCAGGTGTCAGGCTTGATG
G931S *AARS*_R	ACGTTGGATGAGCCAACGTTCTTGCCTGTG
L133H *KARS*_F	ACGTTGGATGATCAGCTGAAGGTCAATGGG
L133H *KARS*_R	ACGTTGGATGCAGGCTGCAGGTGACTATAT

Y173SfsX7 *KARS*_F	ACGTTGGATGCATGACTTGCAACTTCACCC
Y173SfsX7 *KARS*_R	ACGTTGGATGATGCCAAAAGAGCTTCTGGG
I302M *KARS*_F	ACGTTGGATGGATTGAAACTCCCATGATG
I302M *KARS*_R	ACGTTGGATGGTCCAGCTCGTTGTGATAAG

Appendix A3. Primer Extension Assay Primers for NINDS Control Genotyping

Variant	**Extension Primer**
R329H *AARS*	CGTATCGGACAGCTCGG
T562I *AARS*	CCTCTTAGAAAACAGAGTTTA
R729W *AARS*	CTCCATTCAGGCACCTG
E778A *AARS*	GCCTTCACTTTGGCT
G931S *AARS*	CATCCTTGCCACCAC
L133H *KARS*	TGACGATATTTTTGGATGAAGTCAGTG
Y173SfsX7 *KARS*	GGGGGAAAGCTCATCTT
I302M *KARS*	GAACGGCTTGGCCACGGCTCCCCCTGG

Appendix A4. AARS Haplotype Analysis Primers

Primer Name	**Sequence**	**5'tag**	**Size (bp)**
D16S3050_F	CATCTAATAAGTGATACACCCTGG	6FAM	154-174
D16S3050_R	CAAACTGGCTTGTGATTTCT	N/A	
D16S397_F	TCTGGAGACCACTAACTGTA	6FAM	103-117
D16S397_R	ACTCTCCATGAGTCCTGATG	N/A	
D16S3106_F	GAGACCTACAGTCTTTTGCATTTAC	6FAM	166-206
D16S3106_R	TTTTGAAGCTGAGCAGAAGG	N/A	

Appendix A5. Bisulfite Sequencing Primers

Primer	Sequence	Size (bp)
AARS Exon 7_F	AAGTTTGTTTTTTAAAGGGTTGTTTT	162
AARS Exon 7_R	CCATCAACCAATACCACAATAATAAT	
AARS Exon 8_F	TTAAGATAAAATTTTTAGTTGGGAA	177
AARS Exon 8_R	AAAAATAAACCTACCAAAAACTAAAC	
AARS Exon 9_F	TGAAGAAGGATTTAGATATGGTGAAG	230
AARS Exon 9_R	AAAAACATAAAAACCCACAATCAAT	
SOX3 Exon 1_F	AGGGAGTATTTATTTTTTTTGAGTAG	197
SOX3 Exon 1_R	AAAAACCCCAAAATACACAATTCTA	

Appendix A6. Cloning Primers for Aminoacylation and Yeast Complementation Constructs

Primer	Sequence[1]
*AARS*_CDS_F	ggggacaagtttgtacaaaaaagcaggcttcgaaggagatagaaccATGGACTCTACTCTAACAGC
*AARS*_CDS_R	ggggaccactttgtacaagaaagctgggtcGTTCTTTACATCCCCGAGG
*ALA1*locus_F	ggggacaagtttgtacaaaaaagcaggcttcgaaggagatagaaccCTACCAGGACAATTAATC
*ALA1*locus_R	ggggacaagtttgtacaaaaaagcaggcttcgaaggagatagaaccTTAAATGGAAAGCTTCTCC
cyto*KARS*_CDS_F	ggggacaagtttgtacaaaaaagcaggcttcgaaggagatagaaccATGGCGGCCGTGCAGGCGGC
mito*KARS*_CDS_F	ggggacaagtttgtacaaaaaagcaggcttcgaaggagatagaaccATGTTGACGCAAGCTGCTGT
*KARS*_CDS_R	ggggaccactttgtacaagaaagctgggtcGACAGAAGTGCCAACTG
*KRS1*locus_F	ggggacaagtttgtacaaaaaagcaggcttcgaaggagatagaaccGGCTGGCTGAATCCTTGGAA
*KRS1*locus_R	ggggacaagtttgtacaaaaaagcaggcttcgaaggagatagaaccTTAATTTTCTTCTTCCTTTT

[1]Gateway adapter sequences are depicted in lower case while locus specific primer sequences are depicted in upper case

Appendix A7. AARS, ALA1, KARS, and KRS1 Mutagenic Primers

Primer	**Sequence**
N71Y *AARS*_F	CTGAGCAGAGCTGCCTATACCCAGAAGTGCA
N71Y *AARS*_R	TGCACTTCTGGGTATAGGCAGCTCTGCTCAG
R329H *AARS*_F	GAGACGGATTCTCCACCGAGCTGTCCGAT
R329H *AARS*_R	ATCGGACAGCTCGGTGGAGAATCCGTCTC
E778A *AARS*_F	ATGTCTCTCTGTCATGGCAGCCAAAGTGAAGGCTC
E778A *AARS*_R	GAGCCTTCACTTTGGCTGCCATGACAGAGAGACAT
N71Y *ALA1*_F	CTACACCTTGAAAAGGGCTTACTATTCTCAAAAGTGTATCAGAGCTG
N71Y *ALA1*_R	CAGCTCTGATACACTTTTGAGAATAGTAAGCCCTTTTCAAGGTGTAG
R329H *ALA1*_F	GGTAGAGGATATGTTTTGAGACGCATTCTACATAGAGGTGCCCGTTACG
R329H *ALA1*_R	CGTAACGGGCACCTCTATGTAGAATGCGTCTCAAAACATATCCTCTACC
E778A *ALA1*_F	GTTTGCTGCTGATTTGGCTGCTGCAGACAAGCTGC
E778A *ALA1*_R	GCAGCTTGTCTGCAGCAGCCAAATCAGCAGCAAAC
L133H *KARS*_F	GTTCCATGTAGACATCTCACACACTGACTTCATCCAAAAAT
L133H *KARS*_R	ATTTTTGGATGAAGTCAGTGTGTGAGATGTCTACATGGAAC
Y173SfsX7 *KARS*_F	TCTGGGGGAAAGCTCATCTTTTCTATGATCTTCGAG
Y173SfsX7 *KARS*_R	CTCGAAGATCATAGAAAAGATGAGCTTTCCCCCAGA
I302M *KARS*_F	ACTCCCATGATGAACATCATGCCAGGGGGAGC
I302M *KARS*_R	GCTCCCCCTGGCATGATGTTCATCATGGGAGT
L133H *KRS1*_F	GCTCCCCCTGGCATGATGTTCATCATGGGAGT
L133H *KRS1*_R	TTGGCCAAGAACTCAGGATGGGATATAGAAACGTGAAAC
Y173SfsX7 *KRS1*_F	GAGAATCTGGCTCCAAATTGAAATTTTCTATGTTCTTCACGGTG
Y173SfsX7 *KRS1*_R	CACCGTGAAGAACATAGAAAATTTCAATTTGGAGCCAGATTCTC
I302M *KRS1*_F	GAAACTCCAATGATGAACGTTATGGCTGGTGGTGCT
I302M *KRS1*_R	AGCACCACCAGCCATAACGTTCATCATTGGAGTTTC

Appendix A8. C. elegans ars-2 Cloning Primers

Primer	**Sequence**[1]
ce.*ars-2*_F	ggggacaagtttgtacaaaaaagcaggctaaaaATGAAGCACCTGACTGCCTCAGAGG
ce.*ars-2*_R	ggggaccactttgtacaagaaagctgggtTTAATTGATTGCAGCAAGGGCAAA

[1]Gateway adapter sequences are depicted in lower case while locus specific primer sequences are depicted in upper case

Appendix A9. C. elegans ars-2 Mutagenesis Primers

Primer	**Sequence**
R329H *ars-2*_F	gctccgtcgaattcttcatcgtggagttcgttat
R329H *ars-2*_R	ataacgaactccacgatgaagaattcgacggagc
G931S *ars-2*_F	cacagttctcggtggaaaaagtggtggaaaggac
G931S *ars-2*_R	gtcctttccaccacttttttccaccgagaactgtg

REFERENCES

1000 Genomes Project Consortium (2010) A map of human genome variation from population-scale sequencing. Nature 467:1061-1073.

Abramoff MD, Magalhaes PJ, Ram SJ (2004) Image Processing with ImageJ. Biophotonics International 11:36-42.

Achilli F et al. (2009) An ENU-induced mutation in mouse glycyl-tRNA synthetase (GARS) causes peripheral sensory and motor phenotypes creating a model of Charcot-Marie-Tooth type 2D peripheral neuropathy. Dis Model Mech 2:359-373.

Alberts B, Wilson JH, Hunt T (2008) Molecular biology of the cell, 5th Edition. New York: Garland Science.

Alfonso A, Grundahl K, Duerr JS, Han HP, Rand JB (1993) The Caenorhabditis elegans unc-17 gene: a putative vesicular acetylcholine transporter. Science 261:617-619.

Andreev DE, Hirnet J, Terenin IM, Dmitriev SE, Niepmann M, Shatsky IN (2012) Glycyl-tRNA synthetase specifically binds to the poliovirus IRES to activate translation initiation. Nucleic acids research.

Antonellis A, Green ED (2008) The role of aminoacyl-tRNA synthetases in genetic diseases. Annu Rev Genomics Hum Genet 9:87-107.

Antonellis A, Lee-Lin SQ, Wasterlain A, Leo P, Quezado M, Goldfarb LG, Myung K, Burgess S, Fischbeck KH, Green ED (2006) Functional analyses of glycyl-tRNA synthetase mutations suggest a key role for tRNA-charging enzymes in peripheral axons. J Neurosci 26:10397-10406.

Antonellis A, Ellsworth RE, Sambuughin N, Puls I, Abel A, Lee-Lin SQ, Jordanova A, Kremensky I, Christodoulou K, Middleton LT, Sivakumar K, Ionasescu V, Funalot B, Vance JM, Goldfarb LG, Fischbeck KH, Green ED (2003) Glycyl tRNA synthetase mutations in Charcot-Marie-Tooth disease type 2D and distal spinal muscular atrophy type V. Am J Hum Genet 72:1293-1299.

Arif A, Jia J, Mukhopadhyay R, Willard B, Kinter M, Fox PL (2009) Two-site phosphorylation of EPRS coordinates multimodal regulation of noncanonical translational control activity. Mol Cell 35:164-180.

Auer-Grumbach M et al. (2010) Alterations in the ankyrin domain of TRPV4 cause congenital distal SMA, scapuloperoneal SMA and HMSN2C. Nat Genet 42:160-164.

Baldwin AN, Berg P (1966) Transfer ribonucleic acid-induced hydrolysis of valyladenylate bound to isoleucyl ribonucleic acid synthetase. The Journal of biological chemistry 241:839-845.

Baxter RV, Ben Othmane K, Rochelle JM, Stajich JE, Hulette C, Dew-Knight S, Hentati F, Ben Hamida M, Bel S, Stenger JE, Gilbert JR, Pericak-Vance MA, Vance JM (2002) Ganglioside-induced differentiation-associated protein-1 is mutant in Charcot-Marie-Tooth disease type 4A/8q21. Nat Genet 30:21-22.

Beere HM (2001) Stressed to death: regulation of apoptotic signaling pathways by the heat shock proteins. Sci STKE 2001:re1.

Belostotsky R, Ben-Shalom E, Rinat C, Becker-Cohen R, Feinstein S, Zeligson S, Segel R, Elpeleg O, Nassar S, Frishberg Y (2011) Mutations in the mitochondrial seryl-tRNA synthetase cause hyperuricemia, pulmonary hypertension, renal failure in infancy and alkalosis, HUPRA syndrome. Am J Hum Genet 88:193-200.

Bergoffen J, Scherer SS, Wang S, Scott MO, Bone LJ, Paul DL, Chen K, Lensch MW, Chance PF, Fischbeck KH (1993) Connexin mutations in X-linked Charcot-Marie-Tooth disease. Science 262:2039-2042.

Bernard R, De Sandre-Giovannoli A, Delague V, Levy N (2006) Molecular genetics of autosomal-recessive axonal Charcot-Marie-Tooth neuropathies. Neuromolecular medicine 8:87-106.

Betz RC, Schoser BG, Kasper D, Ricker K, Ramirez A, Stein V, Torbergsen T, Lee YA, Nothen MM, Wienker TF, Malin JP, Propping P, Reis A, Mortier W, Jentsch TJ, Vorgerd M, Kubisch C (2001) Mutations in CAV3 cause mechanical hyperirritability of skeletal muscle in rippling muscle disease. Nat Genet 28:218-219.

Biesecker LG et al. (2009) The ClinSeq Project: piloting large-scale genome sequencing for research in genomic medicine. Genome Res 19:1665-1674.

Black MM, Lasek RJ (1977) The presence of transfer RNA in the axoplasm of the squid giant axon. J Neurobiol 8:229-237.

Bock C, Reither S, Mikeska T, Paulsen M, Walter J, Lengauer T (2005) BiQ Analyzer: visualization and quality control for DNA methylation data from bisulfite sequencing. Bioinformatics 21:4067-4068.

Boeke JD, Trueheart J, Natsoulis G, Fink GR (1987) 5-Fluoroorotic acid as a selective agent in yeast molecular genetics. Methods Enzymol 154:164-175.

Boerkoel CF, Takashima H, Garcia CA, Olney RK, Johnson J, Berry K, Russo P, Kennedy S, Teebi AS, Scavina M, Williams LL, Mancias P, Butler IJ, Krajewski K, Shy M, Lupski JR (2002) Charcot-Marie-Tooth disease and related neuropathies: mutation distribution and genotype-phenotype correlation. Annals of neurology 51:190-201.

Bolino A, Muglia M, Conforti FL, LeGuern E, Salih MA, Georgiou DM, Christodoulou K, Hausmanowa-Petrusewicz I, Mandich P, Schenone A, Gambardella A, Bono F, Quattrone A, Devoto M, Monaco AP (2000) Charcot-Marie-Tooth type 4B is caused by mutations in the gene encoding myotubularin-related protein-2. Nat Genet 25:17-19.

Boyer O et al. (2011) INF2 mutations in Charcot-Marie-Tooth disease with glomerulopathy. N Engl J Med 365:2377-2388.

Calahorro F, Ruiz-Rubio M (2011) Caenorhabditis elegans as an experimental tool for the study of complex neurological diseases: Parkinson's disease, Alzheimer's disease and autism spectrum disorder. Invert Neurosci 11:73-83.

Cantalupo G, Alifano P, Roberti V, Bruni CB, Bucci C (2001) Rab-interacting lysosomal protein (RILP): the Rab7 effector required for transport to lysosomes. EMBO J 20:683-693.

Cao H, Weller S, Orth JD, Chen J, Huang B, Chen JL, Stamnes M, McNiven MA (2005) Actin and Arf1-dependent recruitment of a cortactin-dynamin complex to the Golgi regulates post-Golgi transport. Nat Cell Biol 7:483-492.

Carlberg U, Nilsson A, Nygard O (1990) Functional properties of phosphorylated elongation factor 2. Eur J Biochem 191:639-645.

Chance PF, Alderson MK, Leppig KA, Lensch MW, Matsunami N, Smith B, Swanson PD, Odelberg SJ, Disteche CM, Bird TD (1993) DNA deletion associated with hereditary neuropathy with liability to pressure palsies. Cell 72:143-151.

Charcot JM, Marie P (1886) Sur une forme particuliere d'atrophie musculaire progressive, souvent familiale, de´butant pas les pieds and les jambes et atteignant plustard les mains. Rev Med 6:97-138.
Chihara T, Luginbuhl D, Luo L (2007) Cytoplasmic and mitochondrial protein translation in axonal and dendritic terminal arborization. Nat Neurosci 10:828-837.
Chow CY, Zhang Y, Dowling JJ, Jin N, Adamska M, Shiga K, Szigeti K, Shy ME, Li J, Zhang X, Lupski JR, Weisman LS, Meisler MH (2007) Mutation of FIG4 causes neurodegeneration in the pale tremor mouse and patients with CMT4J. Nature 448:68-72.
Chung KW, Sunwoo IN, Kim SM, Park KD, Kim WK, Kim TS, Koo H, Cho M, Lee J, Choi BO (2005) Two missense mutations of EGR2 R359W and GJB1 V136A in a Charcot-Marie-Tooth disease family. Neurogenetics 6:159-163.
Collins RA, Lambowitz AM (1985) RNA splicing in Neurospora mitochondria. Defective splicing of mitochondrial mRNA precursors in the nuclear mutant cyt18-1. Journal of molecular biology 184:413-428.
Colomer J, Gooding R, Angelicheva D, King RH, Guillen-Navarro E, Parman Y, Nascimento A, Conill J, Kalaydjieva L (2006) Clinical spectrum of CMT4C disease in patients homozygous for the p.Arg1109X mutation in SH3TC2. Neuromuscular disorders : NMD 16:449-453.
Cooper DN, Youssoufian H (1988) The CpG dinucleotide and human genetic disease. Hum Genet 78:151-155.
Cotton AM, Avila L, Penaherrera MS, Affleck JG, Robinson WP, Brown CJ (2009) Inactive X chromosome-specific reduction in placental DNA methylation. Hum Mol Genet 18:3544-3552.
Coulondre C, Miller JH, Farabaugh PJ, Gilbert W (1978) Molecular basis of base substitution hotspots in Escherichia coli. Nature 274:775-780.
Crimella C, Tonelli A, Airoldi G, Baschirotto C, D'Angelo MG, Bonato S, Losito L, Trabacca A, Bresolin N, Bassi MT (2010) The GST domain of GDAP1 is a frequent target of mutations in the dominant form of axonal Charcot Marie Tooth type 2K. J Med Genet 47:712-716.
Cuesta A, Pedrola L, Sevilla T, Garcia-Planells J, Chumillas MJ, Mayordomo F, LeGuern E, Marin I, Vilchez JJ, Palau F (2002) The gene encoding ganglioside-induced differentiation-associated protein 1 is mutated in axonal Charcot-Marie-Tooth type 4A disease. Nat Genet 30:22-25.
De Jonghe P, Timmerman V, Ceuterick C, Nelis E, De Vriendt E, Lofgren A, Vercruyssen A, Verellen C, Van Maldergem L, Martin JJ, Van Broeckhoven C (1999) The Thr124Met mutation in the peripheral myelin protein zero (MPZ) gene is associated with a clinically distinct Charcot-Marie-Tooth phenotype. Brain 122 (Pt 2):281-290.
De Sandre-Giovannoli A, Chaouch M, Kozlov S, Vallat JM, Tazir M, Kassouri N, Szepetowski P, Hammadouche T, Vandenberghe A, Stewart CL, Grid D, Levy N (2002) Homozygous defects in LMNA, encoding lamin A/C nuclear-envelope proteins, cause autosomal recessive axonal neuropathy in human (Charcot-Marie-Tooth disorder type 2) and mouse. Am J Hum Genet 70:726-736.

Deinhardt K, Salinas S, Verastegui C, Watson R, Worth D, Hanrahan S, Bucci C, Schiavo G (2006) Rab5 and Rab7 control endocytic sorting along the axonal retrograde transport pathway. Neuron 52:293-305.

Delague V, Jacquier A, Hamadouche T, Poitelon Y, Baudot C, Boccaccio I, Chouery E, Chaouch M, Kassouri N, Jabbour R, Grid D, Megarbane A, Haase G, Levy N (2007) Mutations in FGD4 encoding the Rho GDP/GTP exchange factor FRABIN cause autosomal recessive Charcot-Marie-Tooth type 4H. Am J Hum Genet 81:1-16.

Delarue M (1995) Aminoacyl-tRNA synthetases. Curr Opin Struct Biol 5:48-55.

Deschenes SM, Walcott JL, Wexler TL, Scherer SS, Fischbeck KH (1997) Altered trafficking of mutant connexin32. The Journal of neuroscience : the official journal of the Society for Neuroscience 17:9077-9084.

Dimitriadi M, Hart AC (2010) Neurodegenerative disorders: insights from the nematode Caenorhabditis elegans. Neurobiology of disease 40:4-11.

Dyck PJ, Lambert EH (1968) Lower motor and primary sensory neuron diseases with peroneal muscular atrophy. II. Neurologic, genetic, and electrophysiologic findings in various neuronal degenerations. Arch Neurol 18:619-625.

Dyck PJ, Thomas PK (2005a) Peripheral Neuropathy, 4th Edition. Philadelphia: Elsevier, Inc. .

Dyck PJ, Thomas PK (2005b) Peripheral Neuropathy, 4th Edition. Philadelphia: Elsevier, Inc. .

Eaton HE, Metcalf J, Lacerda AF, Brunetti CR (2012) Accumulation of endogenous LITAF in aggresomes. PLoS One 7:e30003.

Edvardson S, Shaag A, Kolesnikova O, Gomori JM, Tarassov I, Einbinder T, Saada A, Elpeleg O (2007) Deleterious mutation in the mitochondrial arginyl-transfer RNA synthetase gene is associated with pontocerebellar hypoplasia. Am J Hum Genet 81:857-862.

Ehrlich M, Gama-Sosa MA, Huang LH, Midgett RM, Kuo KC, McCune RA, Gehrke C (1982) Amount and distribution of 5-methylcytosine in human DNA from different types of tissues of cells. Nucleic Acids Res 10:2709-2721.

Eldred EW, Schimmel PR (1972) Rapid deacylation by isoleucyl transfer ribonucleic acid synthetase of isoleucine-specific transfer ribonucleic acid aminoacylated with valine. The Journal of biological chemistry 247:2961-2964.

Evgrafov OV et al. (2004) Mutant small heat-shock protein 27 causes axonal Charcot-Marie-Tooth disease and distal hereditary motor neuropathy. Nat Genet 36:602-606.

Exome Variant Server, NHLBI Exome Sequencing Project (ESP), Seattle, WA (URL: http://evs.gs.washington.edu/EVS/) [June 2012].

Fabrizi GM, Cavallaro T, Angiari C, Bertolasi L, Cabrini I, Ferrarini M, Rizzuto N (2004) Giant axon and neurofilament accumulation in Charcot-Marie-Tooth disease type 2E. Neurology 62:1429-1431.

Fabrizi GM, Ferrarini M, Cavallaro T, Cabrini I, Cerini R, Bertolasi L, Rizzuto N (2007a) Two novel mutations in dynamin-2 cause axonal Charcot-Marie-Tooth disease. Neurology 69:291-295.

Fabrizi GM, Cavallaro T, Angiari C, Cabrini I, Taioli F, Malerba G, Bertolasi L, Rizzuto N (2007b) Charcot-Marie-Tooth disease type 2E, a disorder of the cytoskeleton. Brain 130:394-403.

Fersht AR (1977) Editing mechanisms in protein synthesis. Rejection of valine by the isoleucyl-tRNA synthetase. Biochemistry 16:1025-1030.

Froelich CA, First EA (2011) Dominant Intermediate Charcot-Marie-Tooth disorder is not due to a catalytic defect in tyrosyl-tRNA synthetase. Biochemistry 50:7132-7145.

Frommer M, McDonald LE, Millar DS, Collis CM, Watt F, Grigg GW, Molloy PL, Paul CL (1992) A genomic sequencing protocol that yields a positive display of 5-methylcytosine residues in individual DNA strands. Proc Natl Acad Sci U S A 89:1827-1831.

Gallardo E, Claeys KG, Nelis E, Garcia A, Canga A, Combarros O, Timmerman V, De Jonghe P, Berciano J (2008) Magnetic resonance imaging findings of leg musculature in Charcot-Marie-Tooth disease type 2 due to dynamin 2 mutation. J Neurol 255:986-992.

Gazzerro E, Sotgia F, Bruno C, Lisanti MP, Minetti C (2010) Caveolinopathies: from the biology of caveolin-3 to human diseases. European journal of human genetics : EJHG 18:137-145.

Geisler N, Weber K (1981) Self-assembly in Vitro of the 68,000 molecular weight component of the mammalian neurofilament triplet proteins into intermediate-sized filaments. J Mol Biol 151:565-571.

Georgiou DM, Zidar J, Korosec M, Middleton LT, Kyriakides T, Christodoulou K (2002) A novel NF-L mutation Pro22Ser is associated with CMT2 in a large Slovenian family. Neurogenetics 4:93-96.

Gilbert S (2010) Developmental Biology, 9th Edition. Sunderland: Sinauer Associates, Inc. .

Greenblatt MS, Bennett WP, Hollstein M, Harris CC (1994) Mutations in the p53 tumor suppressor gene: clues to cancer etiology and molecular pathogenesis. Cancer Res 54:4855-4878.

Greenfield S, Brostoff S, Eylar EH, Morell P (1973) Protein composition of myelin of the peripheral nervous system. J Neurochem 20:1207-1216.

Hafezparast M et al. (2003) Mutations in dynein link motor neuron degeneration to defects in retrograde transport. Science 300:808-812.

Hahn AF, Brown WF, Koopman WJ, Feasby TE (1990) X-linked dominant hereditary motor and sensory neuropathy. Brain 113 (Pt 5):1511-1525.

Hallam SJ, Jin Y (1998) lin-14 regulates the timing of synaptic remodelling in Caenorhabditis elegans. Nature 395:78-82.

Harding AE, Thomas PK (1980) The clinical features of hereditary motor and sensory neuropathy types I and II. Brain 103:259-280.

Harms MB, Ori-McKenney KM, Scoto M, Tuck EP, Bell S, Ma D, Masi S, Allred P, Al-Lozi M, Reilly MM, Miller LJ, Jani-Acsadi A, Pestronk A, Shy ME, Muntoni F, Vallee RB, Baloh RH (2012) Mutations in the tail domain of DYNC1H1 cause dominant spinal muscular atrophy. Neurology.

Hayasaka K, Himoro M, Sato W, Takada G, Uyemura K, Shimizu N, Bird TD, Conneally PM, Chance PF (1993) Charcot-Marie-Tooth neuropathy type 1B is associated with mutations of the myelin P0 gene. Nat Genet 5:31-34.
Hodapp JA, Carter GT, Lipe HP, Michelson SJ, Kraft GH, Bird TD (2006) Double trouble in hereditary neuropathy: concomitant mutations in the PMP-22 gene and another gene produce novel phenotypes. Arch Neurol 63:112-117.
Hou YM, Westhof E, Giege R (1993) An unusual RNA tertiary interaction has a role for the specific aminoacylation of a transfer RNA. Proc Natl Acad Sci U S A 90:6776-6780.
Inouye H, Tsuruta H, Sedzik J, Uyemura K, Kirschner DA (1999) Tetrameric assembly of full-sequence protein zero myelin glycoprotein by synchrotron x-ray scattering. Biophys J 76:423-437.
Ionasescu VV, Ionasescu R, Searby C (1993) Screening of dominantly inherited Charcot-Marie-Tooth neuropathies. Muscle & nerve 16:1232-1238.
Ishaque A, Roomi MW, Szymanska I, Kowalski S, Eylar EH (1980) The PO glycoprotein of peripheral nerve myelin. Can J Biochem 58:913-921.
Jellinger KA (2010) Basic mechanisms of neurodegeneration: a critical update. J Cell Mol Med 14:457-487.
Jin P, Duan R, Qurashi A, Qin Y, Tian D, Rosser TC, Liu H, Feng Y, Warren ST (2007) Pur alpha binds to rCGG repeats and modulates repeat-mediated neurodegeneration in a Drosophila model of fragile X tremor/ataxia syndrome. Neuron 55:556-564.
Jin Y, Hoskins R, Horvitz HR (1994) Control of type-D GABAergic neuron differentiation by C. elegans UNC-30 homeodomain protein. Nature 372:780-783.
Jin Y, Jorgensen E, Hartwieg E, Horvitz HR (1999) The Caenorhabditis elegans gene unc-25 encodes glutamic acid decarboxylase and is required for synaptic transmission but not synaptic development. The Journal of neuroscience : the official journal of the Society for Neuroscience 19:539-548.
Jordanova A et al. (2006) Disrupted function and axonal distribution of mutant tyrosyl-tRNA synthetase in dominant intermediate Charcot-Marie-Tooth neuropathy. Nat Genet 38:197-202.
Kalaydjieva L, Gresham D, Gooding R, Heather L, Baas F, de Jonge R, Blechschmidt K, Angelicheva D, Chandler D, Worsley P, Rosenthal A, King RH, Thomas PK (2000) N-myc downstream-regulated gene 1 is mutated in hereditary motor and sensory neuropathy-Lom. Am J Hum Genet 67:47-58.
Kennerson ML, Zhu D, Gardner RJ, Storey E, Merory J, Robertson SP, Nicholson GA (2001) Dominant intermediate Charcot-Marie-Tooth neuropathy maps to chromosome 19p12-p13.2. Am J Hum Genet 69:883-888.
Kessels MM, Dong J, Leibig W, Westermann P, Qualmann B (2006) Complexes of syndapin II with dynamin II promote vesicle formation at the trans-Golgi network. J Cell Sci 119:1504-1516.
Kim HJ, Hong SH, Ki CS, Kim BJ, Shim JS, Cho SH, Park JH, Kim JW (2005) A novel locus for X-linked recessive CMT with deafness and optic neuropathy maps to Xq21.32-q24. Neurology 64:1964-1967.
Kim HJ, Sohn KM, Shy ME, Krajewski KM, Hwang M, Park JH, Jang SY, Won HH, Choi BO, Hong SH, Kim BJ, Suh YL, Ki CS, Lee SY, Kim SH, Kim JW (2007)

Mutations in PRPS1, which encodes the phosphoribosyl pyrophosphate synthetase enzyme critical for nucleotide biosynthesis, cause hereditary peripheral neuropathy with hearing loss and optic neuropathy (cmtx5). Am J Hum Genet 81:552-558.

Ko YG, Kang YS, Kim EK, Park SG, Kim S (2000) Nucleolar localization of human methionyl-tRNA synthetase and its role in ribosomal RNA synthesis. J Cell Biol 149:567-574.

Ko YG, Kim EY, Kim T, Park H, Park HS, Choi EJ, Kim S (2001) Glutamine-dependent antiapoptotic interaction of human glutaminyl-tRNA synthetase with apoptosis signal-regulating kinase 1. J Biol Chem 276:6030-6036.

Koenig E (1979) Ribosomal RNA in Mauthner axon: implications for a protein synthesizing machinery in the myelinated axon. Brain Res 174:95-107.

Kovach MJ, Lin JP, Boyadjiev S, Campbell K, Mazzeo L, Herman K, Rimer LA, Frank W, Llewellyn B, Jabs EW, Gelber D, Kimonis VE (1999) A unique point mutation in the PMP22 gene is associated with Charcot-Marie-Tooth disease and deafness. Am J Hum Genet 64:1580-1593.

Kumar NM, Gilula NB (1996) The gap junction communication channel. Cell 84:381-388.

Kurihara S, Adachi Y, Imai C, Araki H, Hattori N, Numakura C, Lin Y, Hayasaka K, Sobue G, Nakashima K (2004) Charcot-Marie-Tooth families in Japan with MPZ Thr124Met mutation. Journal of neurology, neurosurgery, and psychiatry 75:1492-1494.

Kwiatkowski TJ, Jr. et al. (2009) Mutations in the FUS/TLS gene on chromosome 16 cause familial amyotrophic lateral sclerosis. Science 323:1205-1208.

Larkin MA, Blackshields G, Brown NP, Chenna R, McGettigan PA, McWilliam H, Valentin F, Wallace IM, Wilm A, Lopez R, Thompson JD, Gibson TJ, Higgins DG (2007) Clustal W and Clustal X version 2.0. Bioinformatics 23:2947-2948.

Latour P, Thauvin-Robinet C, Baudelet-Mery C, Soichot P, Cusin V, Faivre L, Locatelli MC, Mayencon M, Sarcey A, Broussolle E, Camu W, David A, Rousson R (2010) A major determinant for binding and aminoacylation of tRNA(Ala) in cytoplasmic Alanyl-tRNA synthetase is mutated in dominant axonal charcot-marie-tooth disease. Am J Hum Genet 86:77-82.

Leal A et al. (2009) Identification of the variant Ala335Val of MED25 as responsible for CMT2B2: molecular data, functional studies of the SH3 recognition motif and correlation between wild-type MED25 and PMP22 RNA levels in CMT1A animal models. Neurogenetics.

Lee HJ, Park CH, Lee SJ, Park JW, Choi JH, Ryu GH, Kwon BS (2008) Expression of caveolin-3 immunoreactivities in the developing sciatic nerve of the rat. Muscle & nerve 38:1021-1026.

Lee JW, Beebe K, Nangle LA, Jang J, Longo-Guess CM, Cook SA, Davisson MT, Sundberg JP, Schimmel P, Ackerman SL (2006) Editing-defective tRNA synthetase causes protein misfolding and neurodegeneration. Nature 443:50-55.

Lee YN, Nechushtan H, Figov N, Razin E (2004) The function of lysyl-tRNA synthetase and Ap4A as signaling regulators of MITF activity in FcepsilonRI-activated mast cells. Immunity 20:145-151.

Levitan I, Kaczmarek L (2002) The Neuron, 3rd Edition. Oxford: Oxford University Press.
Li J, Krajewski K, Shy ME, Lewis RA (2002) Hereditary neuropathy with liability to pressure palsy: the electrophysiology fits the name. Neurology 58:1769-1773.
Lin KP, Soong BW, Yang CC, Huang LW, Chang MH, Lee IH, Antonellis A, Lee YC (2011) The Mutational Spectrum in a Cohort of Charcot-Marie-Tooth Disease Type 2 among the Han Chinese in Taiwan. PLoS One 6:e29393.
Lodish HF (2008) Molecular cell biology, 6th Edition. New York: W.H. Freeman.
Lupski JR, de Oca-Luna RM, Slaugenhaupt S, Pentao L, Guzzetta V, Trask BJ, Saucedo-Cardenas O, Barker DF, Killian JM, Garcia CA, Chakravarti A, Patel PI (1991) DNA duplication associated with Charcot-Marie-Tooth disease type 1A. Cell 66:219-232.
Marrosu MG, Vaccargiu S, Marrosu G, Vannelli A, Cianchetti C, Muntoni F (1998) Charcot-Marie-Tooth disease type 2 associated with mutation of the myelin protein zero gene. Neurology 50:1397-1401.
Martyn CN, Hughes RA (1997) Epidemiology of peripheral neuropathy. J Neurol Neurosurg Psychiatry 62:310-318.
McIntire SL, Jorgensen E, Horvitz HR (1993a) Genes required for GABA function in Caenorhabditis elegans. Nature 364:334-337.
McIntire SL, Jorgensen E, Kaplan J, Horvitz HR (1993b) The GABAergic nervous system of Caenorhabditis elegans. Nature 364:337-341.
McIntire SL, Reimer RJ, Schuske K, Edwards RH, Jorgensen EM (1997) Identification and characterization of the vesicular GABA transporter. Nature 389:870-876.
McLaughlin HM, Sakaguchi R, Giblin W, Wilson TE, Biesecker L, Lupski JR, Talbot K, Vance JM, Zuchner S, Lee YC, Kennerson M, Hou YM, Nicholson G, Antonellis A (2012) A Recurrent loss-of-function alanyl-tRNA synthetase (AARS) mutation in patients with charcot-marie-tooth disease type 2N (CMT2N). Human mutation 33:244-253.
McLaughlin HM et al. (2010) Compound heterozygosity for loss-of-function lysyl-tRNA synthetase mutations in a patient with peripheral neuropathy. Am J Hum Genet 87:560-566.
Meggouh F, de Visser M, Arts WF, De Coo RI, van Schaik IN, Baas F (2005) Early onset neuropathy in a compound form of Charcot-Marie-Tooth disease. Ann Neurol 57:589-591.
Mersiyanova IV, Perepelov AV, Polyakov AV, Sitnikov VF, Dadali EL, Oparin RB, Petrin AN, Evgrafov OV (2000) A new variant of Charcot-Marie-Tooth disease type 2 is probably the result of a mutation in the neurofilament-light gene. Am J Hum Genet 67:37-46.
Misko A, Jiang S, Wegorzewska I, Milbrandt J, Baloh RH (2010) Mitofusin 2 is necessary for transport of axonal mitochondria and interacts with the Miro/Milton complex. J Neurosci 30:4232-4240.
Mossessova E, Lima CD (2000) Ulp1-SUMO crystal structure and genetic analysis reveal conserved interactions and a regulatory element essential for cell growth in yeast. Mol Cell 5:865-876.
Motley WW, Talbot K, Fischbeck KH (2010) GARS axonopathy: not every neuron's cup of tRNA. Trends Neurosci 33:59-66.

Motley WW, Seburn KL, Nawaz MH, Miers KE, Cheng J, Antonellis A, Green ED, Talbot K, Yang XL, Fischbeck KH, Burgess RW (2011) Charcot-Marie-Tooth-linked mutant GARS is toxic to peripheral neurons independent of wild-type GARS levels. PLoS genetics 7:e1002399.
Mudge SJ, Williams JH, Eyre HJ, Sutherland GR, Cowan PJ, Power DA (1998) Complex organisation of the 5'-end of the human glycine tRNA synthetase gene. Gene 209:45-50.
Murakami H, Ohta A, Ashigai H, Suga H (2006) A highly flexible tRNA acylation method for non-natural polypeptide synthesis. Nat Methods 3:357-359.
Murakami T, Garcia CA, Reiter LT, Lupski JR (1996) Charcot-Marie-Tooth disease and related inherited neuropathies. Medicine (Baltimore) 75:233-250.
Murphy BC, Scriver CR, Singh SM (2006) CpG methylation accounts for a recurrent mutation (c.1222C>T) in the human PAH gene. Hum Mutat 27:975.
Nangle LA, Zhang W, Xie W, Yang XL, Schimmel P (2007) Charcot-Marie-Tooth disease-associated mutant tRNA synthetases linked to altered dimer interface and neurite distribution defect. Proc Natl Acad Sci U S A 104:11239-11244.
Nelis E, Simokovic S, Timmerman V, Lofgren A, Backhovens H, De Jonghe P, Martin JJ, Van Broeckhoven C (1997) Mutation analysis of the connexin 32 (Cx32) gene in Charcot-Marie-Tooth neuropathy type 1: identification of five new mutations. Hum Mutat 9:47-52.
Nicholson G, Myers S (2006) Intermediate forms of Charcot-Marie-Tooth neuropathy: a review. Neuromolecular Med 8:123-130.
Niemann A, Berger P, Suter U (2006) Pathomechanisms of mutant proteins in Charcot-Marie-Tooth disease. Neuromolecular Med 8:217-242.
Niemann A, Wagner KM, Ruegg M, Suter U (2009) GDAP1 mutations differ in their effects on mitochondrial dynamics and apoptosis depending on the mode of inheritance. Neurobiol Dis 36:509-520.
Nishimura A, Moriya S, Ukai H, Nagai K, Wachi M, Yamada Y (1997) Diadenosine 5',5'''-P1,P4-tetraphosphate (Ap4A) controls the timing of cell division in Escherichia coli. Genes Cells 2:401-413.
Otani A, Slike BM, Dorrell MI, Hood J, Kinder K, Ewalt KL, Cheresh D, Schimmel P, Friedlander M (2002) A fragment of human TrpRS as a potent antagonist of ocular angiogenesis. Proc Natl Acad Sci U S A 99:178-183.
Owczarek A, Safro M, Wolfson AD (2008) Enzymatic tRNA acylation by acid and alpha-hydroxy acid analogues of amino acids. Biochemistry 47:301-307.
Paratcha G, Ledda F, Baars L, Coulpier M, Besset V, Anders J, Scott R, Ibanez CF (2001) Released GFRalpha1 potentiates downstream signaling, neuronal survival, and differentiation via a novel mechanism of recruitment of c-Ret to lipid rafts. Neuron 29:171-184.
Pareek S, Notterpek L, Snipes GJ, Naef R, Sossin W, Laliberte J, Iacampo S, Suter U, Shooter EM, Murphy RA (1997) Neurons promote the translocation of peripheral myelin protein 22 into myelin. The Journal of neuroscience : the official journal of the Society for Neuroscience 17:7754-7762.
Park MC, Kang T, Jin D, Han JM, Kim SB, Park YJ, Cho K, Park YW, Guo M, He W, Yang XL, Schimmel P, Kim S (2012) Secreted human glycyl-tRNA synthetase

implicated in defense against ERK-activated tumorigenesis. Proceedings of the National Academy of Sciences of the United States of America.
Park SG, Choi EC, Kim S (2010) Aminoacyl-tRNA synthetase-interacting multifunctional proteins (AIMPs): a triad for cellular homeostasis. IUBMB Life 62:296-302.
Park SG, Kim HJ, Min YH, Choi EC, Shin YK, Park BJ, Lee SW, Kim S (2005) Human lysyl-tRNA synthetase is secreted to trigger proinflammatory response. Proc Natl Acad Sci U S A 102:6356-6361.
Parton RG (1996) Caveolae and caveolins. Curr Opin Cell Biol 8:542-548.
Petersen SC, Watson JD, Richmond JE, Sarov M, Walthall WW, Miller DM, 3rd (2011) A transcriptional program promotes remodeling of GABAergic synapses in Caenorhabditis elegans. The Journal of neuroscience : the official journal of the Society for Neuroscience 31:15362-15375.
Pierce SB, Chisholm KM, Lynch ED, Lee MK, Walsh T, Opitz JM, Li W, Klevit RE, King MC (2011) Mutations in mitochondrial histidyl tRNA synthetase HARS2 cause ovarian dysgenesis and sensorineural hearing loss of Perrault syndrome. Proc Natl Acad Sci U S A 108:6543-6548.
Pritchard J (2010) Guillain-Barre syndrome. Clin Med 10:399-401.
Purves D, Augustine GJ, Fitzpatrick D, Katz LC, LaMantia A-S, McNamara JO, Williams SM (2001) Neuroscience, 2nd Edition. Sunderland, MA: Sinauer Associates, Inc.
Rice P, Longden I, Bleasby A (2000) EMBOSS: the European Molecular Biology Open Software Suite. Trends Genet 16:276-277.
Rinehart J, Krett B, Rubio MA, Alfonzo JD, Soll D (2005) Saccharomyces cerevisiae imports the cytosolic pathway for Gln-tRNA synthesis into the mitochondrion. Genes Dev 19:583-592.
Rizzuto R, Brini M, Pizzo P, Murgia M, Pozzan T (1995) Chimeric green fluorescent protein as a tool for visualizing subcellular organelles in living cells. Curr Biol 5:635-642.
Rowlands AG, Panniers R, Henshaw EC (1988) The catalytic mechanism of guanine nucleotide exchange factor action and competitive inhibition by phosphorylated eukaryotic initiation factor 2. The Journal of biological chemistry 263:5526-5533.
Ryan MC, Shooter EM, Notterpek L (2002) Aggresome formation in neuropathy models based on peripheral myelin protein 22 mutations. Neurobiology of disease 10:109-118.
Sahin-Calapoglu N, Tan M, Soyoz M, Calapoglu M, Ozcelik N (2009) Novel GDAP1 mutation in a Turkish family with CMT2K (CMT2K with novel GDAP1 mutation). Neuromolecular Med 11:106-113.
Saifi GM, Szigeti K, Wiszniewski W, Shy ME, Krajewski K, Hausmanowa-Petrusewicz I, Kochanski A, Reeser S, Mancias P, Butler I, Lupski JR (2005) SIMPLE mutations in Charcot-Marie-Tooth disease and the potential role of its protein product in protein degradation. Human mutation 25:372-383.
Saito M, Hayashi Y, Suzuki T, Tanaka H, Hozumi I, Tsuji S (1997) Linkage mapping of the gene for Charcot-Marie-Tooth disease type 2 to chromosome 1p (CMT2A) and the clinical features of CMT2A. Neurology 49:1630-1635.

Salazar-Grueso EF, Kim S, Kim H (1991) Embryonic mouse spinal cord motor neuron hybrid cells. Neuroreport 2:505-508.
Santel A, Fuller MT (2001) Control of mitochondrial morphology by a human mitofusin. J Cell Sci 114:867-874.
Saporta AS, Sottile SL, Miller LJ, Feely SM, Siskind CE, Shy ME (2011) Charcot-Marie-Tooth disease subtypes and genetic testing strategies. Ann Neurol 69:22-33.
Saxena S, Bucci C, Weis J, Kruttgen A (2005) The small GTPase Rab7 controls the endosomal trafficking and neuritogenic signaling of the nerve growth factor receptor TrkA. J Neurosci 25:10930-10940.
Scheper GC, van der Klok T, van Andel RJ, van Berkel CG, Sissler M, Smet J, Muravina TI, Serkov SV, Uziel G, Bugiani M, Schiffmann R, Krageloh-Mann I, Smeitink JA, Florentz C, Van Coster R, Pronk JC, van der Knaap MS (2007) Mitochondrial aspartyl-tRNA synthetase deficiency causes leukoencephalopathy with brain stem and spinal cord involvement and lactate elevation. Nat Genet 39:534-539.
Scherer PE, Okamoto T, Chun M, Nishimoto I, Lodish HF, Lisanti MP (1996) Identification, sequence, and expression of caveolin-2 defines a caveolin gene family. Proceedings of the National Academy of Sciences of the United States of America 93:131-135.
Scherer SS, Deschenes SM, Xu YT, Grinspan JB, Fischbeck KH, Paul DL (1995) Connexin32 is a myelin-related protein in the PNS and CNS. J Neurosci 15:8281-8294.
Schulze-Lohoff E, Zanner S, Ogilvie A, Sterzel RB (1995) Vasoactive diadenosine polyphosphates promote growth of cultured renal mesangial cells. Hypertension 26:899-904.
Schuske K, Beg AA, Jorgensen EM (2004) The GABA nervous system in C. elegans. Trends in neurosciences 27:407-414.
Seburn KL, Nangle LA, Cox GA, Schimmel P, Burgess RW (2006) An active dominant mutation of glycyl-tRNA synthetase causes neuropathy in a Charcot-Marie-Tooth 2D mouse model. Neuron 51:715-726.
Selker EU, Stevens JN (1985) DNA methylation at asymmetric sites is associated with numerous transition mutations. Proc Natl Acad Sci U S A 82:8114-8118.
Senderek J, Bergmann C, Weber S, Ketelsen UP, Schorle H, Rudnik-Schoneborn S, Buttner R, Buchheim E, Zerres K (2003a) Mutation of the SBF2 gene, encoding a novel member of the myotubularin family, in Charcot-Marie-Tooth neuropathy type 4B2/11p15. Hum Mol Genet 12:349-356.
Senderek J, Bergmann C, Ramaekers VT, Nelis E, Bernert G, Makowski A, Zuchner S, De Jonghe P, Rudnik-Schoneborn S, Zerres K, Schroder JM (2003b) Mutations in the ganglioside-induced differentiation-associated protein-1 (GDAP1) gene in intermediate type autosomal recessive Charcot-Marie-Tooth neuropathy. Brain 126:642-649.
Senderek J et al. (2003c) Mutations in a gene encoding a novel SH3/TPR domain protein cause autosomal recessive Charcot-Marie-Tooth type 4C neuropathy. Am J Hum Genet 73:1106-1119.
Shitivelband S, Hou YM (2005) Breaking the stereo barrier of amino acid attachment to tRNA by a single nucleotide. J Mol Biol 348:513-521.

Skre H (1974) Genetic and clinical aspects of Charcot-Marie-Tooth's disease. Clin Genet 6:98-118.
Snipes GJ, Suter U, Welcher AA, Shooter EM (1992) Characterization of a novel peripheral nervous system myelin protein (PMP-22/SR13). J Cell Biol 117:225-238.
Sofola OA, Jin P, Qin Y, Duan R, Liu H, de Haro M, Nelson DL, Botas J (2007) RNA-binding proteins hnRNP A2/B1 and CUGBP1 suppress fragile X CGG premutation repeat-induced neurodegeneration in a Drosophila model of FXTAS. Neuron 55:565-571.
Spinosa MR, Progida C, De Luca A, Colucci AM, Alifano P, Bucci C (2008) Functional characterization of Rab7 mutant proteins associated with Charcot-Marie-Tooth type 2B disease. J Neurosci 28:1640-1648.
Sreedharan J, Blair IP, Tripathi VB, Hu X, Vance C, Rogelj B, Ackerley S, Durnall JC, Williams KL, Buratti E, Baralle F, de Belleroche J, Mitchell JD, Leigh PN, Al-Chalabi A, Miller CC, Nicholson G, Shaw CE (2008) TDP-43 mutations in familial and sporadic amyotrophic lateral sclerosis. Science 319:1668-1672.
Stark LA, Hay RT (1998) Human immunodeficiency virus type 1 (HIV-1) viral protein R (Vpr) interacts with Lys-tRNA synthetase: implications for priming of HIV-1 reverse transcription. J Virol 72:3037-3044.
Stojkovic T, Latour P, Vandenberghe A, Hurtevent JF, Vermersch P (1999) Sensorineural deafness in X-linked Charcot-Marie-Tooth disease with connexin 32 mutation (R142Q). Neurology 52:1010-1014.
Storkebaum E, Leitao-Goncalves R, Godenschwege T, Nangle L, Mejia M, Bosmans I, Ooms T, Jacobs A, Van Dijck P, Yang XL, Schimmel P, Norga K, Timmerman V, Callaerts P, Jordanova A (2009) Dominant mutations in the tyrosyl-tRNA synthetase gene recapitulate in Drosophila features of human Charcot-Marie-Tooth neuropathy. Proc Natl Acad Sci U S A 106:11782-11787.
Street VA, Bennett CL, Goldy JD, Shirk AJ, Kleopa KA, Tempel BL, Lipe HP, Scherer SS, Bird TD, Chance PF (2003) Mutation of a putative protein degradation gene LITAF/SIMPLE in Charcot-Marie-Tooth disease 1C. Neurology 60:22-26.
Stum M, McLaughlin HM, Kleinbrink EL, Miers KE, Ackerman SL, Seburn KL, Antonellis A, Burgess RW (2011) An assessment of mechanisms underlying peripheral axonal degeneration caused by aminoacyl-tRNA synthetase mutations. Mol Cell Neurosci 46:432-443.
Tang BS, Zhao GH, Luo W, Xia K, Cai F, Pan Q, Zhang RX, Zhang FF, Liu XM, Chen B, Zhang C, Shen L, Jiang H, Long ZG, Dai HP (2005) Small heat-shock protein 22 mutated in autosomal dominant Charcot-Marie-Tooth disease type 2L. Hum Genet 116:222-224.
Taylor AM, Berchtold NC, Perreau VM, Tu CH, Li Jeon N, Cotman CW (2009) Axonal mRNA in uninjured and regenerating cortical mammalian axons. The Journal of neuroscience : the official journal of the Society for Neuroscience 29:4697-4707.
Thompson AJ, Cronin MS, Kirschner DA (2002) Myelin protein zero exists as dimers and tetramers in native membranes of Xenopus laevis peripheral nerve. J Neurosci Res 67:766-771.
Tolkunova E, Park H, Xia J, King MP, Davidson E (2000) The human lysyl-tRNA synthetase gene encodes both the cytoplasmic and mitochondrial enzymes by

means of an unusual alternative splicing of the primary transcript. J Biol Chem 275:35063-35069.
Tooth HH (1886) The peroneal type of progressive muscular atrophy. Cambridge: University of Cambridge.
Tsalik EL, Hobert O (2003) Functional mapping of neurons that control locomotory behavior in Caenorhabditis elegans. Journal of neurobiology 56:178-197.
Valentijn LJ, Bolhuis PA, Zorn I, Hoogendijk JE, van den Bosch N, Hensels GW, Stanton VP, Jr., Housman DE, Fischbeck KH, Ross DA, et al. (1992) The peripheral myelin gene PMP-22/GAS-3 is duplicated in Charcot-Marie-Tooth disease type 1A. Nat Genet 1:166-170.
Vartanian A, Prudovsky I, Suzuki H, Dal Pra I, Kisselev L (1997) Opposite effects of cell differentiation and apoptosis on Ap3A/Ap4A ratio in human cell cultures. FEBS letters 415:160-162.
Verhoeven K, De Jonghe P, Coen K, Verpoorten N, Auer-Grumbach M, Kwon JM, FitzPatrick D, Schmedding E, De Vriendt E, Jacobs A, Van Gerwen V, Wagner K, Hartung HP, Timmerman V (2003) Mutations in the small GTP-ase late endosomal protein RAB7 cause Charcot-Marie-Tooth type 2B neuropathy. Am J Hum Genet 72:722-727.
Verhoeven K et al. (2006) MFN2 mutation distribution and genotype/phenotype correlation in Charcot-Marie-Tooth type 2. Brain 129:2093-2102.
Vincent AM, Callaghan BC, Smith AL, Feldman EL (2011) Diabetic neuropathy: cellular mechanisms as therapeutic targets. Nat Rev Neurol 7:573-583.
Voet D, Voet JG, Pratt CW (1999) Fundamentals of biochemistry. New York: Wiley.
Wakasugi K, Schimmel P (1999a) Two distinct cytokines released from a human aminoacyl-tRNA synthetase. Science 284:147-151.
Wakasugi K, Schimmel P (1999b) Highly differentiated motifs responsible for two cytokine activities of a split human tRNA synthetase. J Biol Chem 274:23155-23159.
Wakasugi K, Slike BM, Hood J, Otani A, Ewalt KL, Friedlander M, Cheresh DA, Schimmel P (2002) A human aminoacyl-tRNA synthetase as a regulator of angiogenesis. Proc Natl Acad Sci U S A 99:173-177.
Wan M, Lee SS, Zhang X, Houwink-Manville I, Song HR, Amir RE, Budden S, Naidu S, Pereira JL, Lo IF, Zoghbi HY, Schanen NC, Francke U (1999) Rett syndrome and beyond: recurrent spontaneous and familial MECP2 mutations at CpG hotspots. Am J Hum Genet 65:1520-1529.
Warner LE, Mancias P, Butler IJ, McDonald CM, Keppen L, Koob KG, Lupski JR (1998) Mutations in the early growth response 2 (EGR2) gene are associated with hereditary myelinopathies. Nat Genet 18:382-384.
Warner LE, Hilz MJ, Appel SH, Killian JM, Kolodry EH, Karpati G, Carpenter S, Watters GV, Wheeler C, Witt D, Bodell A, Nelis E, Van Broeckhoven C, Lupski JR (1996) Clinical phenotypes of different MPZ (P0) mutations may include Charcot-Marie-Tooth type 1B, Dejerine-Sottas, and congenital hypomyelination. Neuron 17:451-460.
Waxman S, Kocsis J, Stys P (1995) The Axon. Oxford: Oxford University Press, Inc. .
Weedon MN, Hastings R, Caswell R, Xie W, Paszkiewicz K, Antoniadi T, Williams M, King C, Greenhalgh L, Newbury-Ecob R, Ellard S (2011) Exome sequencing

identifies a DYNC1H1 mutation in a large pedigree with dominant axonal Charcot-Marie-Tooth disease. American journal of human genetics 89:308-312.
White JG, Albertson DG, Anness MA (1978) Connectivity changes in a class of motoneurone during the development of a nematode. Nature 271:764-766.
Williams TM, Lisanti MP (2004) The Caveolin genes: from cell biology to medicine. Ann Med 36:584-595.
Xie W, Nangle LA, Zhang W, Schimmel P, Yang XL (2007) Long-range structural effects of a Charcot-Marie-Tooth disease-causing mutation in human glycyl-tRNA synthetase. Proc Natl Acad Sci U S A 104:9976-9981.
Yum SW, Kleopa KA, Shumas S, Scherer SS (2002) Diverse trafficking abnormalities of connexin32 mutants causing CMTX. Neurobiol Dis 11:43-52.
Zaher HS, Green R (2009) Fidelity at the molecular level: lessons from protein synthesis. Cell 136:746-762.
Zhai J, Lin H, Julien JP, Schlaepfer WW (2007) Disruption of neurofilament network with aggregation of light neurofilament protein: a common pathway leading to motor neuron degeneration due to Charcot-Marie-Tooth disease-linked mutations in NFL and HSPB1. Hum Mol Genet 16:3103-3116.
Zhao C, Takita J, Tanaka Y, Setou M, Nakagawa T, Takeda S, Yang HW, Terada S, Nakata T, Takei Y, Saito M, Tsuji S, Hayashi Y, Hirokawa N (2001) Charcot-Marie-Tooth disease type 2A caused by mutation in a microtubule motor KIF1Bbeta. Cell 105:587-597.
Zuchner S, Noureddine M, Kennerson M, Verhoeven K, Claeys K, De Jonghe P, Merory J, Oliveira SA, Speer MC, Stenger JE, Walizada G, Zhu D, Pericak-Vance MA, Nicholson G, Timmerman V, Vance JM (2005) Mutations in the pleckstrin homology domain of dynamin 2 cause dominant intermediate Charcot-Marie-Tooth disease. Nat Genet 37:289-294.
Zuchner S et al. (2004) Mutations in the mitochondrial GTPase mitofusin 2 cause Charcot-Marie-Tooth neuropathy type 2A. Nat Genet 36:449-451.